

Bayesian Causal Inference in Doubly Gaussian DAG–probit Models

Rasool Tahmasbi^{1*}, Keyvan Tahmasbi^b

^aUniversity of Colorado, Boulder, USA

^bDepartment of Statistics, Shahid Beheshti University, Tehran, Iran

*Corresponding author: Rasool Tahmasbi; Rasool.Tahmasbi@Colorado.edu

Abstract

We consider modeling a binary response variable together with a set of covariates for two groups under observational data. The grouping variable can be the confounding variable (the common cause of treatment and outcome), gender, case/control, ethnicity, etc. Given the covariates and a binary latent variable, the goal is to construct two directed acyclic graphs (DAGs), while sharing some common parameters. The set of nodes, which represent the variables, are the same for both groups but the directed edges between nodes, which represent the causal relationships between the variables, can be potentially different. For each group, we also estimate the effect size for each node. We assume that each group follows a Gaussian distribution under its DAG. Given the parent nodes, the joint distribution of DAG is conditionally independent due to the Markov property of DAGs. We introduce the concept of Gaussian DAG–probit model under two groups and hence doubly Gaussian DAG–probit model. To estimate the skeleton of the DAGs and the model parameters, we took samples from the posterior distribution of doubly Gaussian DAG–probit model via MCMC method. We validated the proposed method using a comprehensive simulation experiment and applied it on two real datasets. Furthermore, we validated the results of the real data analysis using well-known experimental studies to show the value of the proposed grouping variable in the causality domain.

Keywords: Bayesian Causal Inference; Causal Effects; do Calculus; Graphical Models; MCMC; Modified Cholesky Decomposition; Observational study;

1 Introduction

The goal of etiological research is to uncover causal effects, whilst prediction research aims to predict an outcome with the best accuracy. Causal and prediction research usually require different methods, and yet their findings may be meaningless if the right method is not used. Machine-learning (ML) systems have made astounding progress in analyzing data patterns, but ML algorithms cannot tell whether a crowing rooster makes the sun rise, or the other way around (Pearl and Mackenzie (2020)). So by just training a model on historical data we cannot say anything about the causes or the direction of causation, which is crucial as well. More granular distinction between the causality and prediction methods can be found in Ramspek et al. (2021) and Gische, West, and Voelkle (2021).

Type of data availability is also important for picking the right causality model. The gold standard data for answering the "what if" questions, which are related to the causal effect discovery, is *randomized* data. However, it is often not feasible to run randomized experiments due to the ethical issues, costs, or running time. In this case, causal inferences can be obtained from *observational* data (Hernán and Robins (2010)).

Estimating causality from observational data is essential in many data science questions but can be a challenging task. Some mathematical models such as Directed Acyclic Graph (DAG) and Structural Equation Model (SEM) are important tools to infer the causal effects based on observational data. DAGs have been extensively used to construct statistical models embodying conditional independence relations in graphical models (Lauritzen (1996)) while causal DAGs will be instrumental to define the notion of causal effect (Pearl et al. (2000)). Some models such as DoWhy (Sharma and Kiciman (2020)) assume that the causal graph is known and the goal is to estimate the effect sizes.

Gaussian graphical models (GGM) are also used in many causal discovery problems. GGM is a statistical framework defined with respect to a graph, in which the nodes index a collection of jointly Gaussian random variables and the edges represent the conditional independence relations among the variables. A number of papers have studied covariance estimation in the context of GMM selection. For example, M. Chen, Ren, Zhao, and Zhou (2016) estimated the covariate-adjusted GMM using asymptotic theory. They showed that for each finite subgraph, their estimator is asymptotically normal and efficient. Cai, Li, Liu, and Xie (2013) introduced a sparse

high dimensional multivariate regression model for studying conditional independence relationships among a set of genes adjusting for possible genetic effects. They presented a covariate-adjusted precision matrix estimation method using a constrained ℓ_1 minimization.

The problem of latent variables, where all the variables (both observed and latent) are jointly Gaussian, is studied by [Chandrasekaran, Parrilo, and Willsky \(2012\)](#). [Chandrasekaran et al. \(2012\)](#) studied the case when the graph is sparse and there are a few additional latent components in the DAG structure. They proposed a convex program based on ℓ_1 and nuclear norm regularized maximum likelihood for latent-variable graphical model selection. [Wu, Zhao, Fang, and Deng \(2017\)](#) proposed a method for learning latent variable graphical models via ℓ_1 and trace penalized D-trace loss. Gaussian latent variables also have many applications in the generative models such as variational autoencoder (VAE) models, introduced by [Kingma and Welling \(2013\)](#). Learning individual-level causal effects (ILCE) from observational data, which is important for the policy makers, is studied by [Louizos et al. \(2017\)](#). Examples of ILCE include understanding the effect of medications on a patient’s health, or of teaching methods on a student’s chance of graduation. Their approach is based on the VAE to estimate the causal effects of the latent variables on large datasets. For a comprehensive review on theoretical properties and optimalities of the estimation of structured covariance and precision matrices, see [Cai, Ren, and Zhou \(2016\)](#) and the references therein.

Motivated by the probit regression model, [Guo, Levina, Michailidis, and Zhu \(2015\)](#) introduced the probit graphical model. [Castelletti and Consonni \(2021\)](#) extended the probit graphical models by introducing DAG–probit models. For DAG–probit model, they considered a binary response which is potentially affected by a set of continuous variables. Their model assumes that there is just one DAG.

In reality, there are many cases when we should model our data for different groups, separately. The grouping variable can be gender, different ethnicities, or case/control studies. For example, it is well known that the physiological differences between men and women affect drug activity, including pharmacokinetics and pharmacodynamics. If we pick a model that does not properly take genders into account, then the results will be biased, a serious problem which is called *gender bias in research* (see [Holdcroft \(2007\)](#) and [Aragón, Pietri, and Powell \(2023\)](#)). As another example, our metabolism changes with age ([Pontzer et al. \(2021\)](#)) and therefore a method that can model the age differences is preferred. The results of comparing the outcome between two groups can sometimes be confounded and even reversed by an unrecognised third variable. This concept is known as *Simpson’s Paradox* and confounding variable can be gender, ethnicity, etc.

In this paper, we introduce the *doubly Gaussian DAG–probit model* in Section 2 by allowing groups to have different DAGs while some of the model parameters are shared between the groups. Allowing a model with the flexibility to have different structures for different groups can potentially take care of Simpson paradox and can reduce gender bias in research. The proposed model is driven for binary grouping variables but can be extended for any non-binary grouping variable as well. The shared parameters can be the common edges between the two groups, a common cut-off parameter or nodes variance. As an example, [Qiao, Qian, James, and Guo \(2020\)](#) studied the network of EEG (electroencephalogram) signals on alcoholic and control groups. They expressed that since the graphical structures for alcoholic and non-alcoholic groups share some common edges, it is advantageous to jointly estimate two networks. For estimating the heritability using genome data, it is common to assume that the effect of SNPs (single-nucleotide polymorphism) are the same for all individuals (check our paper [Evans et al. \(2018\)](#)). Therefore, we assume that the effect of a gene for all individuals (even in different groups) is the same and changes in the phenotypes are due to the differences in the gene network, which enables us to jointly estimate this parameter from all groups.

Choice of priors can speed up the MCMC algorithm and simplify the posterior formula. Our priors for the model parameters are presented in Section 3. After computing the posteriors for the parameters, we present our MCMC algorithm in Section 4. [Dawid and Musio \(2022\)](#) expressed and contrasted two distinct problem areas for statistical causality: studying the likely effects of an intervention (effects of causes) and studying whether there is a causal link between the observed exposure and outcome in an individual case (causes of effects). The effect of interventions in terms of the observed probabilities using *do calculus* is computed in section 5 and causes of effects can be estimated from the last step of our MCMC Algorithm.

To assess the performance of the proposed method, a comprehensive simulation study is performed in Section 6. We provide several evaluation metrics to check the MCMC algorithm and model performance. We apply our method on two well-known real datasets and illustrate the results in Section 7. We use the genome network data of breast cancer for the first example and compare our results with the well-known published genetics papers to validate our outputs in Section 7.1. For the second real data analysis, we study the impact of airborne particles on the cardiovascular mortality rate (CMR) in Section 7.2. The final points for discussion are presented in Section 8. Some proof of the posteriors together with more simulation results are provided in Appendix.

2 Methodology

Let $\mathcal{D} = (V, E)$ be a DAG, where $V = \{1, \dots, q\}$ is a set of vertices (or nodes) and $E \subseteq V \times V$ a set of edges whose elements are $(u, v) \equiv u \rightarrow v$, such that if $(u, v) \in E$ then $(v, u) \notin E$. In addition, \mathcal{D} contains no cycles. For a given node v , if $u \rightarrow v \in E$, we say that u is a *parent* of v (conversely v is a *child* of u). The parent set of v in \mathcal{D} is denoted by $\text{pa}(v)$, the set of children by $\text{ch}(v)$. Moreover, we denote by $\text{fa}(v) = v \cup \text{pa}(v)$ the *family* of v in

\mathcal{D} . Finally, we say that a DAG is complete if all vertices are joined by an edge. For further theory and notation on DAGs we refer to [Lauritzen \(1996\)](#).

A DAG can be expressed by a probabilistic model via conditional dependence structure between its random variables. We consider a collection of random variables (X_1, \dots, X_q) and assume that their joint probability density function $f(\mathbf{x})$ is Markov w.r.t. \mathcal{D} , so that it admits the following factorization

$$f(x_1, \dots, x_q) = \prod_{j=1}^q f(x_j | \mathbf{x}_{\text{pa}(j)}). \quad (1)$$

2.1 Gaussian Graphical Models

Graphical models provide a suitable language to decompose many complex real-world problems through conditional independence constraints. Gaussian Graphical Models (GGMs) are extensively used in many research areas, such as genomics, proteomics, neuroimaging, and psychology, to study the partial correlation structure of a set of variables. This structure is visualized by drawing an undirected network, in which the variables constitute the nodes and the partial correlations the edges.

GGMs are tightly linked to precision matrices. Suppose $\mathbf{X} = (X_1, \dots, X_q)'$ follows a multivariate Gaussian distribution $\mathcal{N}_q(\boldsymbol{\mu}, \boldsymbol{\Sigma})$ with dimension q . Without loss of generality, we can assume the mean of X_i is zero. The precision matrix $\boldsymbol{\Omega} = \boldsymbol{\Sigma}^{-1}$ with $\boldsymbol{\Omega} = [\omega_{ij}]_{i,j=1,\dots,q}$ describes the graphical structure of its corresponding Gaussian graph. If the (i, j) th entry of the precision matrix ω_{ij} is equal to zero, then X_i and X_j are independent conditioning on all other variables $X_k, k \neq i, j$. Correspondingly, no edge exists between X_i and variable X_j in the graphical structure of Gaussian graphical model. If $\omega_{ij} \neq 0$, then X_i and X_j are conditionally dependent and they are therefore connected in the graphical structure. Partial correlation can be written in terms of the precision matrix. For the precision matrix $\boldsymbol{\Omega}$, the partial correlation between two variables X_i and X_j given all other nodes, i.e., $V \setminus \{i, j\}$ is given by

$$\rho_{ij} := \rho_{ij | V \setminus \{i, j\}} = -\frac{\omega_{ij}}{\sqrt{\omega_{ii}\omega_{jj}}}. \quad (2)$$

[Lafit, Tuerlinckx, Myin-Germeys, and Ceulemans \(2019\)](#) used a partial correlation screening approach for controlling the false positive rate in sparse GMMs. Under Gaussian assumption with mean zero, i.e., $X_1, \dots, X_q | \boldsymbol{\Omega} \sim \mathcal{N}_q(\mathbf{0}, \boldsymbol{\Omega}^{-1})$, we can rewrite (1) as

$$f(x_1, \dots, x_q | \boldsymbol{\Omega}) = \prod_{j=1}^q f_{\mathcal{N}}(x_j | \mu_j(\mathbf{x}_{\text{pa}(j)}), \sigma_j^2), \quad (3)$$

where $f_{\mathcal{N}}(\cdot | \mu, \sigma^2)$ denotes the normal density having mean μ and variance σ^2 . In this section, we will show how to compute $\mu_j(\mathbf{x}_{\text{pa}(j)})$ and σ_j^2 .

For a given DAG, we can always reorder the nodes using topological sorting to have a *parent ordering* of the nodes which numerically relabels the nodes so that if $i \rightarrow j$ (i is a child of j) then $i < j$, for any $i, j \in V$ ([Knuth \(1997\)](#)). Clearly node 1 will not have any children.

Equation (3) can be written as a *structural equation model*

$$\mathbf{L}'\mathbf{X} = \boldsymbol{\epsilon}, \quad (4)$$

where $\mathbf{X} = (X_1, \dots, X_q)'$ and $\mathbf{L} = [L_{ij}]_{i,j=1,\dots,q}$ is a lower-triangular matrix of coefficients with $L_{ij} \in \mathbb{R}$, $L_{ii} = 1$ and $L_{ij} \neq 0$ if and only if $i \rightarrow j$. \mathbf{L} is a lower-triangular matrix because of the parent ordering. So $L_{ij} = 0$ if and only if $i > j$ or $i \not\rightarrow j$. Moreover, $\boldsymbol{\epsilon}$ is a $q \times 1$ vector of error terms, $\boldsymbol{\epsilon} \sim \mathcal{N}_q(\mathbf{0}, \mathbf{D})$, where $\mathbf{D} = \text{diag}(\boldsymbol{\sigma}^2)$ and $\boldsymbol{\sigma}^2$ is the $q \times 1$ vector of conditional variances whose j -th element is $\sigma_j^2 = \text{Var}(X_j | \mathbf{x}_{\text{pa}(j)}, \boldsymbol{\Omega})$.

Taking variance on both sides of (4), we can show that

$$\boldsymbol{\Omega} = \mathbf{L}\mathbf{D}^{-1}\mathbf{L}', \quad (5)$$

which is the *modified Cholesky decomposition* of $\boldsymbol{\Omega}$ (see [Pourahmadi \(2007\)](#)). In fact any positive definite matrix $\boldsymbol{\Omega}$ can be uniquely decomposed as $\boldsymbol{\Omega} = \mathbf{L}\mathbf{D}^{-1}\mathbf{L}'$, where \mathbf{L} is a lower triangular matrix with unit diagonal entries, and \mathbf{D} is a diagonal matrix with positive diagonal entries (see, e.g., [Golub and Van Loan \(2013\)](#)). [Rothman, Levina, and Zhu \(2010\)](#) presented a new approach for the Cholesky-based covariance regularization in high dimensions. [Guo, Levina, Michailidis, and Zhu \(2011\)](#) considered an automated approach using the lasso to estimate sparse graphical models by selecting sets of edges common to all groups, as well as group-specific edges.

Since the joint probability density function $f(\mathbf{x})$ is Markov w.r.t. \mathcal{D} , we can use multivariate Gaussian conditional distribution to compute $\mu_j(\mathbf{x}_{\text{pa}(j)})$ and σ_j^2 in (3). For any given $q \times q$ matrix \mathbf{A} , denote by $\mathbf{A}_{\leq j \geq}$ the $|\text{pa}(j)| \times |\text{pa}(j)|$ submatrix of \mathbf{A} with indexes corresponding to $\text{pa}(j)$, $\mathbf{A}_{\leq j >}$ the $|\text{pa}(j)| \times 1$ submatrix of \mathbf{A} , and $\mathbf{A}_{< j >} := \mathbf{A}_{jj}$ where the parent nodes, $\text{pa}(j)$, can be extracted from \mathcal{D} . Therefore,

$$\mu_j(\mathbf{x}_{\text{pa}(j)}) = -\mathbf{L}_{\leq j >} \mathbf{x}_{\text{pa}(j)}, \quad (6)$$

where $\mathbf{L}_{\prec j \succ} = -\boldsymbol{\Sigma}_{\prec j \succeq}^{-1} \boldsymbol{\Sigma}_{\prec j \succ}$ and

$$\sigma_j^2 = \boldsymbol{\Sigma}_{\prec j \succ} - \boldsymbol{\Sigma}'_{\prec j \succ} \boldsymbol{\Sigma}_{\prec j \succeq}^{-1} \boldsymbol{\Sigma}_{\prec j \succ}. \quad (7)$$

The proof is based on the Gaussian conditional distributions of node j given its parent nodes, $\text{pa}(j)$. For the cases when $\text{pa}(j)$ is empty set, we set $\mu_j(\mathbf{x}_{\text{pa}(j)}) = \mathbf{0}$ and $\sigma_j^2 = \boldsymbol{\Sigma}_{\prec j \succ}$.

2.2 DAG-Probit Model

DAG-Probit model is defined in [Castelletti and Consommi \(2021\)](#). They assumed that X_1 is a latent variable and the binary variable $Y \in \{0, 1\}$ is observed. For a given threshold $\theta \in \mathbb{R}$, define

$$Y = \begin{cases} 0 & \text{if } X_1 < \theta, \\ 1 & \text{if } X_1 \geq \theta. \end{cases} \quad (8)$$

Without loss of generality, they assumed that the variance of X_1 is 1, i.e., $\sigma_1^2 = 1$. In reality, X_1 is not observed and we are interested in distribution of (Y, X_2, \dots, X_q) . By including the latent variable X_1 in the model and using (3) and (8), the joint density of (Y, X_1, \dots, X_q) becomes

$$f(y, x_1, \dots, x_q | \mathcal{D}, \mathbf{D}, \mathbf{L}, \theta) = \prod_{j=1}^q f_{\mathcal{N}}(x_j | \mu_j(\mathbf{x}_{\text{pa}(j)}), \sigma_j^2) \cdot \mathbb{1}(\theta_{y_i-1} < x_1 \leq \theta_{y_i}), \quad (9)$$

where the notation $\theta_{-1} := -\infty, \theta_0 := \theta$ and $\theta_1 := \infty$ is used.

For a sample size of n with observations $(y_i, x_{i,1}, \dots, x_{i,q})$, the *augmented* likelihood can be written as

$$\begin{aligned} f(\mathbf{y}, \mathbf{X} | \mathcal{D}, \mathbf{D}, \mathbf{L}, \theta) &= \prod_{i=1}^n f(y_i, x_{i,1}, \dots, x_{i,q} | \mathcal{D}, \mathbf{D}, \mathbf{L}) \cdot \mathbb{1}(\theta_{y_i-1} < x_{i,1} \leq \theta_{y_i}) \\ &= \prod_{j=1}^q f_{\mathcal{N}_n}(\mathbf{X}_j | -\mathbf{X}_{\text{pa}(j)} \mathbf{L}_{\prec j \succ}, \sigma_j^2 \mathbf{I}_n) \cdot \prod_{i=1}^n \mathbb{1}(\theta_{y_i-1} < x_{i,1} \leq \theta_{y_i}) \end{aligned} \quad (10)$$

where $\mathbf{y} = (y_1, \dots, y_n)'$, $\mathbf{X} := (\mathbf{X}_1, \dots, \mathbf{X}_q)$ is the $n \times q$ augmented data matrix, \mathbf{X}_s is the submatrix of \mathbf{X} with columns s and $\mathbf{X}_{-1} := (\mathbf{X}_2, \dots, \mathbf{X}_q)$.

2.3 Doubly Gaussian DAG-Probit Model

We assume there are two groups of data, $\mathbf{X}^{(1)}$ and $\mathbf{X}^{(2)}$ with the corresponding DAG's $\mathcal{D}^{(1)} = (V, E^{(1)})$ and $\mathcal{D}^{(2)} = (V, E^{(2)})$. The set of vertices are the same for both groups but potentially they can have different sets of edges. For each group $k \in \{1, 2\}$, $\mathbf{X}^{(k)}$ follows a Gaussian distribution with sample size n_k . Furthermore, we also have observed the binary random vector $\mathbf{y}^{(k)}$ of size n_k , related to the latent variables $X_1^{(k)}$ defined in (8). We assume that σ_j^2 is equal for both groups, i.e., $\text{Var}(X_j | \mathbf{x}_{\text{pa}(j)}^{(1)}) = \text{Var}(X_j | \mathbf{x}_{\text{pa}(j)}^{(2)})$, therefore $\mathbf{D} := \mathbf{D}^{(1)} = \mathbf{D}^{(2)}$. The skeleton of $\mathcal{D}^{(k)}$ can have effect on the $\mathbf{L}^{(k)}$ as well, because $L_{ij} = 0$ if and only if $i \not\rightarrow j$, so they can be different as well as the precision matrices $\boldsymbol{\Omega}^{(1)}$ and $\boldsymbol{\Omega}^{(2)}$.

The augmented likelihood for the doubly Gaussian DAG-probit model can be written as

$$\begin{aligned} &f(\mathbf{y}^{(1)}, \mathbf{y}^{(2)}, \mathbf{X}^{(1)}, \mathbf{X}^{(2)} | \mathcal{D}^{(1)}, \mathcal{D}^{(2)}, \mathbf{D}, \mathbf{L}^{(1)}, \mathbf{L}^{(2)}, \theta) \\ &= \prod_{k=1}^2 f(\mathbf{y}^{(k)}, \mathbf{X}^{(k)} | \mathcal{D}^{(k)}, \mathbf{D}, \mathbf{L}^{(k)}, \theta) \\ &= \prod_{j=1}^q f_{\mathcal{N}_{n_1}}(\mathbf{X}_j^{(1)} | \hat{\boldsymbol{\mu}}^{(1)}, \sigma_j^2 \mathbf{I}_{n_1}) f_{\mathcal{N}_{n_2}}(\mathbf{X}_j^{(2)} | \hat{\boldsymbol{\mu}}^{(2)}, \sigma_j^2 \mathbf{I}_{n_2}) \times \prod_{i=1}^{n_1} \mathbb{1}(\theta_{y_i-1} < x_{i,1}^{(1)} \leq \theta_{y_i}) \prod_{i=1}^{n_2} \mathbb{1}(\theta_{y_i-1} < x_{i,1}^{(2)} \leq \theta_{y_i}), \end{aligned} \quad (11)$$

where $\hat{\boldsymbol{\mu}}^{(k)} := -\mathbf{X}_{\text{pa}(j)}^{(k)} \mathbf{L}_{\prec j \succ}^{(k)}$ and we assumed the cut-off parameter θ is the same for both groups.

3 Bayesian Inference

This section concerns priors for $(\mathcal{D}^{(1)}, \mathcal{D}^{(2)}, \mathbf{D}, \mathbf{L}^{(1)}, \mathbf{L}^{(2)}, \theta)$ and we review different models in the literature. We try to pick the conjugate priors to make the equations simpler and the computations faster. In section 4, we will compute the posteriors for each of the parameters.

3.1 Prior on DAG $\mathcal{D}^{(k)}$

Random graph famously studied by Erdős and Rényi [Erdős, Rényi, et al. \(1960\)](#). For generating random graphs on DAGs, we refer to [Karrer and Newman \(2009\)](#). Let $\mathbf{A}^{\mathcal{D}}$ be the 0–1 adjacency matrix of the skeleton of the parent ordering DAG \mathcal{D} whose (i, j) th element is denoted by $\mathbf{A}_{ij}^{\mathcal{D}}$. Clearly, $\mathbf{A}_{ij}^{\mathcal{D}} = 0$ for $i \leq j$ because of the parent ordering and no self-loops.

Assuming the probability of edge inclusion is ξ , we assign a Bernoulli prior independently to each element $\mathbf{A}_{ij}^{\mathcal{D}}$, that is

$$f(\mathbf{A}^{\mathcal{D}}) = \xi^{|\mathbf{A}^{\mathcal{D}}|} (1 - \xi)^{\frac{q(q-1)}{2} - |\mathbf{A}^{\mathcal{D}}|}, \quad (12)$$

where $|\mathbf{A}^{\mathcal{D}}|$ denotes the number of edges in the skeleton. [Cao, Khare, and Ghosh \(2019\)](#) also used independent identically distributed Bernoulli random variables as the prior on the probability of edges which corresponds to an Erdős–Rényi type of distribution.

For the prior on DAG's $\mathcal{D}^{(k)}$, we independently set

$$f(\mathcal{D}^{(k)}) \propto f(\mathbf{A}^{\mathcal{D}^{(k)}}), \quad (13)$$

where $k \in \{1, 2\}$.

3.2 Prior on the Modified Cholesky Decomposition

Since $\mathbf{L}_{ij} = 0$ either if there is no edge from i to j or $i > j$, so a Gaussian DAG model restricts Σ (and Ω) to a lower-dimensional space by imposing sparsity constraints encoded in \mathcal{D} on \mathbf{L} . This constraint is important for both frequentist and Bayesian methods.

On the frequentist side, a variety of penalized likelihood methods for sparse estimation of \mathbf{L} exist in the literature; see the references in [Cao et al. \(2019\)](#). Some of those methods, such as those in [Shojaie and Michailidis \(2010\)](#); [Yu and Bien \(2017\)](#), constrain the sparsity pattern in \mathbf{L} to be banded. We assume no constraints on the sparsity pattern in this paper. [Gaskins and Daniels \(2013\)](#) used a nonparametric prior for covariance estimation.

On the Bayesian side, the first class of priors on the restricted space of covariance matrices corresponding to a Gaussian DAG model was initially developed in [Geiger and Heckerman \(2002\)](#); [Smith and Kohn \(2002\)](#). [Li and Zhang \(2019\)](#) reparameterized the likelihood of a matrix of Gaussian graphical model and obtained the full conditional distribution of the parameters in Cholesky factor. Using the asymptotic distribution of all parameters in the Cholesky factor, they obtained a shrinkage Bayesian estimator for large precision matrix. [Cao et al. \(2019\)](#) considered a hierarchical Gaussian DAG model with DAG-Wishart priors on the covariance matrix and independent Bernoulli priors for each edge in the DAG. A standard choice of conjugate prior is the Wishart distribution, i.e., $\Omega \sim W_q(a, \mathbf{U})$ having expectation $a\mathbf{U}^{-1}$, where $a > q - 1$. The priors in [Geiger and Heckerman \(2002\)](#) can be considered as analogs of the G-Wishart distribution for concentration graph models. [Ben-David, Li, Massam, and Rajaratnam \(2015\)](#) introduced a class of DAG-Wishart distributions with multiple shape parameters. Their class of distributions is defined for arbitrary DAG models and offers a flexible framework for Bayesian inference in Gaussian DAG models, and generalizes previous Wishart-based priors for DAG models.

For the cases when \mathcal{D} is complete, ([Ben-David et al., 2015](#), Supplemental Section B) derived the Hyper Morkov properties of the DAG-Wishart as

$$\sigma_j^2 \sim \text{I-Ga} \left(\frac{a_j}{2} - \frac{|\text{pa}(j)|}{2} - 1, \frac{1}{2} \mathbf{U}_{\prec j \succ} \right), \quad (14)$$

and

$$\mathbf{L}_{\preceq j \succ} | \sigma_j^2 \sim \mathcal{N}_{|\text{pa}(j)|} \left(\mathbf{0}, \sigma_j^2 \mathbf{U}_{\preceq j \succ}^{-1} \right), \quad (15)$$

for the Cholesky parameters, where $a_j = a + q - 2j + 3$ and $\text{I-Ga}(\alpha, \beta)$ is an Inverse-Gamma distribution with shape $\alpha > 0$ and rate $\beta > 0$ having expectation $\beta/(\alpha - 1)$. When \mathcal{D} is not complete, by setting $\mathbf{U} = g\mathbf{I}_q$ in equations (14) and (15), ([Castelletti & Consolmi, 2021](#), Supplementary) showed that

$$\sigma_j^2 \sim \text{I-Ga} \left(\frac{a_j}{2}, \frac{g}{2} \right), \quad (16)$$

$$\mathbf{L}_{\preceq j \succ} | \sigma_j^2 \sim \mathcal{N}_{|\text{pa}(j)|} \left(\mathbf{0}, \frac{1}{g} \sigma_j^2 \mathbf{I}_{|\text{pa}(j)|} \right), \quad (17)$$

where $a_j = a + |\text{pa}(j)| - q + 1$ and \mathbf{I}_q is the identity matrix and $g > 0$ is a hyperparameter.

For the case where there are 2 sparse DAGs, we need to properly define the priors for \mathbf{D} , $\mathbf{L}^{(1)}$ and $\mathbf{L}^{(2)}$. Lets define the prior for σ_j^2 as

$$\sigma_j^2 \sim \text{I-Ga} \left(\frac{a_j^{(1)} + a_j^{(2)}}{2}, \frac{g_1 + g_2}{2} \right), \quad (18)$$

where $a_j^{(k)} = a + |\text{pa}^{(k)}(j)| - q + 1$.

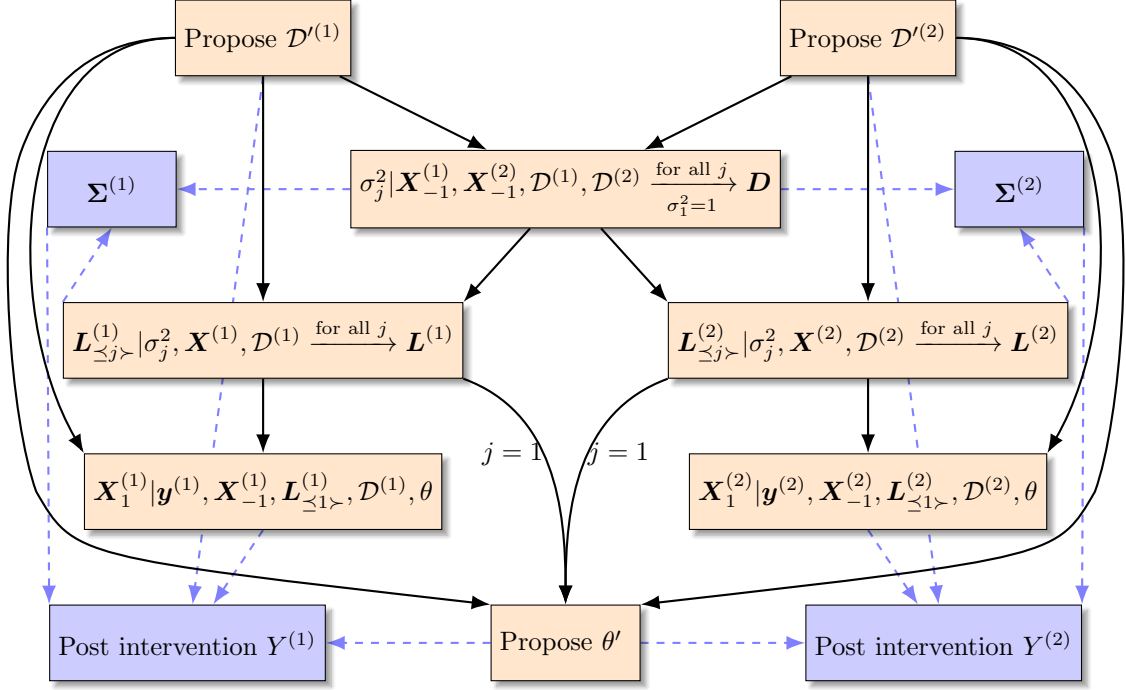


Figure 1: Proposed MCMC scheme for doubly Gaussian DAG-probit models. In the proposed method, \mathbf{D} and θ will be estimated jointly using all the observed data, $\{\mathbf{y}^{(1)}, \mathbf{y}^{(2)}, \mathbf{X}_{-1}^{(1)}, \mathbf{X}_{-1}^{(2)}\}$, while $\mathcal{D}^{(k)}$, $\mathbf{L}^{(k)}$ and $\mathbf{X}_1^{(k)}$ will be estimated separately for each group $k \in \{1, 2\}$. The blue nodes and blue dashed edges are related to the causal effect estimation.

The prior distribution for $\mathbf{L}^{(k)}$, as discussed in Section 2.3, depends on the skeleton of $\mathcal{D}^{(k)}$ too. Therefore, the prior for $\mathbf{L}^{(k)}$ becomes

$$\mathbf{L}_{\leq j}^{(k)} | \sigma_j^2 \sim \mathcal{N}_{|\text{pa}^{(k)}(j)|} \left(\mathbf{0}, \frac{1}{g_k} \sigma_j^2 \mathbf{I}_{|\text{pa}^{(k)}(j)|} \right), \quad (19)$$

where $\text{pa}^{(k)}(j)$ is the parent nodes for node j in DAG $\mathcal{D}^{(k)}$.

In this paper, we use equations (18) and (19) as the priors. We also set $a = q$ and $g_k = 1/n_k$ for our simulations in section 6.

3.3 Prior Distribution on θ

We assign a flat improper prior to the threshold $\theta \in \mathbb{R}$, i.e., $f(\theta) \propto 1$. This choice of prior will make the posterior of θ proper, as well. For the proof check (Castelletti & Consonni, 2021, Proposition 4.1).

4 MCMC for Doubly Gaussian DAG-Probit Models

We assume there are two groups of data, $\mathbf{X}^{(1)}$ and $\mathbf{X}^{(2)}$ with the corresponding DAGs $\mathcal{D}^{(1)}$ and $\mathcal{D}^{(2)}$. We first present the full likelihood distribution of the model given the input data $\{\mathbf{y}^{(1)}, \mathbf{y}^{(2)}, \mathbf{X}_{-1}^{(1)}, \mathbf{X}_{-1}^{(2)}\}$ and then find the posterior distributions for the model parameters. The goal is to estimate some of the model parameters using the joint distribution. The schematic view of the algorithm is presented in Figure 1. We will provide more info on the MCMC algorithm in Section 4.8.

4.1 Full Posterior Distribution

The full posterior distribution is used to find the posteriors or acceptance rates for $\mathcal{D}^{(k)}$, $\mathbf{L}^{(k)}$, \mathbf{D} , $\mathbf{X}_1^{(k)}$ and θ in the subsequent sections.

Given $\{\mathbf{y}^{(1)}, \mathbf{y}^{(2)}, \mathbf{X}_{-1}^{(1)}, \mathbf{X}_{-1}^{(2)}\}$ as the input, the full posterior distribution is

$$\begin{aligned} & f(\mathcal{D}^{(1)}, \mathcal{D}^{(2)}, \mathbf{L}^{(1)}, \mathbf{L}^{(2)}, \mathbf{D}, \mathbf{X}_1^{(1)}, \mathbf{X}_1^{(2)}, \theta | \mathbf{y}^{(1)}, \mathbf{y}^{(2)}, \mathbf{X}_{-1}^{(1)}, \mathbf{X}_{-1}^{(2)}) \\ & \propto \prod_{k=1}^2 f(\mathbf{y}^{(k)}, \mathbf{X}^{(k)} | \mathcal{D}^{(k)}, \mathbf{L}^{(k)}, \mathbf{D}, \theta) f(\mathbf{L}^{(k)} | \mathbf{D}, \mathcal{D}^{(k)}) f(\mathcal{D}^{(k)}) \times f(\mathbf{D} | \mathcal{D}^{(1)}, \mathcal{D}^{(2)}), \end{aligned} \quad (20)$$

where the first term is defined in (11), $f(\mathcal{D}|\mathcal{D}^{(1)}, \mathcal{D}^{(2)})$ and $f(\mathcal{L}^{(k)}|\mathcal{D}, \mathcal{D}^{(k)})$ are defined in equations (18) and (19), and $f(\mathcal{D}^{(k)})$ is defined in (13). The proof of the full posterior distribution is presented in Appendix A.

4.2 Update of $\mathcal{D}^{(k)}$

The first step at each MCMC iteration is to propose two new DAG's $\mathcal{D}'^{(1)}$ and $\mathcal{D}'^{(2)}$ from suitable proposal distributions $q(\mathcal{D}'^{(1)}|\mathcal{D}^{(1)})$ and $q(\mathcal{D}'^{(2)}|\mathcal{D}^{(2)})$. Given the current DAG $\mathcal{D}^{(k)}$, we construct $\mathcal{D}'^{(k)}$ by randomly selecting one of the following operators: **Insert**($i \rightarrow j$), **Delete**($i \rightarrow j$) or **Reverse**($i \rightarrow j$). The operator **Insert** adds the edge $i \rightarrow j$ with probability ξ if this edge does not exist in $\mathcal{D}^{(k)}$, **Delete** removes the existing edge $i \rightarrow j$ with probability $1 - \xi$, and the operator **Reverse** changes the direction of an existing edge, i.e., converting $i \rightarrow j$ to $i \leftarrow j$. **Reverse**($i \rightarrow j$) operator is equivalent to removing $i \rightarrow j$ followed by adding the reverse edge, i.e., **Reverse**($i \rightarrow j$) := **Delete**($i \rightarrow j$) + **Insert**($j \rightarrow i$).

All of these operators must not violate the DAG assumptions, especially they should not create any loop, so we check if the proposed DAG is valid or not at each MCMC iteration. If the proposed DAG has loop, we simply reject it and continue proposing new DAGs until we end up with a valid one. This process ensures that the proposed DAG is valid.

The next step is to accept or reject the proposed valid DAG $\mathcal{D}'^{(k)}$. We use the algorithm proposed by Wang and Li (2012) for Bayesian model determination in Gaussian graphical models under G-Wishart prior distributions. This algorithm is based on PAS (Partial Analytic Structure) algorithm proposed by Godsill (2001), which is based on the reversible jump proposal schemes and takes into account the partial analytic structure of the DAG model.

It is important to mention that **Insert**($i \rightarrow j$) and **Delete**($i \rightarrow j$) operators just make changes in the $\text{pa}(j)$, so the Cholesky parameters under the new and old DAGs differ only with respect to their j -th component, but for the **Reverse**($i \rightarrow j$) operator, both $\text{pa}(i)$ and $\text{pa}(j)$ will change. As a result, the acceptance probabilities for these two cases are different and we present them separately.

4.2.1 Acceptance Probability for Insert and Delete Operators

Under **Insert**($i \rightarrow j$) and **Delete**($i \rightarrow j$) operators, the acceptance probability for $\mathcal{D}'^{(k)}$ for $j \in \{2, \dots, q\}$ is given by

$$\alpha_{\mathcal{D}'^{(k)}} = \min \left\{ 1, \frac{m(\mathbf{X}_j^{(k)}|\mathbf{X}_{\text{pa}_{\mathcal{D}'^{(k)}}(j)}^{(k)}, \mathcal{D}'^{(k)})}{m(\mathbf{X}_j^{(k)}|\mathbf{X}_{\text{pa}_{\mathcal{D}^{(k)}}(j)}^{(k)}, \mathcal{D}^{(k)})} \cdot \frac{f(\mathcal{D}'^{(k)})}{f(\mathcal{D}^{(k)})} \cdot \frac{q(\mathcal{D}^{(k)}|\mathcal{D}'^{(k)})}{q(\mathcal{D}'^{(k)}|\mathcal{D}^{(k)})} \right\}, \quad (21)$$

where for $\mathcal{D} \in \{\mathcal{D}^{(1)}, \mathcal{D}^{(2)}, \mathcal{D}'^{(1)}, \mathcal{D}'^{(2)}\}$,

$$\begin{aligned} & m(\mathbf{X}_j^{(k)}|\mathbf{X}_{\text{pa}_{\mathcal{D}}(j)}^{(k)}, \mathcal{D}) \\ &= (2\pi)^{-\frac{n_k}{2}} \frac{|\mathbf{T}_j^{(k)}|^{1/2}}{|\hat{\mathbf{T}}_j^{(k)}|^{1/2}} \cdot \frac{\Gamma(a_j^{\mathcal{D}}/2 + n_k/2)}{\Gamma(a_j^{\mathcal{D}}/2)} \left[\frac{1}{2} g_k \right]^{a_j^{\mathcal{D}}/2} \left[\frac{1}{2} \left(g_k + \mathbf{X}_j'^{(k)} \mathbf{X}_j^{(k)} - \hat{\mathbf{L}}_j^{(k)} \hat{\mathbf{T}}_j^{(k)} \hat{\mathbf{L}}_j^{(k)} \right) \right]^{-(a_j^{\mathcal{D}} + n_k)/2}, \end{aligned} \quad (22)$$

and

$$\begin{aligned} \mathbf{T}_j^{(k)} &= g_k \mathbf{I}_{|\text{pa}_{\mathcal{D}}(j)|}, \\ \hat{\mathbf{T}}_j^{(k)} &= \mathbf{T}_j^{(k)} + \mathbf{X}_{\text{pa}_{\mathcal{D}}(j)}'^{(k)} \mathbf{X}_{\text{pa}_{\mathcal{D}}(j)}^{(k)}, \\ \hat{\mathbf{L}}_j^{(k)} &= \left(\hat{\mathbf{T}}_j^{(k)} \right)^{-1} \mathbf{X}_{\text{pa}_{\mathcal{D}}(j)}'^{(k)} \mathbf{X}_j^{(k)}, \end{aligned} \quad (23)$$

with $a_j^{\mathcal{D}} = a + |\text{pa}_{\mathcal{D}}(j)| - q + 1$.

For $j = 1$, because we fixed $\sigma_1^2 = 1$, we have

$$m(\mathbf{X}_1^{(k)}|\mathbf{X}_{\text{pa}_{\mathcal{D}}(1)}^{(k)}, \mathcal{D}) = (2\pi)^{-\frac{n_k}{2}} \frac{|\mathbf{T}_1^{(k)}|^{1/2}}{|\hat{\mathbf{T}}_1^{(k)}|^{1/2}} \cdot \exp \left\{ -\frac{1}{2} \left(\mathbf{X}_1'^{(k)} \mathbf{X}_1^{(k)} - \hat{\mathbf{L}}_1^{(k)} \hat{\mathbf{T}}_1^{(k)} \hat{\mathbf{L}}_1^{(k)} \right) \right\}. \quad (24)$$

The proof for both $j = 1$ and $j > 1$ cases is given in Appendix B.1.

4.2.2 Acceptance Probability for Reverse Operator

For **Delete**($i \rightarrow j$) operator, both the parents for the nodes i and j will change. So, the acceptance probability for $\mathcal{D}'^{(k)}$ becomes

$$\alpha_{\mathcal{D}'^{(k)}} = \min \left\{ 1, \frac{m(\mathbf{X}_i^{(k)}|\mathbf{X}_{\text{pa}_{\mathcal{D}'^{(k)}}(i)}^{(k)}, \mathcal{D}'^{(k)}) m(\mathbf{X}_j^{(k)}|\mathbf{X}_{\text{pa}_{\mathcal{D}'^{(k)}}(j)}^{(k)}, \mathcal{D}'^{(k)})}{m(\mathbf{X}_i^{(k)}|\mathbf{X}_{\text{pa}_{\mathcal{D}^{(k)}}(i)}^{(k)}, \mathcal{D}^{(k)}) m(\mathbf{X}_j^{(k)}|\mathbf{X}_{\text{pa}_{\mathcal{D}^{(k)}}(j)}^{(k)}, \mathcal{D}^{(k)})} \cdot \frac{f(\mathcal{D}'^{(k)})}{f(\mathcal{D}^{(k)})} \cdot \frac{q(\mathcal{D}^{(k)}|\mathcal{D}'^{(k)})}{q(\mathcal{D}'^{(k)}|\mathcal{D}^{(k)})} \right\}, \quad (25)$$

where $m(\cdot)$ is defined in (22) and (24) for $j > 1$ and $j = 1$, respectively. For the proof, check Appendix B.2.

Finally, using equation (13), the term $f(\mathcal{D}'^{(k)})/f(\mathcal{D}^{(k)})$ defined in equations (21) and (25) is equal to $\xi/(1-\xi)$, $(1-\xi)/\xi$ and 1, respectively for **Insert**, **Delete** and **Reverse** operators with ξ as the probability of edge inclusion. Let's denote by $\mathbb{O}^{\mathcal{D}}$ the set of *valid* operators in \mathcal{D} . The probability of transition from \mathcal{D} to \mathcal{D}' is then equal to $q(\mathcal{D}'|\mathcal{D}) = 1/|\mathbb{O}^{\mathcal{D}}|$. For transitioning from DAG \mathcal{D} with q nodes and $|E|$ edges to \mathcal{D}' , the number of **Delete**, **Reverse** and **Insert** operators are $|E|$, $|E|$ and $q(q-1)/2 - |E|$ respectively, but some of the **Reverse** and **Insert** operators might not be valid, because they can create loops. Since \mathcal{D} and \mathcal{D}' only differ at most in one edge, so $q(\mathcal{D}^{(k)}|\mathcal{D}'^{(k)})/q(\mathcal{D}'^{(k)}|\mathcal{D}^{(k)}) \approx 1$ for sparse \mathcal{D} .

4.3 Update of $L^{(k)}$

For $j \in \{2, \dots, q\}$, we have

$$\mathbf{L}_{\leq j}^{(k)} | \sigma_j^2, \mathbf{X}^{(k)}, \mathcal{D}^{(k)} \sim \mathcal{N}_{|\text{pa}^{(k)}(j)|} \left(-\hat{\mathbf{L}}_j^{(k)}, \sigma_j^2 (\bar{\mathbf{T}}_j^{(k)})^{-1} \right). \quad (26)$$

Moreover, for node 1 we have

$$\mathbf{L}_{\leq 1}^{(k)} | \mathbf{X}^{(k)}, \mathcal{D}^{(k)} \sim \mathcal{N}_{|\text{pa}^{(k)}(1)|} \left(-\hat{\mathbf{L}}_1^{(k)}, (\bar{\mathbf{T}}_1^{(k)})^{-1} \right). \quad (27)$$

The proofs for $j = 1$ and $j > 1$ are given in Appendix C.1.

4.4 Update of D

We update D using information from both groups. For $j \in \{2, \dots, q\}$,

$$\sigma_j^2 | \mathbf{X}^{(1)}, \mathbf{X}^{(2)}, \mathcal{D}^{(1)}, \mathcal{D}^{(2)} \sim \text{I-Ga} \left(\frac{\alpha^{(1)}}{2} + \frac{\alpha^{(2)}}{2}, \frac{\beta^{(1)}}{2} + \frac{\beta^{(2)}}{2} \right), \quad (28)$$

where $\alpha^{(k)} = a_j^{(k)} + n_k$ and $\beta^{(k)} = g_k + \mathbf{X}_j^{(k)'} \mathbf{X}_j^{(k)} - \hat{\mathbf{L}}_j^{(k)} \bar{\mathbf{T}}_j^{(k)} \hat{\mathbf{L}}_j^{(k)}$ for $k \in \{1, 2\}$. For node 1, we set $\sigma_1^2 = 1$. The proof is given in Appendix C.2.

4.5 Update of $\mathbf{X}_1^{(k)}$

Since $\mathbf{X}_1^{(k)}$ is the latent variable, we need to get a sample from its posterior distribution, which follows

$$\mathbf{X}_1^{(k)} | \mathbf{y}^{(k)}, \mathbf{X}_{-1}^{(k)}, \mathbf{L}_{\leq 1}^{(k)}, \mathcal{D}^{(k)}, \theta \sim \mathcal{N}_{n_k} \left(-\mathbf{X}_{\text{pa}(1)}^{(k)} \mathbf{L}_{\leq 1}^{(k)}, \mathbf{I}_{n_k} \right), \quad (29)$$

truncated at θ where n_k is the sample size of the k -th group. Clearly this equation is not a function of D because $\sigma_1^2 = 1$. For the proof, check [Castelletti and Consonni \(2021\)](#).

4.6 Update of θ

To update the cut-off θ , we propose a new θ' using Metropolis Hastings method with the proposal distribution $\theta'|\theta \sim \mathcal{N}(\theta, \sigma_0^2)$, so the transition kernel becomes $q(\theta'|\theta) = f_{\mathcal{N}}(\theta'|\theta, \sigma_0^2)$ where σ_0^2 is a hyperparameter. We accept θ' with probability

$$\alpha_{\theta} = \min\{1, r_{\theta}\}, \quad (30)$$

where

$$r_{\theta} = \frac{\prod_{i=1}^{n_1} \Psi(y_i^{(1)}, \theta' | -\mathbf{x}_{\text{pa}(1)}^{(1)} \mathbf{L}_{\leq 1}^{(1)}, 1) \prod_{i=1}^{n_2} \Psi(y_i^{(2)}, \theta' | -\mathbf{x}_{\text{pa}(1)}^{(2)} \mathbf{L}_{\leq 1}^{(2)}, 1) f_{\mathcal{N}}(\theta|\theta', \sigma_0^2)}{\prod_{i=1}^{n_1} \Psi(y_i^{(1)}, \theta | -\mathbf{x}_{\text{pa}(1)}^{(1)} \mathbf{L}_{\leq 1}^{(1)}, 1) \prod_{i=1}^{n_2} \Psi(y_i^{(2)}, \theta | -\mathbf{x}_{\text{pa}(1)}^{(2)} \mathbf{L}_{\leq 1}^{(2)}, 1) f_{\mathcal{N}}(\theta'|\theta, \sigma_0^2)}, \quad (31)$$

and $\Psi(y, \eta|\mu, \sigma^2) = |y - \Phi(\eta|\mu, \sigma^2)|$. In fact, $\Psi(y, \eta|\mu, \sigma^2)$ is either the CDF or the survival function of a $\mathcal{N}(\mu, \sigma^2)$ distribution for $y = 0$ and $y = 1$, respectively. The proof is presented in Appendix D.

4.7 Initial DAGs for $\mathcal{D}^{(k)}$

The number of different combinations to initialize $\mathcal{D}^{(k)}$ is equal to $2^{q(q-1)/2}$. Choosing appropriate initial values for $\mathcal{D}^{(1)}[0]$ and $\mathcal{D}^{(2)}[0]$ can exponentially speed up the convergence of MCMC algorithm. To speed up the computations, we propose the following method.

We showed in Equation (5) that Ω can be uniquely decomposed into

$$\Omega = \mathbf{L} \mathbf{D}^{-1} \mathbf{L}', \quad (32)$$

where the non-zero elements of L correspond to the edges in \mathcal{D} . Unfortunately, we cannot estimate L given \mathbf{X}_{-1} because \mathbf{X}_1 is a latent variable. But, Ω_{-1}^{-1} is the covariance matrix of \mathbf{X}_{-1} , and can be decomposed into

$$\Omega_{-1}^{-1} = \mathbf{L}_{-1} \mathbf{D}_{-1}^{-1} \mathbf{L}'_{-1} \quad (33)$$

using modified Cholesky decomposition method. So, we can initialize \mathcal{D} by binarizing the non-zero elements of the estimated \mathbf{L}_{-1} matrix. The following proposition shows the relation between \mathbf{L}_{-1} and \mathbf{L} , and states that it is the corresponding submatrix of \mathbf{L} .

Proposition 1 *Let's reorder the matrix \mathbf{X} as $\mathbf{X}^* = (\mathbf{X}_{-1}, \mathbf{X}_1)$ and let $\text{cov}(\mathbf{X}^*) = \mathbf{\Omega}^{-1}$ with $\mathbf{\Omega} = \mathbf{L}\mathbf{D}^{-1}\mathbf{L}'$. If we partition \mathbf{L} into*

$$\mathbf{L} = \begin{pmatrix} \mathbf{L}_{11} & \mathbf{0} \\ \mathbf{L}_{2,1} & \mathbf{L}_{22} \end{pmatrix} \quad (34)$$

then $\mathbf{L}_{-1} = \mathbf{L}_{11}$, where \mathbf{L}_{-1} is the lower-triangular matrix from the decomposition of $\mathbf{\Omega}_{-1}$.

For the proof check Appendix E. So we use the non-zero elements of

$$\hat{\mathbf{L}} := \begin{pmatrix} \mathbf{0} & \mathbf{0} \\ \mathbf{0} & \mathbf{L}_{-1} \end{pmatrix} \quad (35)$$

for initializing $\mathcal{D} \in \{\mathcal{D}^{(1)}, \mathcal{D}^{(2)}\}$.

4.8 MCMC Algorithm

The MCMC Scheme for this method is depicted in Fig 1. Using the samples from the posteriors, we estimate the model parameters at the end of the algorithm. The proposed MCMC is presented in Algorithm 1.

Algorithm 1: MCMC algorithm for the proposed method on doubly Gaussian–probit DAG models.

Input: $\{\mathbf{y}^{(1)}, \mathbf{y}^{(2)}, \mathbf{X}_{-1}^{(1)}, \mathbf{X}_{-1}^{(2)}\}$
Output: T samples from posterior distribution (20)

- 1 Initialize $\mathcal{D}^{(1)}[0]$ and $\mathcal{D}^{(2)}[0]$ with (35), set the cut-off $\theta[0] = 0$, and the latent variables $\mathbf{x}_1^{(1)}[0], \mathbf{x}_1^{(2)}[0] \sim \mathcal{N}(0, 1)$ truncated at $\theta[0]$;
- 2 **for** $t = 1, \dots, T$ **do**
- 3 **for** $k \in \{1, 2\}$ **do**
- 4 Given $\mathcal{D}^{(k)}[t-1]$, randomly select a valid operator;
- 5 Sample $\mathcal{D}'^{(k)}[t]$ from $q(\mathcal{D}'^{(k)}|\mathcal{D}^{(k)})$ with acceptance probability $\alpha_{\mathcal{D}'^{(k)}}$ defined in (21) for the **Insert** and **Delete** operators or with acceptance probability defined in (25) if the selected operator is **Reverse**;
- 6 **end**
- 7 Sample $\mathbf{D}[t]$ from $I\text{-Ga}(\cdot, \cdot)$ defined in (28) using information from both groups;
- 8 **for** $k \in \{1, 2\}$ **do**
- 9 Sample $\mathbf{L}^{(k)}[t]$ from (26);
- 10 Sample $\mathbf{X}_1^{(k)}[t]$ from (29);
- 11 **end**
- 12 Update $\theta[t]$ with acceptance probability $\alpha_\theta = \min\{1, r_\theta\}$ defined in (30);
- 13 **for** $k \in \{1, 2\}$ **do**
- 14 Compute the post intervention $\mathbb{E}\left(Y^{(k)} \mid \text{do}(X_s^{(k)} = \tilde{x}^{(k)}), \mathbf{\Sigma}^{(k)}, \theta\right)$ from (40);
- 15 **end**
- 16 **end**
- 17 The elements of $\hat{\mathcal{D}}^{(k)}$ can be estimated by comparing $\hat{\xi}^{(k)}(i \rightarrow j)$ defined in (36) with a threshold;

For each group $k \in \{1, 2\}$, the posterior probabilities of edge inclusion can be computed via

$$\hat{\xi}^{(k)}(i \rightarrow j) = \frac{1}{T-B} \sum_{t=B}^T \mathbb{1}_{i \rightarrow j}(\mathcal{D}^{(k)}[t]), \quad (36)$$

where $\mathbb{1}_{i \rightarrow j}(\mathcal{D}^{(k)}[t])$ is 1 if there is an edge $i \rightarrow j$ in the $\mathcal{D}^{(k)}[t]$, and 0 otherwise. We can compare $\hat{\xi}^{(k)}(i \rightarrow j)$ with a threshold, say 0.5, to estimate the final $\hat{\mathcal{D}}^{(k)}$.

5 Causal Effects

Given two disjoint sets of variables, X and Y , the *causal effect* of X on Y , denoted by $f(y | \text{do}(x))$, is a function from X to the space of probability distributions on Y . The goal of $\text{do}(x)$ calculus is to generate probabilistic formulas for the effect of interventions in terms of the observed probabilities. For each realization x of X , $f(y | \text{do}(x))$ gives the probability of $Y = y$ induced by deleting all equations corresponding to variables in X and substituting $X = x$ in the remaining equations (Pearl (2009)). In fact, $\text{do}(\cdot)$ operator marks an action or an intervention in the model. In an algebraic model, we replace certain functions with a constant $X = x$, and in a graph we remove edges going into the target of intervention, but preserve edges going out of the target. The graph corresponding to the reduced set of equations is a subgraph of \mathcal{D} from which all arrows entering x have been pruned.

The effect of interventions of $\text{do}(X_s = x_s)$ for $s \in \{2, \dots, q\}$ can be expressed in a simple *truncated factorization* formula as following

$$f(x_1, \dots, x_q | \text{do}(X_s = \tilde{x})) = \begin{cases} \prod_{j=1, j \neq s}^q f(x_j | \text{pa}(x_j)) \Big|_{x_s = \tilde{x}} & \text{if } x_s = \tilde{x}, \\ 0 & \text{otherwise.} \end{cases} \quad (37)$$

This equation reflects the removal of the term $f(x_i | \text{pa}(x_i))$ from the product of (1), since $\text{pa}(x_i)$ no longer influences X_i and can be seen as a transformation between the pre- (1) and post-intervention (37) distributions.

For the latent variable X_1 , the post-intervention distribution can be calculated as

$$f(x_1 | \text{do}(X_s = \tilde{x})) = \int f(x_1 | \tilde{x}, \mathbf{x}_{\text{pa}(s)}) f(\mathbf{x}_{\text{pa}(s)}) d\mathbf{x}_{\text{pa}(s)}. \quad (38)$$

For more details on the post-intervention distribution, take a look at the Theorem 3.2.2 in Pearl (2009).

Using the conditional Gaussian distribution, Castelletti and Consonni (2021) showed that

$$f(x_1 | \text{do}(X_s = \tilde{x}), \Sigma) = f_{\mathcal{N}}(x_1 | \gamma_s \tilde{x}, \sigma_{\text{do}}^2), \quad (39)$$

where

$$\begin{aligned} \sigma_{\text{do}}^2 &= \frac{\delta_1^2}{1 - (\gamma' \mathbf{T}^{-1} \gamma) / \delta_1^2}, \\ \delta_1^2 &= \Sigma_{1 | \text{fa}(s)}, \\ (\gamma_s, \gamma') &= \Sigma_{1, \text{fa}(s)} (\Sigma_{\text{fa}(s), \text{fa}(s)})^{-1}, \\ \mathbf{T} &= (\Sigma_{\text{fa}(s), \text{fa}(s)})^{-1} + \frac{1}{\delta_1^2} \gamma \gamma'. \end{aligned}$$

Inspired by the Bartlett's decomposition, Silva and Ghahramani (2009) called the set $(\delta_1^2, \gamma_s, \gamma')$ as the Bartlett parameters of Σ . Bartlett's decomposition, defined in Brown, Le, and Zidek (1994), allows the definition of its density function by the joint density of $(\delta_1^2, \gamma_s, \gamma')$. The closed form of the distribution of the corresponding Bartlett parameters is presented in (Silva & Ghahramani, 2009, Lemma 1) which are related to the equations (14) and (15).

Since X_1 is a latent variable, the post-intervention average for the observed binary variable Y , $\mathbb{E}(Y | \text{do}(X_s = \tilde{x}), \Sigma, \theta)$ can be computed by

$$\begin{aligned} \mathbb{E}(Y | \text{do}(X_s = \tilde{x}), \Sigma, \theta) &= \mathbb{P}(Y = 1 | \text{do}(X_s = \tilde{x}), \Sigma, \theta) \\ &= \mathbb{P}(X_1 > \theta | \text{do}(X_s = \tilde{x}), \Sigma) \\ &= 1 - \Phi\left(\frac{\theta - \gamma_s \tilde{x}}{\sqrt{\sigma_{\text{do}}^2}}\right), \end{aligned} \quad (40)$$

where $\Phi(\cdot)$ is the c.d.f. of a standard normal distribution. Figure (1) shows the input parameters and steps to compute (40) for $Y^{(k)}$, where we estimate it by substituting $\Sigma^{(k)}$ and θ with their simulated values at each step of the MCMC discussed in Section 4.

6 Simulation

We ran a comprehensive simulation to assess the performance of the proposed method. We ran the simulations for sample sizes $n_1, n_2 \in \{50, 100, 200, 500, 1000\}$, number of nodes $q \in \{10, 20, 30, 40, 50\}$, and probability of edge inclusion $\xi \in \{0.1, 0.2, 0.3, 0.4\}$. The number of runs/replications for each scenario is 25. We did not run our algorithm for $(q = 40, \xi = 0.4)$, $(q = 50, \xi = 0.3)$ and $(q = 50, \xi = 0.4)$ because sample sizes larger than 1,000 are needed for bigger DAGs.

For each run, we applied Algorithm 1 with $T = 5,000$ MCMC iterations and discarded the first $B = 1,000$ burn-in iterations. We also set $g_k = 1/n_k$ and $a = q$ in the prior on the Cholesky parameters of (18), and $\sigma_0^2 = 0.5$ for the proposal density of the cut-off in (31).

Table 1: AUC computed from the average ROC curves in Figure 2 for different sample sizes and DAG sizes, q . The probability of edge inclusion is $\xi = 0.1$ for this table.

n_1	n_2	q				
		10	20	30	40	50
50	50	0.9843	0.9756	0.9628	0.9468	0.8653
50	100	0.9823	0.9751	0.9701	0.9598	0.9184
100	100	0.9906	0.9853	0.9777	0.9707	0.9554
100	200	0.9912	0.9843	0.9774	0.9704	0.9617
200	200	0.9991	0.9886	0.9826	0.9712	0.9725
500	500	0.9944	0.9951	0.9802	0.9804	0.9785
1000	500	0.9975	0.9942	0.9828	0.9817	0.9787
1000	1000	0.9956	0.9948	0.9836	0.9815	0.9824

The receiver operating characteristic (ROC) curve is a good method for showing the performance of a binary classification problem. In our case, the binary classification is to assess if an edge $i \rightarrow j$ exists. To plot ROC, we need to compute the *sensitivity* and *specificity* indexes, which can be computed from the actual and predicted conditions. To simplify the plots and have an overall evaluation metric, we concatenated the lower elements of $\mathcal{D}^{(1)}$ and $\mathcal{D}^{(2)}$ as the actual condition, and concatenated the lower elements of $\hat{\mathcal{D}}^{(1)}$ and $\hat{\mathcal{D}}^{(2)}$ estimated form (36) as the predicted condition. The results are plotted in Figure 2 for different scenarios with $\xi = 0.1$. We added ROC plots for $\xi \in \{0.2, 0.3, 0.4\}$ in Appendix F. The area under curve (AUC) is also computed and presented in Table 1 for $\xi = 0.1$. AUC gets better as the sample size increases. A bigger sample size is also needed to improve the AUC if the number of nodes gets bigger. We added AUC tables for $\xi \in \{0.2, 0.3, 0.4\}$ in Appendix.

At each step t of the MCMC iteration, we compute the partial correlations $\hat{\rho}_{ij}^{(k)}[t]; k = 1, 2$ defined in (2) using the estimated precision matrix $\hat{\Omega}^{(k)}[t]$ and compare them with the true partial correlations. We take average over all the iterations after discarding the burn-in iterations (B), i.e., for each run we compute

$$\frac{1}{T-B} \sum_{t=B}^T \frac{1}{q(q-1)/2} \sum_{i<j} \rho_{ij}^{(k)}[t] - \hat{\rho}_{ij}^{(k)}[t]. \quad (41)$$

The boxplot for equation (41) and different runs are plotted in Figure 3 for $\xi = 0.1$. In almost all the cases, the difference is less than 5% and the average is around zero, depicting the stability of the proposed method. We removed some of the boxplots for big (n_1, n_2) to save space. Similar to (41), we also depicted the same boxplot for the absolute differences, i.e.,

$$\frac{1}{T-B} \sum_{t=B}^T \frac{1}{q(q-1)/2} \sum_{i<j} \left| \rho_{ij}^{(k)}[t] - \hat{\rho}_{ij}^{(k)}[t] \right|, \quad (42)$$

in Figure 4 for $\xi = 0.1$. We added more plots for $\xi > 0.1$ in Appendix F. We can see that the average absolute difference converges to zero as the sample size increases.

In order to show the stability of the estimated post-intervention values defined in (40), the difference between the actual effect size and the estimated effect size is quantified for all the incoming edges to node 1. The actual effect size is computed using $(\Sigma^{(k)}, \theta)$ and the predicted effect size is computed from the $(\hat{\Sigma}^{(k)}, \hat{\theta})$, i.e.,

$$\mathbb{E}(Y | \text{do}(X_s = \tilde{x}), \Sigma, \theta) - \mathbb{E}(Y | \text{do}(X_s = \tilde{x}), \hat{\Sigma}, \hat{\theta}), \quad (43)$$

where the results are plotted in Figure 5.

The estimated cut-off parameter θ is also unbiased and its variance shrinks quickly as sample size increases. The estimated θ together with the 95% confidence intervals for different scenarios are plotted in Figure 6.

We ran all of the scenarios on a AMD RYZEN 7 with 8-Core 3.6 GHz CPU. The average running time for each scenario is plotted in Figure 7. In each panel, the computational time increases as the number of nodes, q , increases. Probability of edge, ξ , also has a direct effect on the average time. It seems both q and ξ parameters increase the time in a non-linear fashion, because both of them increases the size of $\text{pa}(\cdot)$ and make it slower to compute equations in (23). For all the panels, the sample sizes (n_1, n_2) has a little effect on the computational time, which makes it feasible to run the proposed algorithm on large sample sizes.

7 Real Data

In this section we apply our method on two well-known real datasets. The first dataset, introduced by Desmedt et al. (2007b), is the breast cancer gene data, studied in many causality papers and clinical cancer researches such as Rueda et al. (2019), Momenzadeh, Sehhati, and Rabbani (2020), Bertucci, Finetti, Goncalves, and Birnbaum

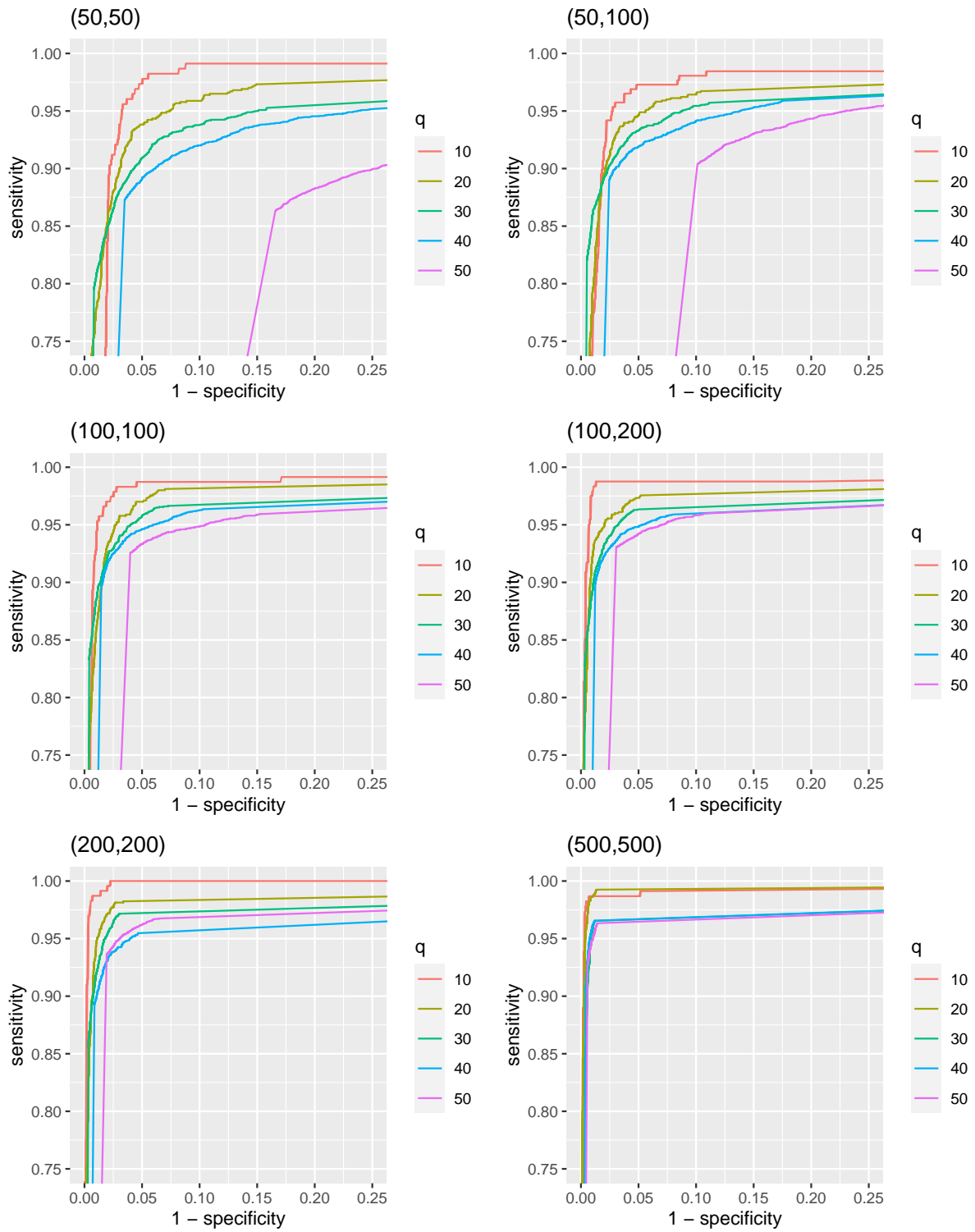


Figure 2: ROC for $\xi = 0.1$. Each plot is for different sample sizes (n_1, n_2) . Different colors represent different DAG sizes, q .

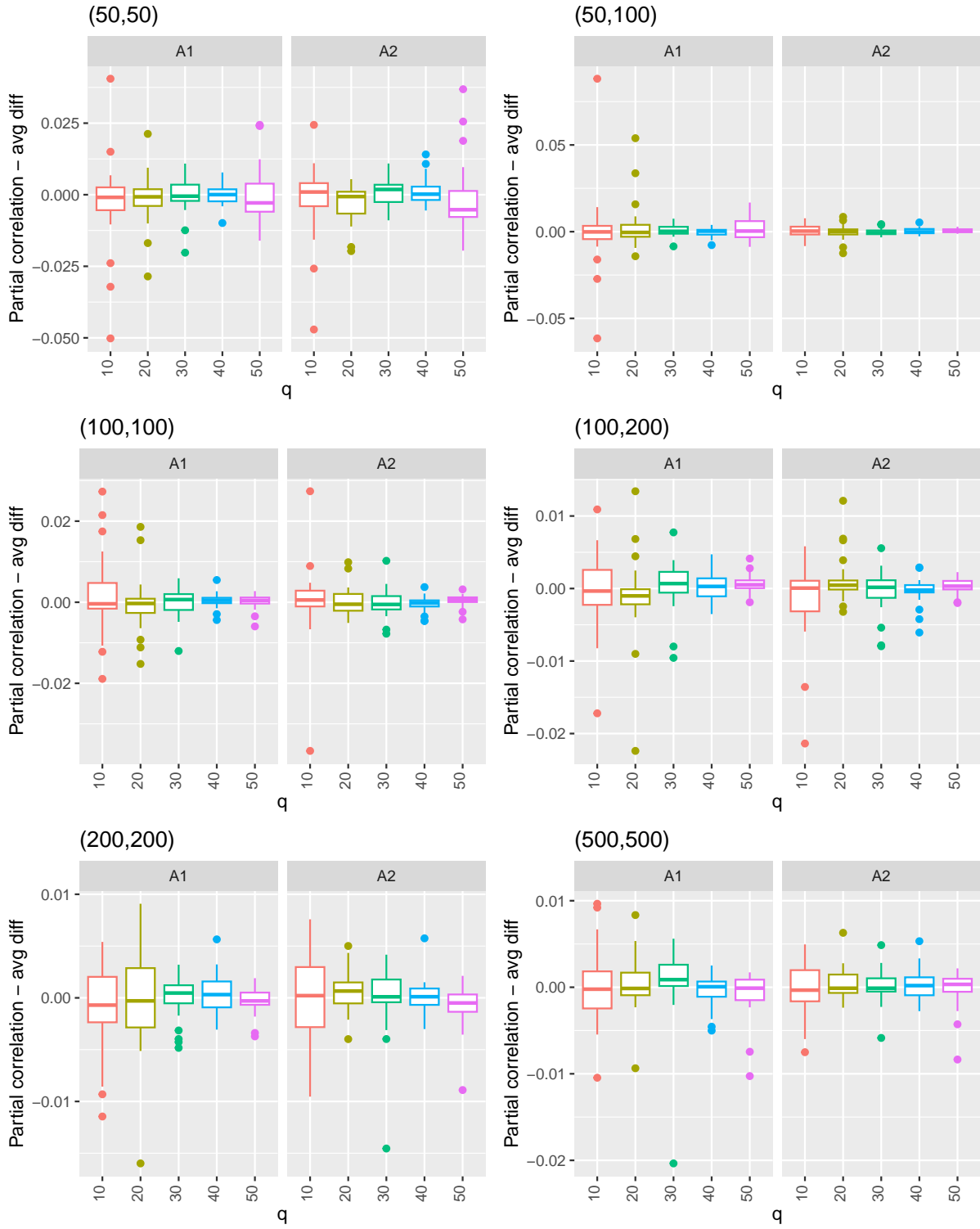


Figure 3: Boxplot for the difference between the estimated and true partial correlations defined in (41) for $T = 5000$ iterations and $\xi = 0.1$. As the sample size increases, the average difference decreases.

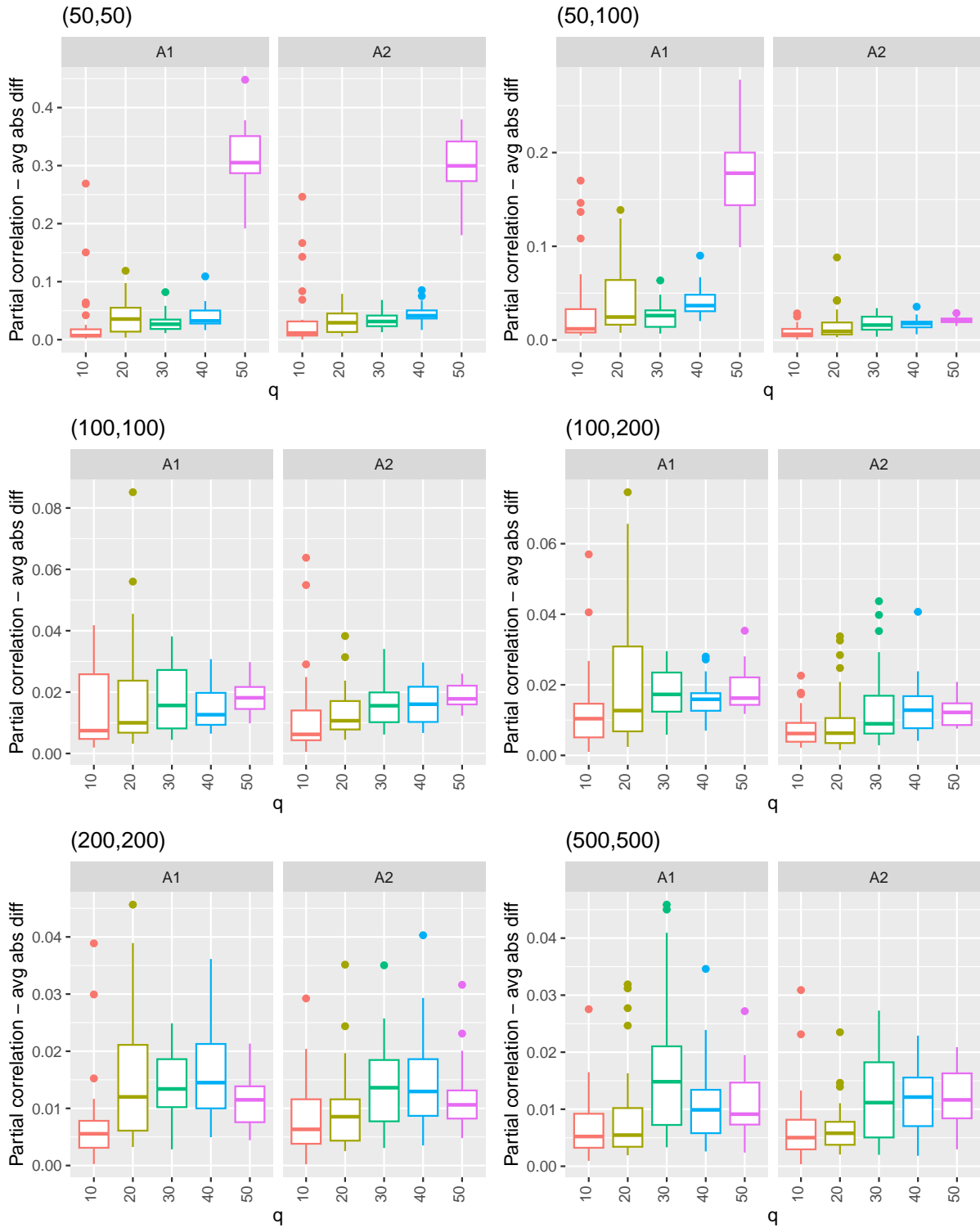


Figure 4: Boxplot for the absolute difference between the estimated and true partial correlations defined in (42) for $T = 5000$ iterations and $\xi = 0.1$. As the sample size increases, the absolute difference decreases.

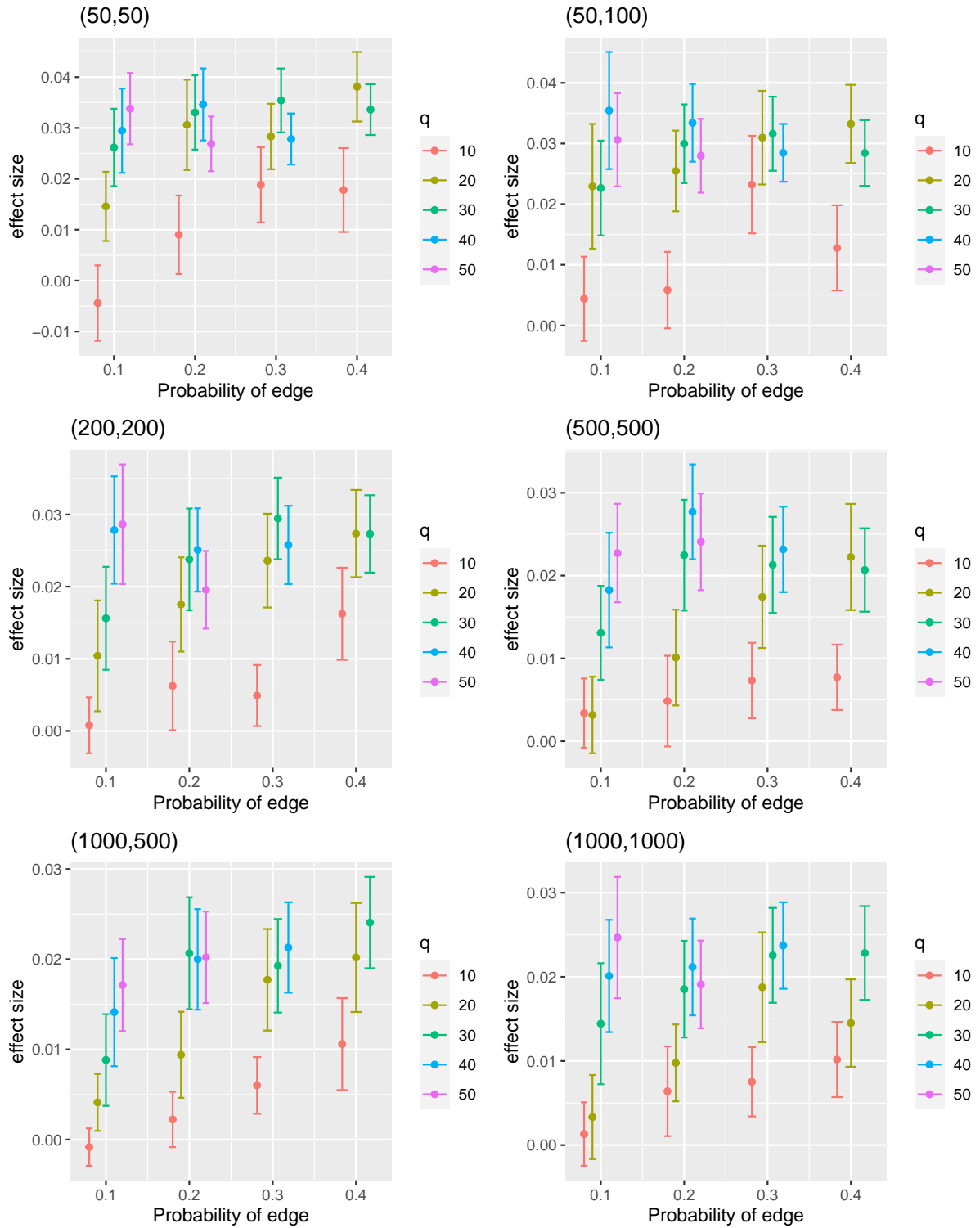


Figure 5: Errorbar for the difference between the estimated and true effect sizes defined in (40) for $T = 5000$ iterations. The error range are almost the same for different sample sizes but it decreases for smaller DAGs.

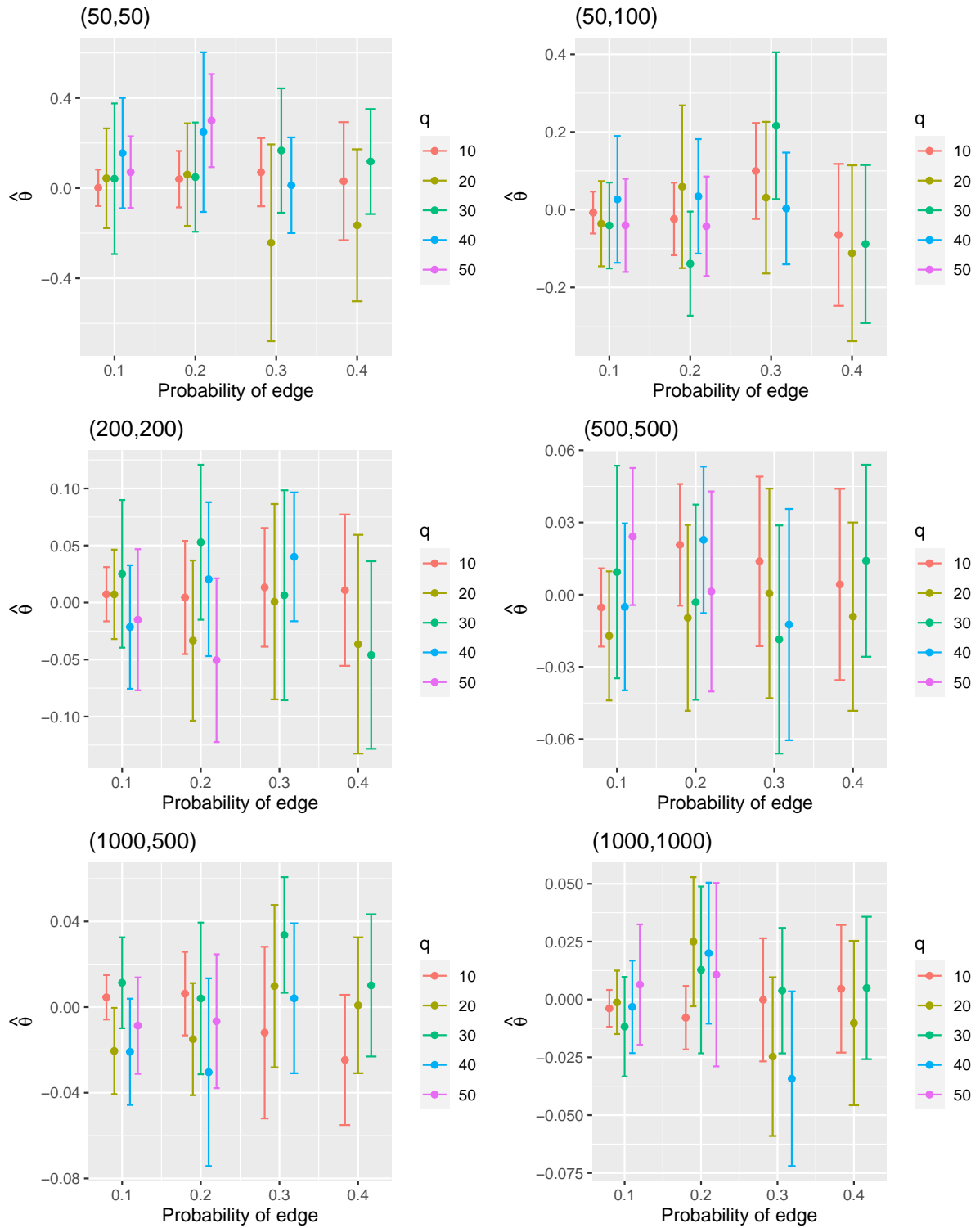


Figure 6: Estimated cut-off parameter together with 95% confidence interval for different scenarios with for $T = 5,000$ iterations.

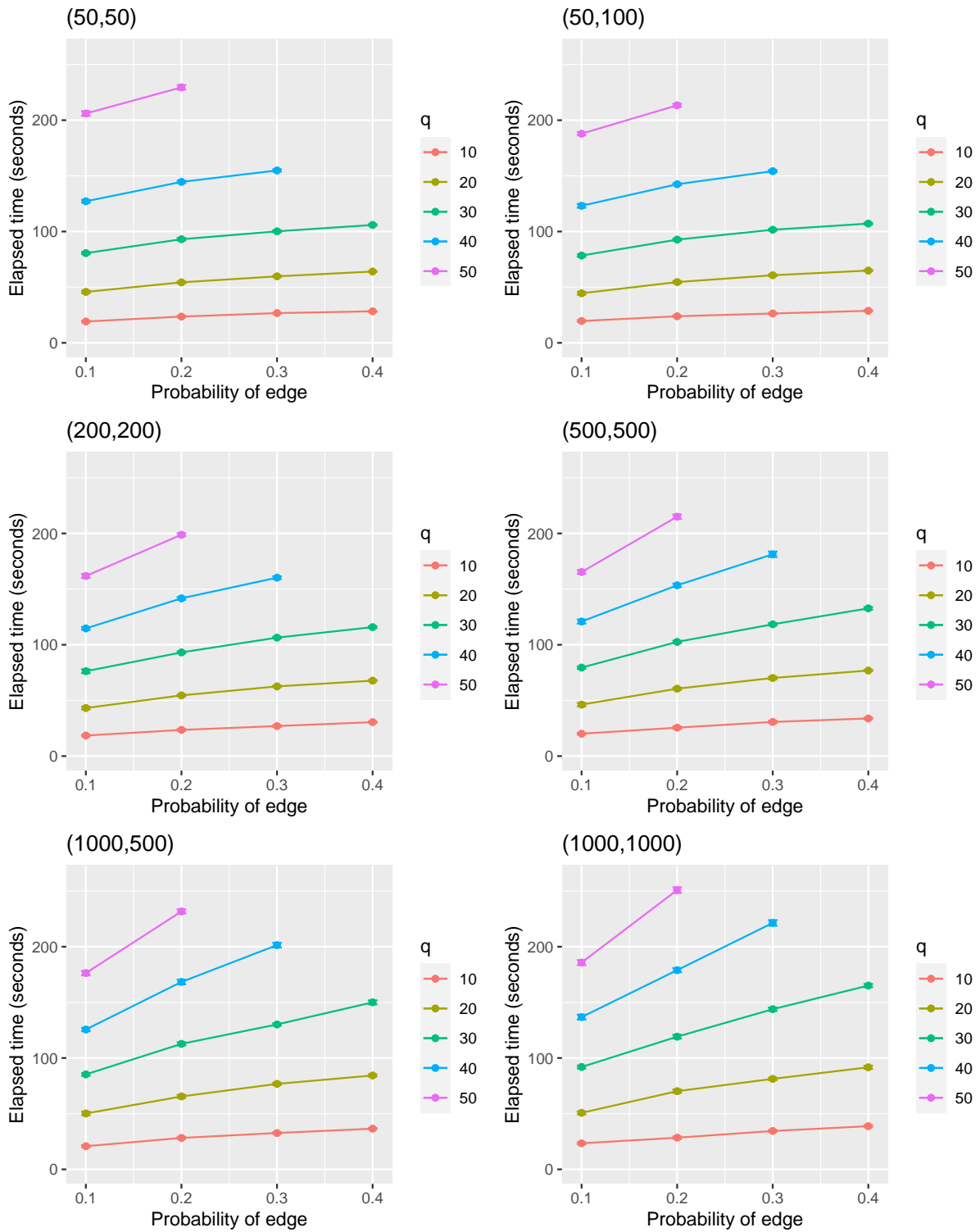


Figure 7: Average computation time for 5,000 replications with 1,000 burn-in. We removed $(n_1, n_2) \in \{(100, 100), (100, 200)\}$ to save space.

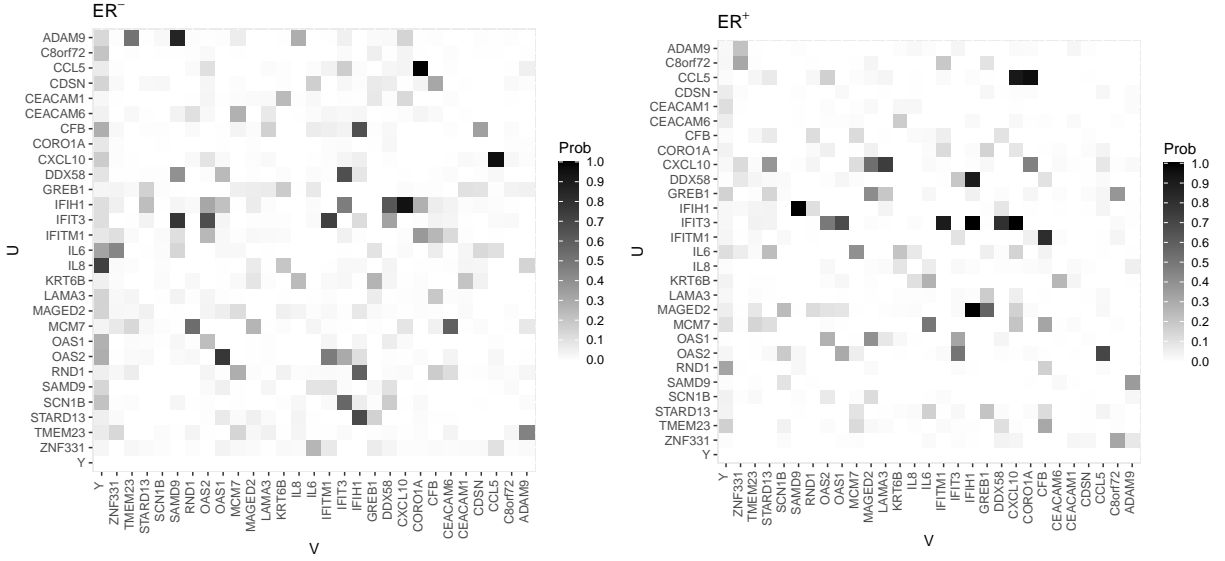


Figure 8: Heat map with estimated marginal posterior probabilities of edge inclusion for each edge $u \rightarrow v$ for $A^{(1)}$ (left) and $A^{(2)}$ (right). The left plot is for ER^- breast cancers and the right plot is for ER^+ . IL-8 is highly expressed in ER^- breast cancers [Todorović-Raković and Milovanović \(2013\)](#), a clear difference between the left and right plots with a direct effect on Y .

(2020), [Poirion, Jing, Chaudhary, Huang, and Garmire \(2021\)](#) and [Miao et al. \(2022\)](#). The network of gene expression data of a set of genes is expected to be sparse ([Cai, Li, Liu, and Xie \(2016\)](#)), which makes it suitable for the proposed method. We also validate our results with several clinical studies.

For the second dataset, we study the effect of airborne particles on the cardiovascular mortality rate (CRM) available in [Rappold \(2020\)](#). This data is also studied by [Bahadori, Tchetgen, and Heckerman \(2022\)](#). Similar data was also used to check the air quality of Los Angeles County using counterfactual evaluation [M.-j. Chen \(2021\)](#).

7.1 Breast Cancer Data

Breast cancer is the second leading cause of cancer-related mortality among women worldwide [Mansoori et al. \(2019\)](#). Finding the underlying gene’s causal graph is one of the important topics in recent cancer research. For example, [Si et al. \(2021\)](#) conducted a research on identifying causality and genetic correlation on breast and ovarian cancers. The authors expressed that identifying genetic correlations can provide useful etiological insights and help prioritise likely causal relationships and can be used to identify direct causal relations and shared genetic risks for an exposure–outcome pair. Furthermore, evaluating the gene’s causal effect on metastasis due to a hypothetical intervention on a specific gene may help understand which genes are more relevant.

Recently, a 76-gene prognostic signature able to predict distant metastases in patients with breast cancer was reported and the outcomes were independently validated with clinical risk assessment [Desmedt et al. \(2007b\)](#). Gene expression profiling of frozen samples from 198 systemically untreated patients was performed at the Bordet Institute, blinded to genomic risk. Survival analyses, done by an independent statistician, were performed with the genomic risk and adjusted for the clinical risk. The data can be downloaded from the National Center for Biotechnology Information website [Desmedt et al. \(2007a\)](#). We denote by the binary response variable Y as the occurrence of distant metastasis, i.e., $Y = 1$ if the cancer is metastatic and $Y = 0$ otherwise. The data were also studied by [Castelletti and Consolmi \(2021\)](#) with one DAG on $q = 28$ genes. We also use the same set of genes. This dataset is suitable for this study because the precision matrix for gene expression data is expected to be sparse ([Cai, Li, et al. \(2016\)](#)).

If breast cancer cells have estrogen receptors, it is called ER positive breast cancer (ER^+), otherwise it is called ER negative (ER^-). When the estrogen and progesterone hormones attach to these receptors, they induce tumor-cell growth. [Saha Roy and Vadlamudi \(2012\)](#) showed that ER signaling contributes to metastasis, and explored possible therapeutic targets to block ER-driven metastasis. They expressed that deregulation of ER coregulators or ER extranuclear signaling has potential to promote metastasis in ER^+ breast cancer cells. Recently, [Bertucci](#)

Table 2: The number of the observations per group for the breast cancer data.

	ER negative (ER ⁻)	ER positive (ER ⁺)
cancer cell is not metastatic, $Y = 0$	41	106
cancer cell is metastatic, $Y = 1$	23	28

et al. (2020) analyzed gene expression data from 5,342 clinically-proven breast cancer data and concluded that the expression profiles were very different in ER⁺/HER2⁻ and ER⁻ Basal subtypes. So, we divide the data into two groups, ER⁻ and ER⁺. Table 2 summarized the sample size based on the response variable Y and ER status.

We ran the proposed algorithm 1 with $TT = 200,000$ iterations and 50,000 burn-in. The heat map with estimated marginal posterior probabilities of edge inclusion for each edge $u \rightarrow v$ is plotted in figure (8). The left plot is for ER⁻ breast cancer cells and the right plot is for ER⁺. We converted the heatmap into a DAG using threshold 0.5 shown in figure 9. To make the DAG bigger, we removed a few isolated nodes. The causal effect of each gene on Y is shown in figure 10 using equation (40). Genes can have positive or negative effects on other genes or on the response variable, too. For example, gene A can influence the expression of gene B but not otherwise and we showed this relationship by adding the edge $A \rightarrow B$ in the corresponding DAG. But this influence can be in the positive or negative direction, meaning that the increase in expression of A can increase the expression of B (positive effect), or increase in the expression of A can lead to decrease in the expression of B (negative effect). Since the direction of the gene’s effect on the response variable Y can not be inferred from the causal effect plot, we also computed the partial correlations (2) and plotted them in figure 11.

In order to validate our causal gene graph, we summarize our results and compared them with the top tier clinical and research breast cancer studies in the following paragraphs.

As can be seen in figure 10, IL-8 is highly expressed in ER⁻ breast cancer cells but not in ER⁺. This gene has also no direct edge to the node Y for ER⁺ group, a clear difference between the left and right plots in figure 9. Todorović-Raković and Milovanović (2013) showed that the IL-8 gene is highly expressed in ER⁻ breast cancer cells. Such gene expressions in different groups such as different ethnicities or different cells, are important in the Simpson’s paradox context. The proposed method can provide a powerful tool to check these changes and can provide more data driven guidance for biologists and other practical sciences.

IFIH1, SAMD9, IFITM1, IFIT3, OAS1, OAS2, CXCL10, CCL5 and CORO1A genes are common between the two groups. This observation is consistent with the results of research done by Magbanua et al. (2015). They expressed that the interferon signaling genes, such as IFIT2, IFIT1, IFITM1, IFIH1 and EML2 are associated with the recurrence-free survival (RFS) in breast tumors which was also confirmed by path analysis.

As another example, there is a strong probability of edge inclusion from gene IL-8 to IL-6 in the research by Castelletti and Consonni (2021), but we could not see this edge when we grouped the cells based on the ER⁻ and ER⁺ in figure 8. Weitkamp, Reinsberg, and Bartmann (2002) also mentioned that the overall correlation between IL-6 and IL-8 is $\rho = 0.50$ (p-value < 0.001), using a sample size of 182. $\rho = 0.50$ is not a strong correlation, and their study was not on breast cancer cells. The aim of their study was to evaluate the correlation of IL-6 and IL-8 values during neonatal clinical infection and to assess whether IL-8 would be a more beneficial infection marker. Besides the data quality and sample size, One possible explanation can be related to Simpson’s paradox. Since the goal of this study is not to check the Simpson’s paradox, we refer the readers to Wagner (1982) for more information on Simpson’s paradox.

Mouly et al. (2019) showed the RND1 gene is involved in oncogenesis and response to cancer therapeutics. Okada et al. (2015) identified the RND1 gene as a candidate metastasis suppressor in basal-like and triple-negative breast cancer through bioinformatics analysis. Triple negative breast cancer is ER⁻, progesterone receptor-negative and HER2-negative. Inactivation of RND1 in mammary epithelial cells induced highly undifferentiated and invasive tumors in mice. Although there is no direct edge connecting RND1 to Y in figure 9, this gene is connected to other genes in ER⁻ DAG while it is isolated in ER⁺. The partial correlation between this gene and the connected genes (MCM7 and IFIH1) for ER⁻ in figure 11 is negative, which can possibly explain why removing RND1 from mice results in more tumors, although we do not know the effect direction of MCM7 and IFIH1 on Y and this hypothesis needs more research, we thought it is good to illustrate the concept of negative effects of one gene on other genes or on the response variable.

In a recent paper published in 2022, the authors showed that the Melanoma-associated antigen D2 (MAGED2) gene positively regulated breast cancer cell metastasis Thakur et al. (2022). This gene also affects both ER⁺ and ER⁻ breast cancer groups (Figure 10). Jia et al. (2019) also showed that the MAGE gene family, such as MAGED2, is influential on breast cancer.

7.2 Cardiovascular Mortality Rate

For the second real data analysis, we study the impact of PM2.5 particle level on the cardiovascular mortality rate (CMR). The PM2.5 particle level and the mortality rate are measured by $\mu g/m^3$ and the number of annual deaths due to cardiovascular conditions per 100,000 people, respectively. The data comprises 2,132 counties and is provided by the US National Studies on Air Pollution and Health and is publicly available under U.S. Public Domain license Rappold (2020). To simplify the experiment setup, we use only the data for 2010. A

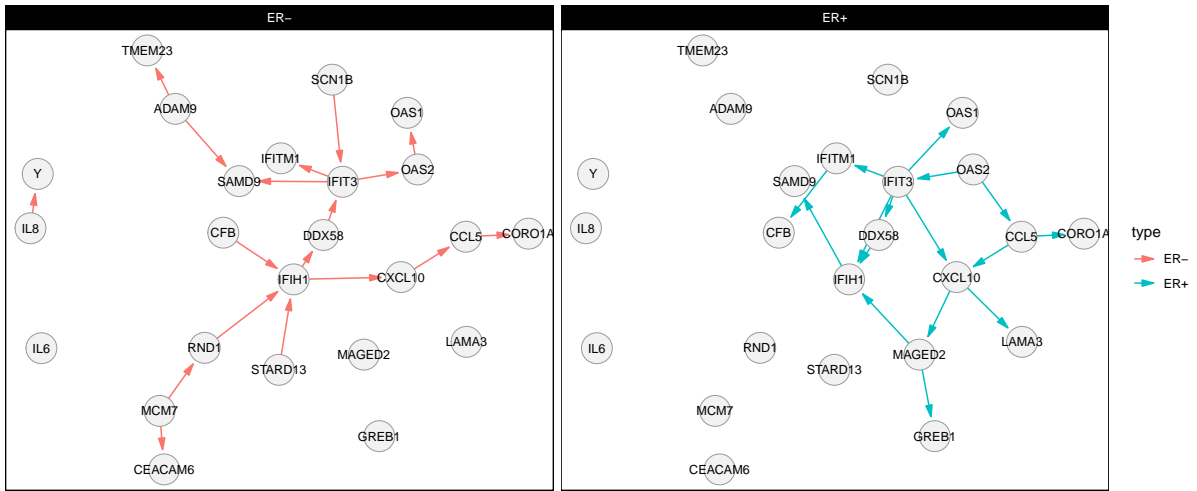


Figure 9: Graph of the gene network for breast cancer. Left plot is for the ER⁻ breast cancers and the right plot is for ER⁺, which shows obvious differences in the gene network connections. Genes IFIH1, SAMD9, IFITM1, IFIT3, OAS1, OAS2, CXCL10, CCL5 and CORO1A are common connecting nodes between the two groups.

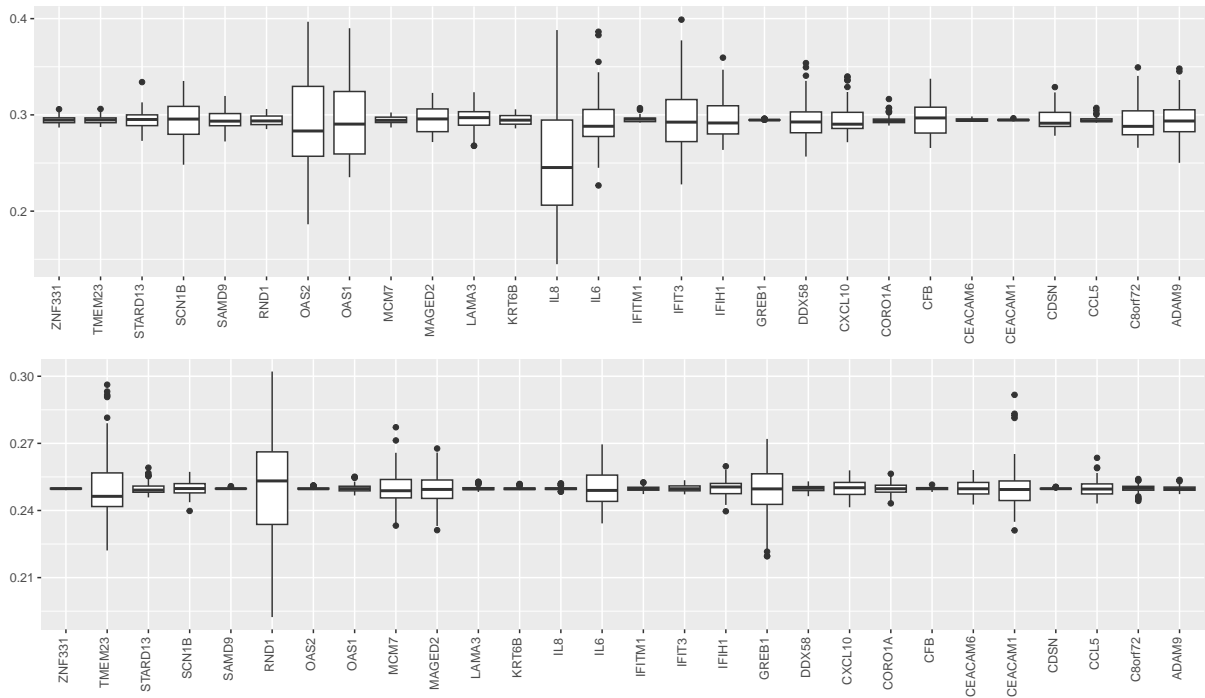


Figure 10: Box-plots of BMA estimate of causal effect. The top plot is for ER⁻ breast cancers and the bottom plot is for ER⁺. IL-8 is highly expressed in ER⁻ breast cancers [Todorović-Raković and Milovanović \(2013\)](#), a clear difference between left and right plots.

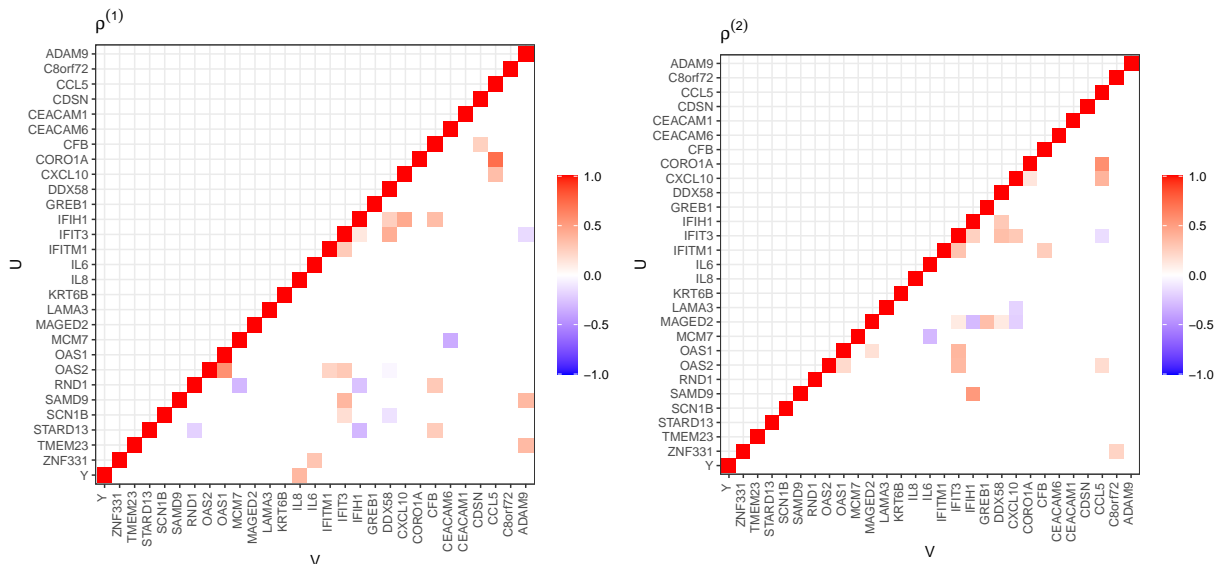


Figure 11: Heat map for estimated partial correlations $\rho^{(1)}$ and $\rho^{(2)}$. Left plot is for the ER^- breast cancers and the right plot is for ER^+ .

Table 3: The number of the observations per group for the CMR data.

	Small city $A^{(1)}$	Big city $A^{(2)}$
Low CRM ($Y = 0$)	432	577
High CRM ($Y = 1$)	520	397

similar approach was taken by Bahadori et al. (2022). The data includes 10 variables such as poverty rate, population, educational attainment, vacant housing units and household income, which we use as confounders. For the response variable Y , we transformed the CMR data into a high and low binary variable by setting the threshold 250. We divided the data into two groups based on the population size. We labeled a county as small if the population was less than 40,000 people and big otherwise. We also removed `SES_index` (Socioeconomic status index) because it has a high correlation with `pctfam_pover` (percentage of families below poverty level) and `femaleHH` (percentage of female household, no husband present). We also included the number of establishments in each county (`establishments`) in our model. The establishments data is included in the Rappold (2020) database too. For more information on the county business pattern establishments, see Bureau (2020).

PM2.5 is the main cause of CMR in both small and big population counties, a clear difference in the heat map of the edge prediction in figures 12 and 13 with big effect size (figure 14). Household income (`HH_inc`) and `femaleHH` are directly connected to CMR for small cities with moderate effect size, while those are indirectly connected to CMR through PM2.5.

Healthcare facility density per 1,000 individuals (`healthfac`) has no direct effect on CMR. `pctfam_pover` has a strong relation with `HH_inc` in both groups, meaning poverty leads to less household income. Educational attainment (`eduattain`) has a direct effect on the `HH_inc` in both groups. Unemployment rate (`unemploy`) is negatively correlated with `HH_inc` in big cities.

8 Conclusion

We considered modeling a binary response variable together with a set of independent variables for two groups under observational data. This work can be extended for groups with more than two elements simply by using $k > 2$ in all equations. We could speed up the MCMC convergence by picking better initial graphs for the DAGs using modified Cholesky decomposition.

In this work, we assumed equal edge inclusion of the edges while we can improve it by adding some weights to the edge inclusion. For example, we can add more weights to the edges coming into node 1, or we can decrease the probability of node inclusion inversely proportionate to the degree of its parent node. This method is useful if someone wants to keep the proposed graph as a sparse DAG at each MCMC iteration.

There are many real examples where there are more than one binary variables in data. This method can model just one binary response variable. Categorical or nominal response variables also have many applications

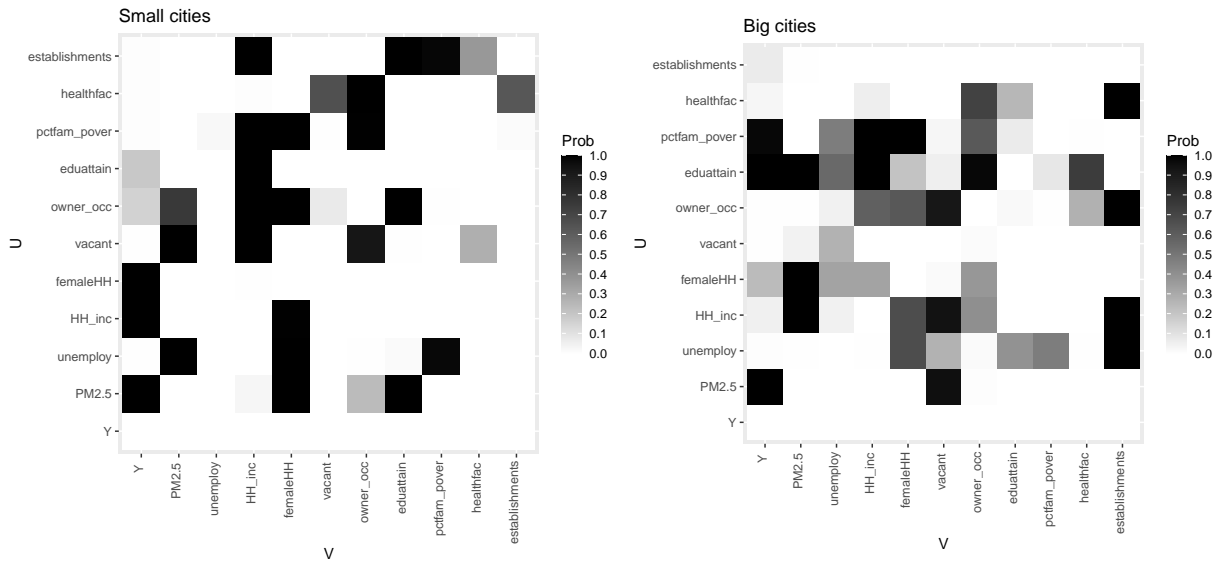


Figure 12: Heat map with estimated marginal posterior probabilities of edge inclusion for each edge $u \rightarrow v$ for $A^{(1)}$ (left) and $A^{(2)}$ (right).

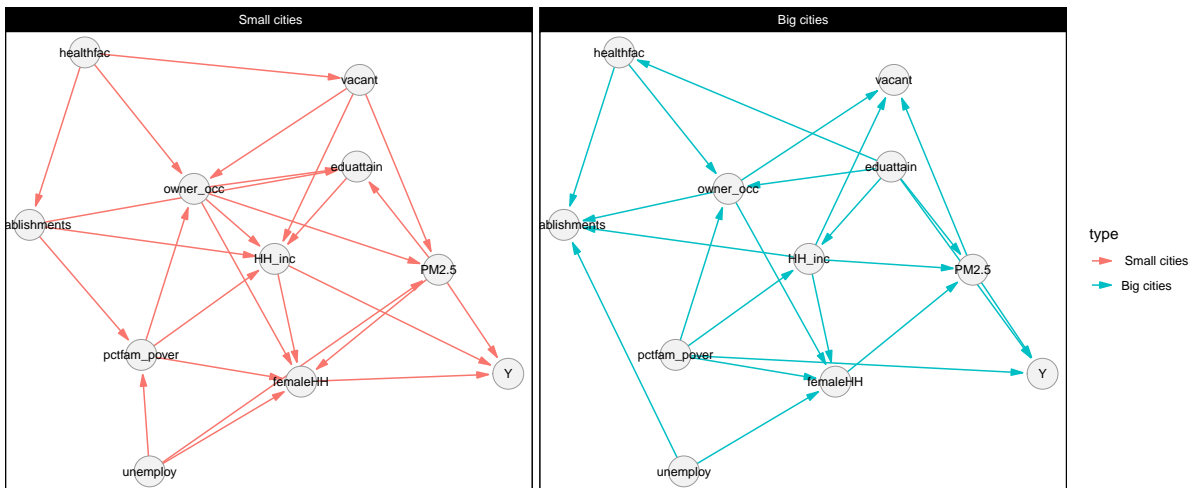


Figure 13: Graph of the nodes. Left plot is for the small cities and the right plot is for the big cities.

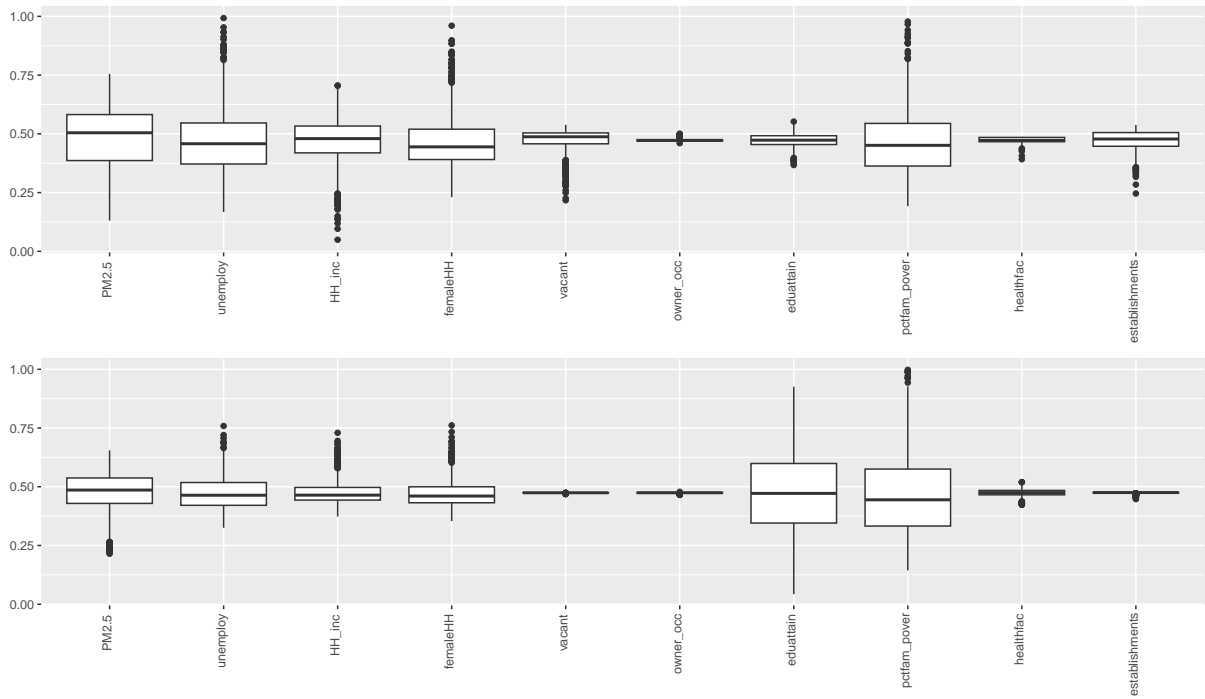


Figure 14: Boxplots of BMA estimate of causal effect.

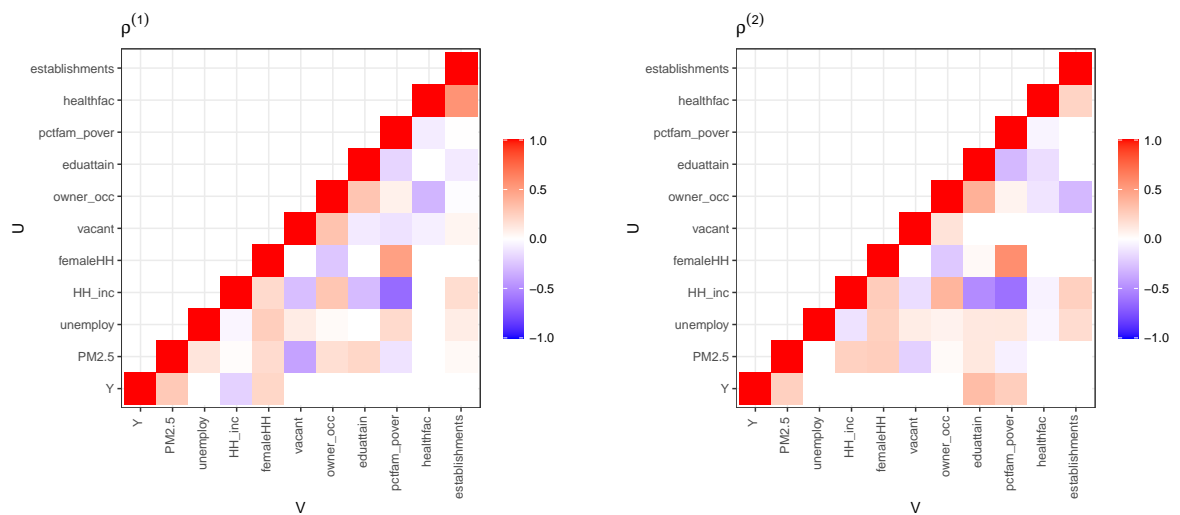


Figure 15: Heat map for estimated partial correlations $\rho^{(1)}$ and $\rho^{(2)}$. Left plot is for the small cities and the right plot is for the big cities.

which are not under the scope of this paper and need more research. Normality assumption of the independent variables is also a limitation of this method which may produce biased outputs.

Regardless of those limitations which are not under the proposed model assumptions, we were able to show that this method could estimate the DAG structure and the model parameters accurately. We also demonstrated its value in real well-known datasets, especially using two DAGs.

References

- Aragón, O. R., Pietri, E. S., & Powell, B. A. (2023). Gender bias in teaching evaluations: the causal role of department gender composition. *Proceedings of the National Academy of Sciences*, *120*(4), e2118466120.
- Bahadori, T., Tchetgen, E. T., & Heckerman, D. (2022). End-to-end balancing for causal continuous treatment-effect estimation. In *International conference on machine learning* (pp. 1313–1326).
- Ben-David, E., Li, T., Massam, H., & Rajaratnam, B. (2015). High dimensional bayesian inference for gaussian directed acyclic graph models. *arXiv preprint arXiv:1109.4371*.
- Bertucci, F., Finetti, P., Goncalves, A., & Birnbaum, D. (2020). The therapeutic response of er+/her2-breast cancers differs according to the molecular basal or luminal subtype. *NPJ Breast Cancer*, *6*(1), 8.
- Brown, P. J., Le, N. D., & Zidek, J. V. (1994). Inference for a covariance matrix. *Aspects of uncertainty: a tribute to DV Lindley*, 77–92.
- Bureau, U. S. C. (2020). *County business patterns by industry: 2020*. Retrieved from <https://www.census.gov/library/visualizations/interactive/county-business-patterns-by-industry-2020.html>
- Cai, T. T., Li, H., Liu, W., & Xie, J. (2013). Covariate-adjusted precision matrix estimation with an application in genetical genomics. *Biometrika*, *100*(1), 139–156.
- Cai, T. T., Li, H., Liu, W., & Xie, J. (2016). Joint estimation of multiple high-dimensional precision matrices. *Statistica Sinica*, *26*(2), 445.
- Cai, T. T., Ren, Z., & Zhou, H. H. (2016). Estimating structured high-dimensional covariance and precision matrices: Optimal rates and adaptive estimation. *Electron. J. Statist*, *10*(1), 1–59.
- Cao, X., Khare, K., & Ghosh, M. (2019). Posterior graph selection and estimation consistency for high-dimensional bayesian dag models. *Annals of Statistics*, *47*(1), 319–348.
- Castelletti, F., & Consonni, G. (2021). Bayesian causal inference in probit graphical models. *Bayesian Analysis*, *16*(4), 1113–1137.
- Chandrasekaran, V., Parrilo, P. A., & Willsky, A. S. (2012). Latent variable graphical model selection via convex optimization. *The Annals of Statistics*, *40*(4), 1935 – 1967.
- Chen, M., Ren, Z., Zhao, H., & Zhou, H. (2016). Asymptotically normal and efficient estimation of covariate-adjusted gaussian graphical model. *Journal of the American Statistical Association*, *111*(513), 394–406.
- Chen, M.-j. (2021). The abatement of particulate matter 2.5 in los angeles county: a counterfactual evaluation. *Environment, Development and Sustainability*, *23*(5), 7063–7088.
- Dawid, A. P., & Musio, M. (2022). Effects of causes and causes of effects. *Annual Review of Statistics and Its Application*, *9*, 261–287.
- Desmedt, C., Piette, F., Loi, S., Wang, Y., Lallemand, F., Haibe-Kains, B., ... others (2007a). *Strong time dependence of the 76-gene prognostic signature*. Retrieved Jun 11, 2007, from <https://www.ncbi.nlm.nih.gov/geo/query/acc.cgi?acc=GSE7390>
- Desmedt, C., Piette, F., Loi, S., Wang, Y., Lallemand, F., Haibe-Kains, B., ... others (2007b). Strong time dependence of the 76-gene prognostic signature for node-negative breast cancer patients in the TRANSBIG multicenter independent validation series. *Clinical cancer research*, *13*(11), 3207–3214.
- Erdős, P., Rényi, A., et al. (1960). On the evolution of random graphs. *Publ. Math. Inst. Hung. Acad. Sci*, *5*(1), 17–60.
- Evans, L. M., Tahmasbi, R., Vrieze, S. I., Abecasis, G. R., Das, S., Gazal, S., ... others (2018). Comparison of methods that use whole genome data to estimate the heritability and genetic architecture of complex traits. *Nature genetics*, *50*(5), 737–745.
- Gaskins, J. T., & Daniels, M. J. (2013). A nonparametric prior for simultaneous covariance estimation. *Biometrika*, *100*(1), 125–138.
- Geiger, D., & Heckerman, D. (2002). Parameter priors for directed acyclic graphical models and the characterization of several probability distributions. *The Annals of Statistics*, *30*(5), 1412–1440.

- Gische, C., West, S. G., & Voelke, M. C. (2021). Forecasting causal effects of interventions versus predicting future outcomes. *Structural Equation Modeling: A Multidisciplinary Journal*, 28(3), 475–492.
- Godsill, S. J. (2001). On the relationship between markov chain monte carlo methods for model uncertainty. *Journal of computational and graphical statistics*, 10(2), 230–248.
- Golub, G. H., & Van Loan, C. F. (2013). *Matrix computations*. JHU press.
- Guo, J., Levina, E., Michailidis, G., & Zhu, J. (2011). Joint estimation of multiple graphical models. *Biometrika*, 98(1), 1–15.
- Guo, J., Levina, E., Michailidis, G., & Zhu, J. (2015). Graphical models for ordinal data. *Journal of Computational and Graphical Statistics*, 24(1), 183–204.
- Hernán, M. A., & Robins, J. M. (2010). *Causal inference*. CRC Boca Raton, FL.
- Holdcroft, A. (2007). *Gender bias in research: how does it affect evidence based medicine?* (Vol. 100) (No. 1). SAGE Publications Sage UK: London, England.
- Jia, B., Zhao, X., Wang, Y., Wang, J., Wang, Y., & Yang, Y. (2019). Prognostic roles of mage family members in breast cancer based on km-plotter data. *Oncology letters*, 18(4), 3501–3516.
- Karrer, B., & Newman, M. E. (2009). Random graph models for directed acyclic networks. *Physical Review E*, 80(4), 046110.
- Kingma, D. P., & Welling, M. (2013). Auto-encoding variational bayes. *arXiv preprint arXiv:1312.6114*.
- Knuth, D. E. (1997). *The art of computer programming* (Vol. 3). Pearson Education.
- Lafit, G., Tuerlinckx, F., Myin-Germeys, I., & Ceulemans, E. (2019). A partial correlation screening approach for controlling the false positive rate in sparse gaussian graphical models. *Scientific reports*, 9(1), 17759.
- Lauritzen, S. L. (1996). *Graphical models* (Vol. 17). Clarendon Press.
- Li, F. Q., & Zhang, X. S. (2019). Bayesian estimation of large precision matrix based on cholesky decomposition. *Acta Mathematica Sinica, English Series*, 35(5), 619–631.
- Louizos, C., Shalit, U., Mooij, J. M., Sontag, D., Zemel, R., & Welling, M. (2017). Causal effect inference with deep latent-variable models. *Advances in neural information processing systems*, 30.
- Magbanua, M. J. M., Wolf, D. M., Yau, C., Davis, S. E., Crothers, J., Au, A., ... others (2015). Serial expression analysis of breast tumors during neoadjuvant chemotherapy reveals changes in cell cycle and immune pathways associated with recurrence and response. *Breast Cancer Research*, 17(1), 1–13.
- Mansoori, B., Mohammadi, A., Ghasabi, M., Shirjang, S., Dehghan, R., Montazeri, V., ... others (2019). mir-142-3p as tumor suppressor mirna in the regulation of tumorigenicity, invasion and migration of human breast cancer by targeting bach-1 expression. *Journal of cellular physiology*, 234(6), 9816–9825.
- Miao, Z., Cao, Q., Liao, R., Chen, X., Li, X., Bai, L., ... others (2022). Elevated transcription and glycosylation of b3gnt5 promotes breast cancer aggressiveness. *Journal of Experimental & Clinical Cancer Research*, 41(1), 169.
- Momenzadeh, M., Sehhati, M., & Rabbani, H. (2020). Using hidden markov model to predict recurrence of breast cancer based on sequential patterns in gene expression profiles. *Journal of Biomedical Informatics*, 111, 103570.
- Mouly, L., Gilhodes, J., Lemarié, A., Cohen-Jonathan Moyal, E., Toulas, C., Favre, G., ... Monferran, S. (2019). The rnd1 small gtpase: main functions and emerging role in oncogenesis. *International Journal of Molecular Sciences*, 20(15), 3612.
- Okada, T., Sinha, S., Esposito, I., Schiavon, G., López-Lago, M. A., Su, W., ... others (2015). The rho gtpase rnd1 suppresses mammary tumorigenesis and emt by restraining ras-mapk signalling. *Nature cell biology*, 17(1), 81–94.
- Pearl, J. (2009). *Causality*. Cambridge university press.
- Pearl, J., & Mackenzie, D. (2020). *AI Can't Reason Why*. Retrieved 1/28/2020, from <https://www.wsj.com/articles/ai-cant-reason-why-1526657442>
- Pearl, J., et al. (2000). Models, reasoning and inference. *Cambridge, UK: CambridgeUniversityPress*, 19(2).
- Poirion, O. B., Jing, Z., Chaudhary, K., Huang, S., & Garmire, L. X. (2021). Deepprog: an ensemble of deep-learning and machine-learning models for prognosis prediction using multi-omics data. *Genome medicine*, 13(1), 1–15.
- Pontzer, H., Yamada, Y., Sagayama, H., Ainslie, P. N., Andersen, L. F., Anderson, L. J., ... others (2021). Daily energy expenditure through the human life course. *Science*, 373(6556), 808–812.
- Pourahmadi, M. (2007). Cholesky decompositions and estimation of a covariance matrix: orthogonality

- of variance–correlation parameters. *Biometrika*, 94(4), 1006–1013.
- Qiao, X., Qian, C., James, G. M., & Guo, S. (2020). Doubly functional graphical models in high dimensions. *Biometrika*, 107(2), 415–431.
- Ramspek, C. L., Steyerberg, E. W., Riley, R. D., Rosendaal, F. R., Dekkers, O. M., Dekker, F. W., & van Diepen, M. (2021). Prediction or causality? a scoping review of their conflation within current observational research. *European journal of epidemiology*, 36, 889–898.
- Rappold, A. (2020). *Annual PM2.5 and cardiovascular mortality rate data: Trends modified by county socioeconomic status in 2,132 us counties*. Retrieved 2019-11-04, from <https://doi.org/10.23719/1506014>
- Rothman, A. J., Levina, E., & Zhu, J. (2010). A new approach to cholesky-based covariance regularization in high dimensions. *Biometrika*, 97(3), 539–550.
- Rueda, O. M., Sammut, S.-J., Seoane, J. A., Chin, S.-F., Caswell-Jin, J. L., Callari, M., ... others (2019). Dynamics of breast-cancer relapse reveal late-recurring er-positive genomic subgroups. *Nature*, 567(7748), 399–404.
- Saha Roy, S., & Vadlamudi, R. K. (2012). Role of estrogen receptor signaling in breast cancer metastasis. *International journal of breast cancer*, 2012.
- Sharma, A., & Kiciman, E. (2020). Dowhy: An end-to-end library for causal inference. *arXiv preprint arXiv:2011.04216*.
- Shojaie, A., & Michailidis, G. (2010). Penalized likelihood methods for estimation of sparse high-dimensional directed acyclic graphs. *Biometrika*, 97(3), 519–538.
- Si, S., Li, J., Tewara, M. A., Li, H., Liu, X., Li, Y., ... others (2021). Identifying causality, genetic correlation, priority and pathways of large-scale complex exposures of breast and ovarian cancers. *British Journal of Cancer*, 125(11), 1570–1581.
- Silva, R., & Ghahramani, Z. (2009). The hidden life of latent variables: Bayesian learning with mixed graph models. *The Journal of Machine Learning Research*, 10, 1187–1238.
- Smith, M., & Kohn, R. (2002). Parsimonious covariance matrix estimation for longitudinal data. *Journal of the American Statistical Association*, 97(460), 1141–1153.
- Thakur, C., Qiu, Y., Zhang, Q., Carruthers, N. J., Yu, M., Bi, Z., ... others (2022). Deletion of mdig enhances h3k36me3 and metastatic potential of the triple negative breast cancer cells. *Iscience*, 25(10), 105057.
- Todorović-Raković, N., & Milovanović, J. (2013). Interleukin-8 in breast cancer progression. *Journal of Interferon & Cytokine Research*, 33(10), 563–570.
- Wagner, C. H. (1982). Simpson’s paradox in real life. *The American Statistician*, 36(1), 46–48.
- Wang, H., & Li, S. Z. (2012). Efficient gaussian graphical model determination under g-wishart prior distributions. *Electron. J. Statist.*, 6, 168–198.
- Weitkamp, J.-H., Reinsberg, J., & Bartmann, P. (2002). Interleukin-8 (il-8) preferable to il-6 as a marker for clinical infection. *Clinical and Vaccine Immunology*, 9(6), 1401–1401.
- Wu, C., Zhao, H., Fang, H., & Deng, M. (2017). Graphical model selection with latent variables. *Electron. J. Statist.*, 11(2), 3485–3521.
- Yu, G., & Bien, J. (2017). Learning local dependence in ordered data. *The Journal of Machine Learning Research*, 18(1), 1354–1413.

Appendix

A Full posterior distribution

The full posterior distribution is

$$\begin{aligned}
& f\left(\mathcal{D}^{(1)}, \mathcal{D}^{(2)}, \mathbf{L}^{(1)}, \mathbf{L}^{(2)}, \mathbf{D}, \mathbf{X}_1^{(1)}, \mathbf{X}_1^{(2)}, \theta | \mathbf{y}^{(1)}, \mathbf{y}^{(2)}, \mathbf{X}_{-1}^{(1)}, \mathbf{X}_{-1}^{(2)}\right) \\
& \propto f\left(\mathbf{y}^{(1)}, \mathbf{y}^{(2)}, \mathbf{X}_{-1}^{(1)}, \mathbf{X}_{-1}^{(2)}, \mathbf{X}_1^{(1)}, \mathbf{X}_1^{(2)} | \mathcal{D}^{(1)}, \mathcal{D}^{(2)}, \mathbf{L}^{(1)}, \mathbf{L}^{(2)}, \mathbf{D}, \theta\right) f\left(\mathcal{D}^{(1)}, \mathcal{D}^{(2)}, \mathbf{L}^{(1)}, \mathbf{L}^{(2)}, \mathbf{D}, \theta\right) \\
& = f\left(\mathbf{y}^{(1)}, \mathbf{y}^{(2)}, \mathbf{X}^{(1)}, \mathbf{X}^{(2)} | \mathcal{D}^{(1)}, \mathcal{D}^{(2)}, \mathbf{L}^{(1)}, \mathbf{L}^{(2)}, \mathbf{D}, \theta\right) f\left(\mathbf{L}^{(1)}, \mathbf{L}^{(2)}, \mathbf{D} | \mathcal{D}^{(1)}, \mathcal{D}^{(2)}, \theta\right) f\left(\mathcal{D}^{(1)}\right) f\left(\mathcal{D}^{(2)}\right) f(\theta) \\
& = \prod_{k=1}^2 f\left(\mathbf{y}^{(k)}, \mathbf{X}^{(k)} | \mathcal{D}^{(k)}, \mathbf{L}^{(k)}, \mathbf{D}, \theta\right) f\left(\mathbf{L}^{(k)} | \mathbf{D}, \mathcal{D}^{(k)}\right) f\left(\mathcal{D}^{(k)}\right) \times f\left(\mathbf{D} | \mathcal{D}^{(1)}, \mathcal{D}^{(2)}\right) f(\theta), \tag{44}
\end{aligned}$$

where $f(\theta) \propto 1$, too.

B Acceptance Probability for $\mathcal{D}^{(k)}$

We summarize the PAS algorithm here at first. Consider N distinct models, $\mathcal{M}_1, \dots, \mathcal{M}_N$, each one with set of parameters $\boldsymbol{\theta}_\nu$ and assume the true data generating model is one of the N models. The associated likelihood function for each model \mathcal{M}_ν is $f(\mathbf{X}|\boldsymbol{\theta}_\nu, \mathcal{M}_\nu)$, where $\mathbf{X} = (X_1, \dots, X_q)$. Consider a move from the current model \mathcal{M}_ν to a new model $\mathcal{M}_{\nu'}$. Suppose

- there exists a subvector $(\boldsymbol{\theta}_{\nu'})_{\mathcal{U}}$ of the parameter $\boldsymbol{\theta}_{\nu'}$ for a new model $\mathcal{M}_{\nu'}$ such that $f((\boldsymbol{\theta}_{\nu'})_{\mathcal{U}} | (\boldsymbol{\theta}_{\nu'})_{-\mathcal{U}}, \mathcal{M}_{\nu'}, \mathbf{X})$ is available in closed form,
- in the current model \mathcal{M}_ν , there exists an equivalent subset of parameters $(\boldsymbol{\theta}_\nu)_{-\mathcal{U}}$ with the same dimension as $(\boldsymbol{\theta}_{\nu'})_{-\mathcal{U}}$.

The PAS algorithm is

- Propose $\mathcal{M}_{\nu'} \sim q(\mathcal{M}_{\nu'}|\mathcal{M}_\nu)$ and set $(\boldsymbol{\theta}_{\nu'})_{-\mathcal{U}} = (\boldsymbol{\theta}_\nu)_{-\mathcal{U}}$.
- Accept $\mathcal{M}_{\nu'}$ with probability $\alpha = \min\{1, r_\nu\}$, where

$$r_\nu = \frac{f(\mathcal{M}_{\nu'} | (\boldsymbol{\theta}_{\nu'})_{-\mathcal{U}}, \mathbf{X}) q(\mathcal{M}_\nu | \mathcal{M}_{\nu'})}{f(\mathcal{M}_\nu | (\boldsymbol{\theta}_\nu)_{-\mathcal{U}}, \mathbf{X}) q(\mathcal{M}_{\nu'} | \mathcal{M}_\nu)} \quad (45)$$

and

$$f(\mathcal{M}_{\nu'} | (\boldsymbol{\theta}_{\nu'})_{-\mathcal{U}}, \mathbf{X}) = \int f(\mathcal{M}_{\nu'}, (\boldsymbol{\theta}_{\nu'})_{\mathcal{U}} | (\boldsymbol{\theta}_{\nu'})_{-\mathcal{U}}, \mathbf{X}) d(\boldsymbol{\theta}_{\nu'})_{\mathcal{U}}. \quad (46)$$

- If $\mathcal{M}_{\nu'}$ is accepted, generate $(\boldsymbol{\theta}_{\nu'})_{\mathcal{U}} \sim f((\boldsymbol{\theta}_{\nu'})_{\mathcal{U}} | (\boldsymbol{\theta}_{\nu'})_{-\mathcal{U}}, \mathcal{M}_{\nu'}, \mathbf{X})$. Otherwise, generate $(\boldsymbol{\theta}_\nu)_{\mathcal{U}} \sim f((\boldsymbol{\theta}_\nu)_{\mathcal{U}} | (\boldsymbol{\theta}_\nu)_{-\mathcal{U}}, \mathcal{M}_\nu, \mathbf{X})$.
- Update the parameters $\boldsymbol{\theta}_{\nu'}$ if $\mathcal{M}_{\nu'}$ is accepted using standard MCMC steps. Otherwise, update the parameters $\boldsymbol{\theta}_\nu$ using standard MCMC steps.

To adapt this algorithm to the proposed method, we need to find which edges been have changed in the new DAGs $\mathcal{D}^{(1)}$ and $\mathcal{D}^{(2)}$ to define the set $\boldsymbol{\theta}_{-\mathcal{U}}$ and them to compute equation (46) for them, accordingly. So, we provide the proofs for the **Insert**($i \rightarrow j$), **Delete**($i \rightarrow j$) and **Reverse**($i \rightarrow j$) operators, separately in the following subsections.

B.1 One Parent Node is Changed

In algorithm 1, new $\mathcal{D}^{(1)}$ and $\mathcal{D}^{(2)}$ are proposed separately, so we need to compute the integral in equation (46) for $k \in \{1, 2\}$ independently. For the operators **Insert**($i \rightarrow j$) and **Delete**($i \rightarrow j$), the difference between the proposed DAG $\mathcal{D}'^{(k)}$ and $\mathcal{D}^{(k)}$ is just one parent node, denoted by node j , so $\mathcal{U} = (\sigma_j^2, \mathbf{L}_{\leq j \succ})$ and the set of parameters in PAS algorithm is $\boldsymbol{\theta} = (\mathbf{D}^{(k)}, \mathbf{L}^{(k)})$. For $j > 1$ and using Bayes theorem, equation (46) becomes

$$\begin{aligned} & f(\mathcal{D}^{(k)} | \mathbf{X}^{(k)}, \boldsymbol{\theta}_{-\mathcal{U}}) \propto f(\mathbf{X}^{(k)}, \boldsymbol{\theta}_{-\mathcal{U}} | \mathcal{D}^{(k)}) f(\mathcal{D}^{(k)}) \\ & = f(\mathcal{D}^{(k)}) \int_{\mathbb{R}^{|\text{pa}(j)|}} \int_0^\infty f(\mathbf{X}^{(k)}, \mathbf{D}^{(k)}, \mathbf{L}^{(k)} | \mathcal{D}^{(k)}) d\mathbf{L}_{\leq j \succ}^{(k)} d\sigma_j^2 \\ & = f(\mathcal{D}^{(k)}) \prod_{r \neq j} f(\mathbf{X}_r^{(k)}, \sigma_r^2, \mathbf{L}_{\leq r \succ}^{(k)} | \mathcal{D}^{(k)}) \times \int \int f(\mathbf{X}_j^{(k)} | \sigma_j^2, \mathbf{L}_{\leq j \succ}^{(k)}) f(\mathbf{L}_{\leq j \succ}^{(k)} | \sigma_j^2) f(\sigma_j^2 | \mathcal{D}^{(k)}) d\mathbf{L}_{\leq j \succ}^{(k)} d\sigma_j^2, \end{aligned} \quad (47)$$

where $f(\sigma_j^2 | \mathcal{D}^{(k)})$ is the prior for σ_j^2 assuming there is just one DAG $\mathcal{D}^{(k)}$, i.e., $\sigma_j^2 | \mathcal{D}^{(k)} \sim \text{I-Ga}\left(\frac{a_j^{(k)}}{2}, \frac{g_k}{2}\right)$.

To simplify the equations, we define

$$m(\mathbf{X}_j^{(k)} | \mathbf{X}_{\text{pa}(j)}^{(k)}, \mathcal{D}^{(k)}) := \int \int f(\mathbf{X}_j^{(k)} | \sigma_j^2, \mathbf{L}_{\leq j \succ}^{(k)}) f(\mathbf{L}_{\leq j \succ}^{(k)} | \sigma_j^2) f(\sigma_j^2 | \mathcal{D}^{(k)}) d\mathbf{L}_{\leq j \succ}^{(k)} d\sigma_j^2. \quad (48)$$

The integrand in (48) can be written as

$$\begin{aligned} & f(\mathbf{X}_j^{(k)} | \sigma_j^2, \mathbf{L}_{\leq j \succ}^{(k)}) f(\mathbf{L}_{\leq j \succ}^{(k)} | \sigma_j^2) f(\sigma_j^2 | \mathcal{D}^{(k)}) \\ & = \frac{1}{(2\pi)^{\frac{n_k}{2}}} |\sigma_j^2 \mathbf{I}_{n_k}|^{-\frac{1}{2}} \exp\left\{-\frac{1}{2\sigma_j^2} (\mathbf{X}_j^{(k)} + \mathbf{X}_{\text{pa}(j)}^{(k)} \mathbf{L}_{\leq j \succ}^{(k)})' (\mathbf{X}_j^{(k)} + \mathbf{X}_{\text{pa}(j)}^{(k)} \mathbf{L}_{\leq j \succ}^{(k)})\right\} \\ & \times \frac{1}{(2\pi)^{\frac{|\text{pa}(j)|}{2}}} \left| \frac{1}{g_k} \sigma_j^2 \mathbf{I}_{|\text{pa}(j)|} \right|^{-\frac{1}{2}} \exp\left\{-\frac{g_k}{2\sigma_j^2} (\mathbf{L}_{\leq j \succ}^{(k)})' \mathbf{L}_{\leq j \succ}^{(k)}\right\} \\ & \times C \cdot (\sigma_j^2)^{-\frac{a_j^{(k)}}{2}-1} \exp\left\{-\frac{g_k}{\sigma_j^2}\right\}, \end{aligned} \quad (49)$$

where $C = \left(\frac{g_j}{2}\right)^{\frac{a_j^{(k)}}{2}} / \Gamma\left(\frac{a_j^{(k)}}{2}\right)$.

By rearranging the terms containing $\mathbf{L}_{\leq j}^{(k)}$ in (49), it is easy to show that

$$\mathbf{L}_{\leq j}^{(k)} | \sigma_j^2, \mathbf{X}^{(k)} \sim \mathcal{N}_{|\text{pa}^{(k)}(j)|} \left(-\hat{\mathbf{L}}_j'^{(k)}, \sigma_j^2 (\bar{\mathbf{T}}_j^{(k)})^{-1} \right), \quad (50)$$

so, the inner integral becomes

$$\int f \left(\mathbf{X}_j^{(k)} | \sigma_j^2, \mathbf{L}_{\leq j}^{(k)} \right) f \left(\mathbf{L}_{\leq j}^{(k)} | \sigma_j^2 \right) d\mathbf{L}_{\leq j}^{(k)} = (2\pi)^{\frac{|\text{pa}^{(k)}(j)|}{2}} \left| \frac{\bar{\mathbf{T}}_j^{(k)}}{\sigma_j^2} \right|^{-\frac{1}{2}} \exp \left\{ \frac{1}{2\sigma_j^2} \hat{\mathbf{L}}_j'^{(k)} \bar{\mathbf{T}}_j^{(k)} \hat{\mathbf{L}}_j^{(k)} \right\}, \quad (51)$$

which is the constant terms in a random variable that follows $\mathcal{N}_{|\text{pa}^{(k)}(j)|} \left(-\hat{\mathbf{L}}_j'^{(k)}, \sigma_j^2 (\bar{\mathbf{T}}_j^{(k)})^{-1} \right)$. Furthermore, using (51) and other terms containing σ_j^2 in (49) together with the prior distribution for $\sigma_j^2 | \mathcal{D}^{(k)}$, we can show that

$$f \left(\sigma_j^2 | \mathbf{X}_j^{(k)}, \mathcal{D}^{(k)} \right) \propto (\sigma_j^2)^{-\frac{n_k}{2} - \frac{a_j^{(k)}}{2} - 1 - \frac{|\text{pa}^{(k)}(j)|}{2} + \frac{|\text{pa}^{(k)}(j)|}{2}} \times \exp \left\{ \frac{-\frac{1}{2} (g_k + \mathbf{X}_j'^{(k)} \mathbf{X}_j^{(k)} - \hat{\mathbf{L}}_j'^{(k)} \bar{\mathbf{T}}_j^{(k)} \hat{\mathbf{L}}_j^{(k)})}{\sigma_j^2} \right\}, \quad (52)$$

where we substitute $\left| \frac{\bar{\mathbf{T}}_j^{(k)}}{\sigma_j^2} \right|^{-\frac{1}{2}} = \sigma_j^2 \frac{|\text{pa}^{(k)}(j)|}{2} \left| \bar{\mathbf{T}}_j^{(k)} \right|^{-\frac{1}{2}}$. It is easy to see that the posterior is

$$\sigma_j^2 | \mathbf{X}_j^{(k)}, \mathcal{D}^{(k)} \sim \text{I-Ga} \left(\frac{a_j^{(k)}}{2} + \frac{n_k}{2}, \frac{1}{2} K^{(k)} \right), \quad (53)$$

where $K^{(k)} = g_k + \mathbf{X}_j'^{(k)} \mathbf{X}_j^{(k)} - \hat{\mathbf{L}}_j'^{(k)} \bar{\mathbf{T}}_j^{(k)} \hat{\mathbf{L}}_j^{(k)}$.

Finally by bringing back the constant terms from (49), the outer integral in (48) becomes

$$\begin{aligned} m(\mathbf{X}_j^{(k)} | \mathbf{X}_{\text{pa}(j)}^{(k)}, \mathcal{D}^{(k)}) &= \int_0^\infty f \left(\sigma_j^2 | \mathbf{X}_j^{(k)}, \mathcal{D}^{(k)} \right) d\sigma_j^2 \\ &= (2\pi)^{-\frac{n_k}{2}} \frac{|\mathbf{T}_j^{(k)}|^{1/2}}{|\bar{\mathbf{T}}_j^{(k)}|^{1/2}} \frac{\Gamma\left(\frac{a_j^{(k)}}{2} + \frac{n_k}{2}\right)}{\Gamma\left(\frac{a_j^{(k)}}{2}\right)} \left(\frac{g_k}{2}\right)^{a_j^{(k)}} \left[\frac{1}{2} (g_k + \mathbf{X}_j'^{(k)} \mathbf{X}_j^{(k)} - \hat{\mathbf{L}}_j'^{(k)} \bar{\mathbf{T}}_j^{(k)} \hat{\mathbf{L}}_j^{(k)}) \right]^{-\left(\frac{a_j^{(k)}}{2} + n_k\right)/2}. \end{aligned} \quad (54)$$

For $j = 1$, since $\sigma_j^2 = 1$ then there would be just one integral, so

$$m(\mathbf{X}_1^{(k)} | \mathbf{X}_{\text{pa}(1)}^{(k)}, \mathcal{D}^{(k)}) := \int f \left(\mathbf{X}_1^{(k)} | \mathbf{L}_{\leq 1}^{(k)} \right) f \left(\mathbf{L}_{\leq 1}^{(k)} \right) d\mathbf{L}_{\leq 1}^{(k)}, \quad (55)$$

which we computed in (51). Bringing back the constant terms from (49) we have

$$m(\mathbf{X}_1^{(k)} | \mathbf{X}_{\text{pa}(1)}^{(k)}, \mathcal{D}^{(k)}) = (2\pi)^{-\frac{n_k}{2}} \frac{|\mathbf{T}_1^{(k)}|^{1/2}}{|\bar{\mathbf{T}}_1^{(k)}|^{1/2}} \cdot \exp \left\{ -\frac{1}{2} \left(\mathbf{X}_1'^{(k)} \mathbf{X}_1^{(k)} - \hat{\mathbf{L}}_1'^{(k)} \bar{\mathbf{T}}_1^{(k)} \hat{\mathbf{L}}_1^{(k)} \right) \right\}. \quad (56)$$

Substituting $f \left(\mathcal{D}^{(k)} | \mathbf{X}^{(k)}, \boldsymbol{\theta}_{-\mathcal{U}} \right)$ into equation (45) completes the proof.

B.2 Two Parent Nodes are Changed

As we explained before, for the **Reverse**($i \rightarrow j$) operator, both $\text{pa}(i)$ and $\text{pa}(j)$ will change. So, we need to account for both nodes i and j . In this case, $\mathcal{U} = (\sigma_i^2, \sigma_j^2, \mathbf{L}_{\leq i}, \mathbf{L}_{\leq j})$ and the set of parameters in PAS algorithm is $\boldsymbol{\theta} = (\mathbf{D}^{(k)}, \mathbf{L}^{(k)})$. For $j > 1$, equation (46) becomes

$$\begin{aligned} f \left(\mathcal{D}^{(k)} | \mathbf{X}^{(k)}, \boldsymbol{\theta}_{-\mathcal{U}} \right) &\propto f \left(\mathbf{X}^{(k)}, \boldsymbol{\theta}_{-\mathcal{U}} | \mathcal{D}^{(k)} \right) f \left(\mathcal{D}^{(k)} \right) \\ &= f \left(\mathcal{D}^{(k)} \right) \int \int \int \int f \left(\mathbf{X}^{(k)}, \mathbf{D}^{(k)}, \mathbf{L}^{(k)} | \mathcal{D}^{(k)} \right) d\mathbf{L}_{\leq i}^{(k)} d\mathbf{L}_{\leq j}^{(k)} d\sigma_i^2 d\sigma_j^2 \\ &= f \left(\mathcal{D}^{(k)} \right) \prod_{r \neq i, j} f \left(\mathbf{X}_r^{(k)}, \sigma_r^2, \mathbf{L}_{\leq r}^{(k)} | \mathcal{D}^{(k)} \right) \times \int \int f \left(\mathbf{X}_i^{(k)} | \sigma_i^2, \mathbf{L}_{\leq i}^{(k)} \right) f \left(\mathbf{L}_{\leq i}^{(k)} | \sigma_i^2 \right) f \left(\sigma_i^2 | \mathcal{D}^{(k)} \right) d\mathbf{L}_{\leq i}^{(k)} d\sigma_i^2 \\ &\quad \times \int \int f \left(\mathbf{X}_j^{(k)} | \sigma_j^2, \mathbf{L}_{\leq j}^{(k)} \right) f \left(\mathbf{L}_{\leq j}^{(k)} | \sigma_j^2 \right) f \left(\sigma_j^2 | \mathcal{D}^{(k)} \right) d\mathbf{L}_{\leq j}^{(k)} d\sigma_j^2 \\ &= f \left(\mathcal{D}^{(k)} \right) \prod_{r \neq i, j} f \left(\mathbf{X}_r^{(k)}, \sigma_r^2, \mathbf{L}_{\leq r}^{(k)} | \mathcal{D}^{(k)} \right) \times m(\mathbf{X}_i^{(k)} | \mathbf{X}_{\text{pa}(i)}^{(k)}, \mathcal{D}^{(k)}) m(\mathbf{X}_j^{(k)} | \mathbf{X}_{\text{pa}(j)}^{(k)}, \mathcal{D}^{(k)}), \end{aligned} \quad (57)$$

where $m(\cdot)$ is defined in (48).

For $j = 1$, we apply the same process that we used before to compute $m(\mathbf{X}_1^{(k)} | \mathbf{X}_{\text{pa}(1)}^{(k)}, \mathcal{D}^{(k)})$, which is defined in (55). Substituting $f(\mathcal{D}^{(k)} | \mathbf{X}^{(k)}, \boldsymbol{\theta}_{-u})$ in equation (45) completes the proof for the **Reverse**($i \rightarrow j$) operator.

C Posteriors for D and $L^{(k)}$

Assuming $\mathcal{D}^{(1)}$ and $\mathcal{D}^{(2)}$ are given, to compute the posteriors for D and $L^{(k)}$, we need to start with the joint probability distribution

$$\begin{aligned} f(\mathbf{X}^{(1)}, \mathbf{X}^{(2)}, D, L^{(1)}, L^{(2)}) &= f(\mathbf{X}^{(1)}, \mathbf{X}^{(2)} | D, L^{(1)}, L^{(2)}) f(L^{(1)}, L^{(2)} | D) f(D) \\ &= \prod_{j=1}^q f(\mathbf{X}_j^{(1)}, \mathbf{X}_j^{(2)} | \sigma_j^2, \mathbf{L}_{\preceq j}^{(1)}, \mathbf{L}_{\preceq j}^{(2)}) f(\mathbf{L}_{\preceq j}^{(1)}, \mathbf{L}_{\preceq j}^{(2)} | \sigma_j^2) f(\sigma_j^2), \end{aligned} \quad (58)$$

and because of the Markov property of Gaussian DAG's, we just need to find the posterior for node j . So

$$\begin{aligned} &f(\mathbf{X}_j^{(1)}, \mathbf{X}_j^{(2)} | \sigma_j^2, \mathbf{L}_{\preceq j}^{(1)}, \mathbf{L}_{\preceq j}^{(2)}) f(\mathbf{L}_{\preceq j}^{(1)}, \mathbf{L}_{\preceq j}^{(2)} | \sigma_j^2) f(\sigma_j^2) \\ &= \frac{1}{(2\pi)^{\frac{n_j}{2}}} |\sigma_j^2 \mathbf{I}_{n_j}|^{-\frac{1}{2}} \exp \left\{ -\frac{1}{2\sigma_j^2} (\mathbf{X}_j^{(1)} + \mathbf{X}_{\text{pa}(j)}^{(1)} \mathbf{L}_{\preceq j}^{(1)})' (\mathbf{X}_j^{(1)} + \mathbf{X}_{\text{pa}(j)}^{(1)} \mathbf{L}_{\preceq j}^{(1)}) \right\} \\ &\times \frac{1}{(2\pi)^{\frac{n_j}{2}}} |\sigma_j^2 \mathbf{I}_{n_j}|^{-\frac{1}{2}} \exp \left\{ -\frac{1}{2\sigma_j^2} (\mathbf{X}_j^{(2)} + \mathbf{X}_{\text{pa}(j)}^{(2)} \mathbf{L}_{\preceq j}^{(2)})' (\mathbf{X}_j^{(2)} + \mathbf{X}_{\text{pa}(j)}^{(2)} \mathbf{L}_{\preceq j}^{(2)}) \right\} \\ &\times \frac{1}{(2\pi)^{\frac{|\text{pa}^{(1)}(j)|}{2}}} \left| \frac{1}{g_1} \sigma_j^2 \mathbf{I}_{|\text{pa}^{(1)}(j)|} \right|^{-\frac{1}{2}} \exp \left\{ -\frac{g_1}{2\sigma_j^2} (\mathbf{L}_{\preceq j}^{(1)})' \mathbf{L}_{\preceq j}^{(1)} \right\} \\ &\times \frac{1}{(2\pi)^{\frac{|\text{pa}^{(2)}(j)|}{2}}} \left| \frac{1}{g_2} \sigma_j^2 \mathbf{I}_{|\text{pa}^{(2)}(j)|} \right|^{-\frac{1}{2}} \exp \left\{ -\frac{g_2}{2\sigma_j^2} (\mathbf{L}_{\preceq j}^{(2)})' \mathbf{L}_{\preceq j}^{(2)} \right\} \\ &\times C \cdot (\sigma_j^2)^{-\frac{a_j^{(1)} + a_j^{(2)}}{2} - 1} \exp \left\{ -\frac{g_1 + g_2}{\sigma_j^2} \right\}, \end{aligned} \quad (59)$$

where $C = \frac{(g_1 + g_2)^{\frac{a_j^{(1)} + a_j^{(2)}}{2}}}{\Gamma(\frac{a_j^{(1)} + a_j^{(2)}}{2})}$, which is not a function of $D^{(k)}$ and $L^{(k)}$.

C.1 Posterior for $L_{\preceq j}^{(k)} | \sigma_j^2, \mathbf{X}^{(k)}$

For each $k \in \{1, 2\}$, the terms with $L_{\preceq j}^{(k)}$ in equation (59) are

$$A^{(k)} := \exp \left\{ -\frac{1}{2\sigma_j^2} \left(\mathbf{X}_j^{\prime(k)} \mathbf{X}_{\text{pa}(j)}^{(k)} \mathbf{L}_{\preceq j}^{(k)} + \mathbf{L}_{\preceq j}^{\prime(k)} \mathbf{X}_{\text{pa}(j)}^{\prime(k)} \mathbf{X}_j^{(k)} + \mathbf{L}_{\preceq j}^{\prime(k)} \mathbf{X}_{\text{pa}(j)}^{\prime(k)} \mathbf{X}_{\text{pa}(j)}^{(k)} \mathbf{L}_{\preceq j}^{(k)} + g_k \mathbf{L}_{\preceq j}^{\prime(k)} \mathbf{L}_{\preceq j}^{(k)} \right) \right\}. \quad (60)$$

Using notations defined in (23), the exponent term in $A^{(k)}$ can be rewritten as

$$\begin{aligned} &-\frac{1}{2\sigma_j^2} \left[\mathbf{L}_{\preceq j}^{\prime(k)} \left(\mathbf{X}_{\text{pa}(j)}^{\prime(k)} \mathbf{X}_{\text{pa}(j)}^{(k)} + g_k \mathbf{I}_{|\text{pa}^{(k)}(j)|} \right) \mathbf{L}_{\preceq j}^{(k)} + \mathbf{L}_{\preceq j}^{\prime(k)} \bar{\mathbf{T}}_j^{(k)} \left(\bar{\mathbf{T}}_j^{(k)} \right)^{-1} \mathbf{X}_{\text{pa}(j)}^{\prime(k)} \mathbf{X}_j^{(k)} + \mathbf{X}_j^{\prime(k)} \mathbf{X}_{\text{pa}(j)}^{(k)} \left(\bar{\mathbf{T}}_j^{\prime(k)} \right)^{-1} \bar{\mathbf{T}}_j^{(k)} \mathbf{L}_{\preceq j}^{(k)} \right] \\ &= -\frac{1}{2\sigma_j^2} \left[\mathbf{L}_{\preceq j}^{\prime(k)} \bar{\mathbf{T}}_j^{(k)} \mathbf{L}_{\preceq j}^{(k)} + \mathbf{L}_{\preceq j}^{\prime(k)} \bar{\mathbf{T}}_j^{(k)} \hat{\mathbf{L}}_j^{(k)} + \hat{\mathbf{L}}_j^{\prime(k)} \bar{\mathbf{T}}_j^{\prime(k)} \mathbf{L}_{\preceq j}^{(k)} \right], \end{aligned} \quad (61)$$

which is proportional to the exponent of a normal distribution, i.e.,

$$A^{(k)} \propto \exp \left\{ -\frac{1}{2\sigma_j^2} \left(\mathbf{L}_{\preceq j}^{(k)} + \hat{\mathbf{L}}_j^{(k)} \right)' \bar{\mathbf{T}}_j^{(k)} \left(\mathbf{L}_{\preceq j}^{(k)} + \hat{\mathbf{L}}_j^{(k)} \right) \right\}. \quad (62)$$

In other words, equation (60) can be written as

$$\mathbf{L}_{\preceq j}^{(k)} | \sigma_j^2, \mathbf{X}^{(k)} \sim \mathcal{N}_{|\text{pa}^{(k)}(j)|} \left(-\hat{\mathbf{L}}_j^{(k)}, \sigma_j^2 (\bar{\mathbf{T}}_j^{(k)})^{-1} \right), \quad (63)$$

which completes the proof.

For case when $j = 1$, because we set $\sigma_1^2 = 1$, we have

$$\mathbf{L}_{\preceq 1}^{(k)} | \mathbf{X}^{(k)} \sim \mathcal{N}_{|\text{pa}^{(k)}(1)|} \left(-\hat{\mathbf{L}}_1^{(k)}, (\bar{\mathbf{T}}_1^{(k)})^{-1} \right). \quad (64)$$

C.2 Posterior for $\sigma_j^2 | \mathbf{X}_j^{(1)}, \mathbf{X}_j^{(2)}$

For $j = 1$, we set $\sigma_1^2 = 1$, so we assume $j > 1$ in this section. The terms with σ_j^2 in equation (59) are

$$\begin{aligned}
& (\sigma_j^2)^{-\frac{n_1}{2} - \frac{n_2}{2} - \frac{a_j^{(1)}}{2} - \frac{a_j^{(2)}}{2} - 1 - \frac{|\text{pa}^{(1)}(j)|}{2} - \frac{|\text{pa}^{(2)}(j)|}{2}} \\
& \times \exp \left\{ -\frac{1}{2\sigma_j^2} \left(\mathbf{X}_j^{\prime(1)} \mathbf{X}_j^{(1)} + \mathbf{X}_j^{\prime(2)} \mathbf{X}_j^{(2)} + g_1 + g_2 \right) \right\} \\
& \times \exp \left\{ -\frac{1}{2\sigma_j^2} \left(\mathbf{X}_j^{\prime(1)} \mathbf{X}_{\text{pa}(j)}^{(1)} \mathbf{L}_{\preceq j}^{(1)} + \mathbf{L}_{\preceq j}^{\prime(1)} \mathbf{X}_{\text{pa}(j)}^{\prime(1)} \mathbf{X}_j^{(1)} + \mathbf{L}_{\preceq j}^{\prime(1)} \mathbf{X}_{\text{pa}(j)}^{(1)} \mathbf{L}_{\preceq j}^{(1)} + g_1 \mathbf{L}_{\preceq j}^{\prime(1)} \mathbf{L}_{\preceq j}^{(1)} \right) \right\} \\
& \times \exp \left\{ -\frac{1}{2\sigma_j^2} \left(\mathbf{X}_j^{\prime(2)} \mathbf{X}_{\text{pa}(j)}^{(2)} \mathbf{L}_{\preceq j}^{(2)} + \mathbf{L}_{\preceq j}^{\prime(2)} \mathbf{X}_{\text{pa}(j)}^{\prime(2)} \mathbf{X}_j^{(2)} + \mathbf{L}_{\preceq j}^{\prime(2)} \mathbf{X}_{\text{pa}(j)}^{(2)} \mathbf{L}_{\preceq j}^{(2)} + g_2 \mathbf{L}_{\preceq j}^{\prime(2)} \mathbf{L}_{\preceq j}^{(2)} \right) \right\} \quad (65)
\end{aligned}$$

Lets denote by $A^{(k)}$ the last two terms in the above equations for $k = 1, 2$, which are a function of $\mathbf{L}_{\preceq j}^{(k)}$. To obtain the marginal posterior for σ_j^2 , we need to integrate $A^{(k)}$ with respect to $\mathbf{L}_{\preceq j}^{(k)}$. We showed that $A^{(k)}$ is proportional to the p.d.f of a normal distribution in equation (62), so

$$\int_{\mathbb{R}^{|\text{pa}^{(k)}(j)|}} A^{(k)} d\mathbf{L}_{\preceq j}^{(k)} = (2\pi)^{\frac{|\text{pa}^{(k)}(j)|}{2}} \left| \frac{\bar{\mathbf{T}}_j^{(k)}}{\sigma_j^2} \right|^{-\frac{1}{2}} \exp \left\{ \frac{1}{2\sigma_j^2} \hat{\mathbf{L}}_j^{\prime(k)} \bar{\mathbf{T}}_j^{(k)} \hat{\mathbf{L}}_j^{(k)} \right\}. \quad (66)$$

Substituting (66) in (65) and using the fact $\left| \frac{\bar{\mathbf{T}}_j^{(k)}}{\sigma_j^2} \right|^{-\frac{1}{2}} = \sigma_j^{\frac{|\text{pa}^{(k)}(j)|}{2}} \left| \bar{\mathbf{T}}_j^{(k)} \right|^{-\frac{1}{2}}$, we have

$$\begin{aligned}
f(\sigma_j^2 | \mathbf{X}_j^{(1)}, \mathbf{X}_j^{(2)}) & \propto (\sigma_j^2)^{-\frac{n_1}{2} - \frac{n_2}{2} - \frac{a_j^{(1)}}{2} - \frac{a_j^{(2)}}{2} - 1 - \frac{|\text{pa}^{(1)}(j)|}{2} - \frac{|\text{pa}^{(2)}(j)|}{2} + \frac{|\text{pa}^{(1)}(j)|}{2} + \frac{|\text{pa}^{(2)}(j)|}{2}} \\
& \times \exp \left\{ \frac{-\frac{1}{2}(g_1 + g_2 + \mathbf{X}_j^{\prime(1)} \mathbf{X}_j^{(1)} + \mathbf{X}_j^{\prime(2)} \mathbf{X}_j^{(2)} - \hat{\mathbf{L}}_j^{\prime(1)} \bar{\mathbf{T}}_j^{(1)} \hat{\mathbf{L}}_j^{(1)} - \hat{\mathbf{L}}_j^{\prime(2)} \bar{\mathbf{T}}_j^{(2)} \hat{\mathbf{L}}_j^{(2)})}{\sigma_j^2} \right\}. \quad (67)
\end{aligned}$$

Therefore the posterior for $\sigma_j^2 | \mathbf{X}_j^{(1)}, \mathbf{X}_j^{(2)}$ becomes

$$\sigma_j^2 | \mathbf{X}_j^{(1)}, \mathbf{X}_j^{(2)} \sim \text{I - Ga} \left(\frac{a_j^{(1)}}{2} + \frac{a_j^{(2)}}{2} + \frac{n_1}{2} + \frac{n_2}{2}, \frac{1}{2} K \right), \quad (68)$$

where $K = \frac{1}{2}(g_1 + g_2 + \mathbf{X}_j^{\prime(1)} \mathbf{X}_j^{(1)} + \mathbf{X}_j^{\prime(2)} \mathbf{X}_j^{(2)} - \hat{\mathbf{L}}_j^{\prime(1)} \bar{\mathbf{T}}_j^{(1)} \hat{\mathbf{L}}_j^{(1)} - \hat{\mathbf{L}}_j^{\prime(2)} \bar{\mathbf{T}}_j^{(2)} \hat{\mathbf{L}}_j^{(2)})$.

D Posterior for $\theta | \mathbf{y}^{(1)}, \mathbf{y}^{(2)}, \mathbf{X}_{-1}^{(1)}, \mathbf{X}_{-1}^{(2)}, \mathbf{D}, \mathbf{L}^{(1)}, \mathbf{L}^{(2)}, \mathcal{D}^{(1)}, \mathcal{D}^{(2)}$

The posterior for θ can be written as

$$f(\theta | \mathbf{y}^{(1)}, \mathbf{y}^{(2)}, \mathbf{X}_{-1}^{(1)}, \mathbf{X}_{-1}^{(2)}, \mathbf{D}, \mathbf{L}^{(1)}, \mathbf{L}^{(2)}, \mathcal{D}^{(1)}, \mathcal{D}^{(2)}) \propto f(\mathbf{y}^{(1)}, \mathbf{y}^{(2)}, \mathbf{X}_{-1}^{(1)}, \mathbf{X}_{-1}^{(2)} | \mathbf{D}, \mathbf{L}^{(1)}, \mathbf{L}^{(2)}, \mathcal{D}^{(1)}, \mathcal{D}^{(2)}, \theta) f(\theta), \quad (69)$$

where $f(\theta) \propto 1$. To simplify the equations, we omit $\mathcal{D}^{(1)}$ and $\mathcal{D}^{(2)}$. By seperating $\mathbf{X}_1^{(k)}$, the full likelihood function can be written as

$$\begin{aligned}
& f(\mathbf{y}^{(1)}, \mathbf{y}^{(2)}, \mathbf{X}^{(1)}, \mathbf{X}^{(2)} | \mathbf{D}, \mathbf{L}^{(1)}, \mathbf{L}^{(2)}, \theta) \\
& = \prod_{j=2}^q f_{\mathcal{N}_{n_1}}(\mathbf{X}_j^{(1)} | -\mathbf{X}_{\text{pa}(j)}^{(1)} \mathbf{L}_{\preceq j}^{(1)}, \sigma_j^2 \mathbf{I}_{n_1}) \cdot f_{\mathcal{N}_{n_1}}(\mathbf{X}_1^{(1)} | -\mathbf{X}_{\text{pa}(1)}^{(1)} \mathbf{L}_{\preceq 1}^{(1)}, \mathbf{I}_{n_1}) \cdot \prod_{i=1}^{n_1} \mathbb{1}(\theta_{y_i^{(1)}-1} < x_{i,1}^{(1)} \leq \theta_{y_i^{(1)}}) \\
& \times \prod_{j=2}^q f_{\mathcal{N}_{n_2}}(\mathbf{X}_j^{(2)} | -\mathbf{X}_{\text{pa}(j)}^{(2)} \mathbf{L}_{\preceq j}^{(2)}, \sigma_j^2 \mathbf{I}_{n_2}) \cdot f_{\mathcal{N}_{n_2}}(\mathbf{X}_1^{(2)} | -\mathbf{X}_{\text{pa}(1)}^{(2)} \mathbf{L}_{\preceq 1}^{(2)}, \mathbf{I}_{n_2}) \cdot \prod_{i=1}^{n_2} \mathbb{1}(\theta_{y_i^{(2)}-1} < x_{i,1}^{(2)} \leq \theta_{y_i^{(2)}}) \\
& = \prod_{k=1}^2 f(\mathbf{X}_{-1}^{(k)} | \mathbf{D}, \mathbf{L}^{(k)}) f_{\mathcal{N}_{n_k}}(\mathbf{X}_1^{(k)} | -\mathbf{X}_{\text{pa}(1)}^{(k)} \mathbf{L}_{\preceq 1}^{(k)}, \mathbf{I}_{n_k}) \cdot \prod_{i=1}^{n_k} \mathbb{1}(\theta_{y_i^{(k)}-1} < x_{i,1}^{(k)} \leq \theta_{y_i^{(k)}}), \quad (70)
\end{aligned}$$

where $f(\mathbf{X}_{-1}^{(k)} | \mathbf{D}, \mathbf{L}^{(k)})$ does not depend on θ .

In order to get the marginal distribution, we need to take integral from both sides of (70) with respect to $\mathbf{X}_1^{(1)}$ and $\mathbf{X}_1^{(2)}$, i.e.,

$$\begin{aligned} & \int \int f(\mathbf{y}^{(1)}, \mathbf{y}^{(2)}, \mathbf{X}^{(1)}, \mathbf{X}^{(2)} | \mathcal{D}, \mathbf{L}^{(1)}, \mathbf{L}^{(2)}, \theta) d\mathbf{X}_1^{(1)} d\mathbf{X}_1^{(2)} \\ & \propto \prod_{k=1}^2 \int f_{\mathcal{N}_{n_k}}(\mathbf{X}_1^{(k)} | -\mathbf{X}_{\text{pa}(1)}^{(k)} \mathbf{L}_{\leq 1}^{(k)}, \mathbf{I}_{n_k}) \cdot \prod_{i=1}^{n_k} \mathbb{1}(\theta_{y_i^{(k)}-1} < x_{i,1}^{(k)} \leq \theta_{y_i^{(k)}}) d\mathbf{X}_1^{(k)} \\ & = \prod_{k=1}^2 \prod_{i=1}^{n_k} \int f_{\mathcal{N}}(x_{i,1}^{(k)} | -\mathbf{x}_{\text{pa}(1)}^{(k)} \mathbf{L}_{\leq 1}^{(k)}, 1) \mathbb{1}(\theta_{y_i^{(k)}-1} < x_{i,1}^{(k)} \leq \theta_{y_i^{(k)}}) dx_{i,1}^{(k)}, \end{aligned} \quad (71)$$

where $\theta_{-1} := -\infty, \theta_0 := \theta, \theta_1 := \infty$ and

$$\int f_{\mathcal{N}}(x_{i,1}^{(k)} | -\mathbf{x}_{\text{pa}(1)}^{(k)} \mathbf{L}_{\leq 1}^{(k)}, 1) \mathbb{1}(\theta_{y_i^{(k)}-1} < x_{i,1}^{(k)} \leq \theta_{y_i^{(k)}}) dx_{i,1}^{(k)} = \int_{\theta_{y_i^{(k)}-1}}^{\theta_{y_i^{(k)}}} f_{\mathcal{N}}(x_{i,1}^{(k)} | -\mathbf{x}_{\text{pa}(1)}^{(k)} \mathbf{L}_{\leq 1}^{(k)}, 1) dx_{i,1}^{(k)}$$

is either the CDF or the survival function of a $\mathcal{N}(-\mathbf{x}_{\text{pa}(1)}^{(k)} \mathbf{L}_{\leq 1}^{(k)}, 1)$ distribution for $y_i^{(k)} = 0$ and $y_i^{(k)} = 1$, respectively.

Therefore,

$$f(\theta | \mathbf{y}^{(1)}, \mathbf{y}^{(2)}, \mathbf{X}_{-1}^{(1)}, \mathbf{X}_{-1}^{(2)}, \mathcal{D}^{(1)}, \mathcal{D}^{(2)}) \propto \prod_{k=1}^2 \prod_{i=1}^{n_k} \Psi(y_i^{(k)}, \theta | -\mathbf{x}_{\text{pa}(1)}^{(k)} \mathbf{L}_{\leq 1}^{(k)}, 1), \quad (72)$$

where $\Psi(y, \eta | \mu, \sigma^2) := |y - \Phi(\eta | \mu, \sigma^2)|$. In fact, $\Psi(y, \eta | \mu, \sigma^2)$ is a notation for the CDF or the survival function of a $\mathcal{N}(\mu, \sigma^2)$ distribution for $y = 0$ and $y = 1$, respectively.

E Proof of proposition 1

We first need to reorder the matrix \mathbf{X} as $\mathbf{X}^* = (\mathbf{X}_{-1}, \mathbf{X}_1)$ and let $\text{cov}(\mathbf{X}^*) = \mathbf{\Omega}^{-1}$. The matrix $\mathbf{\Omega}$ can also be partitioned as

$$\mathbf{\Omega} = \begin{pmatrix} \mathbf{\Omega}_{11} & \mathbf{\Omega}_{12} \\ \mathbf{\Omega}_{21} & \mathbf{\Omega}_{22} \end{pmatrix}. \quad (73)$$

Using Cholesky decomposition, we can decompose $\mathbf{\Omega}$ into

$$\mathbf{\Omega} = \mathbf{L}\mathbf{L}' = \begin{pmatrix} \mathbf{L}_{11} & \mathbf{0} \\ \mathbf{L}_{21} & \mathbf{L}_{22} \end{pmatrix} \begin{pmatrix} \mathbf{L}'_{11} & \mathbf{L}'_{21} \\ \mathbf{0} & \mathbf{L}'_{22} \end{pmatrix}. \quad (74)$$

By equating the submatrices in (73) and (74), we have $\mathbf{\Omega}_{11} = \mathbf{L}_{11}\mathbf{L}'_{11}$, $\mathbf{\Omega}_{12} = \mathbf{L}_{11}\mathbf{L}'_{21}$ and $\mathbf{\Omega}_{22} = \mathbf{L}_{21}\mathbf{L}'_{21} + \mathbf{L}_{22}\mathbf{L}'_{22}$. These equations can be written as

$$\begin{aligned} \mathbf{L}_{11} &= \mathbf{\Omega}_{11}^{1/2} \\ \mathbf{L}'_{21} &= \mathbf{\Omega}_{11}^{-1/2} \mathbf{\Omega}_{12} \\ \mathbf{L}_{22} &= \left(\mathbf{\Omega}_{22} - \mathbf{\Omega}_{11}^{-1/2} \mathbf{\Omega}'_{12} \mathbf{\Omega}_{12} \mathbf{\Omega}_{11}^{-1/2} \right)^{1/2}, \end{aligned} \quad (75)$$

where the square root for the matrix A is defined by $A = A^{1/2} A'^{1/2}$. On the other hand, $\mathbf{\Omega}_{-1} := \mathbf{\Omega}_{11} = \text{cov}(\mathbf{X}_{-1})$ can be decomposed to $\mathbf{L}_{-1}\mathbf{L}'_{-1}$, so $\mathbf{\Omega}_{11}^{1/2} = \mathbf{L}_{-1}$, which completes the proof that $\mathbf{L}_{11} = \mathbf{L}_{-1}$.

F Simulation results

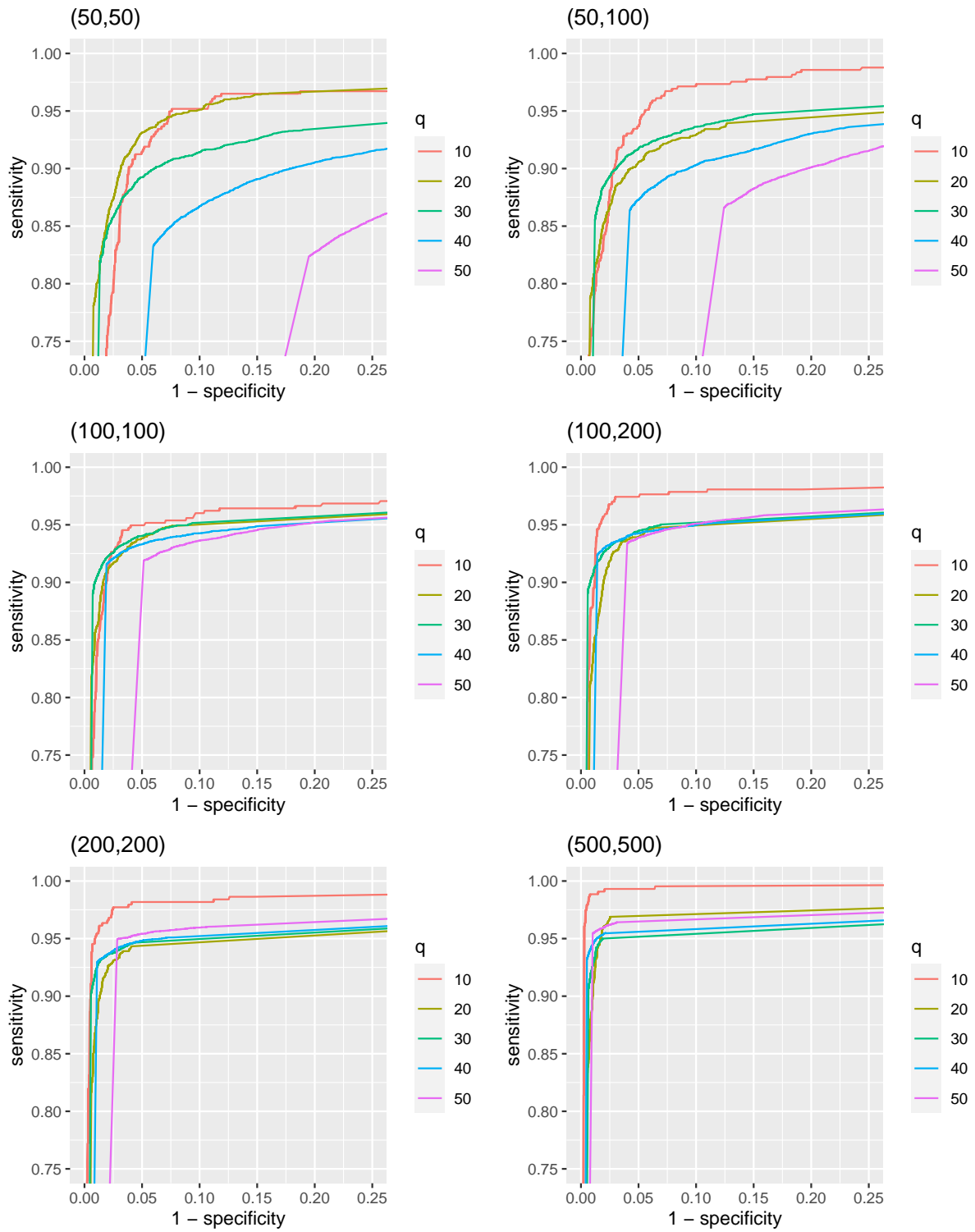


Figure 16: ROC for $\xi = 0.2$. Each plot is for different sample sizes (n_1, n_2) . Different colors represent different DAG sizes, q .

Table 4: Area under the curve (AUC) for different sample sizes and DAG sizes, q and the probability of edge inclusion $\xi = 0.2$.

n_1	n_2	q				
		10	20	30	40	50
50	50	0.9679	0.9703	0.9488	0.9133	0.8307
50	100	0.9820	0.9574	0.9602	0.9345	0.8879
100	100	0.9740	0.9675	0.9686	0.9598	0.9442
100	200	0.9850	0.9661	0.9694	0.9651	0.9550
200	200	0.9895	0.9664	0.9689	0.9679	0.9638
500	500	0.9959	0.9802	0.9711	0.9744	0.9765
1000	500	0.9960	0.9795	0.9707	0.9746	0.9759
1000	1000	0.9971	0.9749	0.9695	0.9751	0.9789

Table 5: Area under the curve (AUC) for different sample sizes and DAG sizes, q and the probability of edge inclusion $\xi = 0.3$.

n_1	n_2	q			
		10	20	30	40
50	50	0.9597	0.9473	0.9303	0.8784
50	100	0.9636	0.9550	0.9446	0.9097
100	100	0.9811	0.9591	0.9562	0.9484
100	200	0.9847	0.9573	0.9644	0.9589
200	200	0.9813	0.9598	0.9671	0.9670
500	500	0.9887	0.9635	0.9686	0.9740
1000	500	0.9857	0.9580	0.9669	0.9741
1000	1000	0.9847	0.9585	0.9680	0.9734

Table 6: Area under the curve (AUC) for different sample sizes and DAG sizes, q and the probability of edge inclusion $\xi = 0.4$.

n_1	n_2	q		
		10	20	30
50	50	0.9416	0.9259	0.8880
50	100	0.9606	0.9418	0.9215
100	100	0.9667	0.9530	0.9449
100	200	0.9692	0.9572	0.9556
200	200	0.9671	0.9530	0.9644
500	500	0.9788	0.9605	0.9651
1000	500	0.9765	0.9569	0.9661
1000	1000	0.9855	0.9600	0.9705

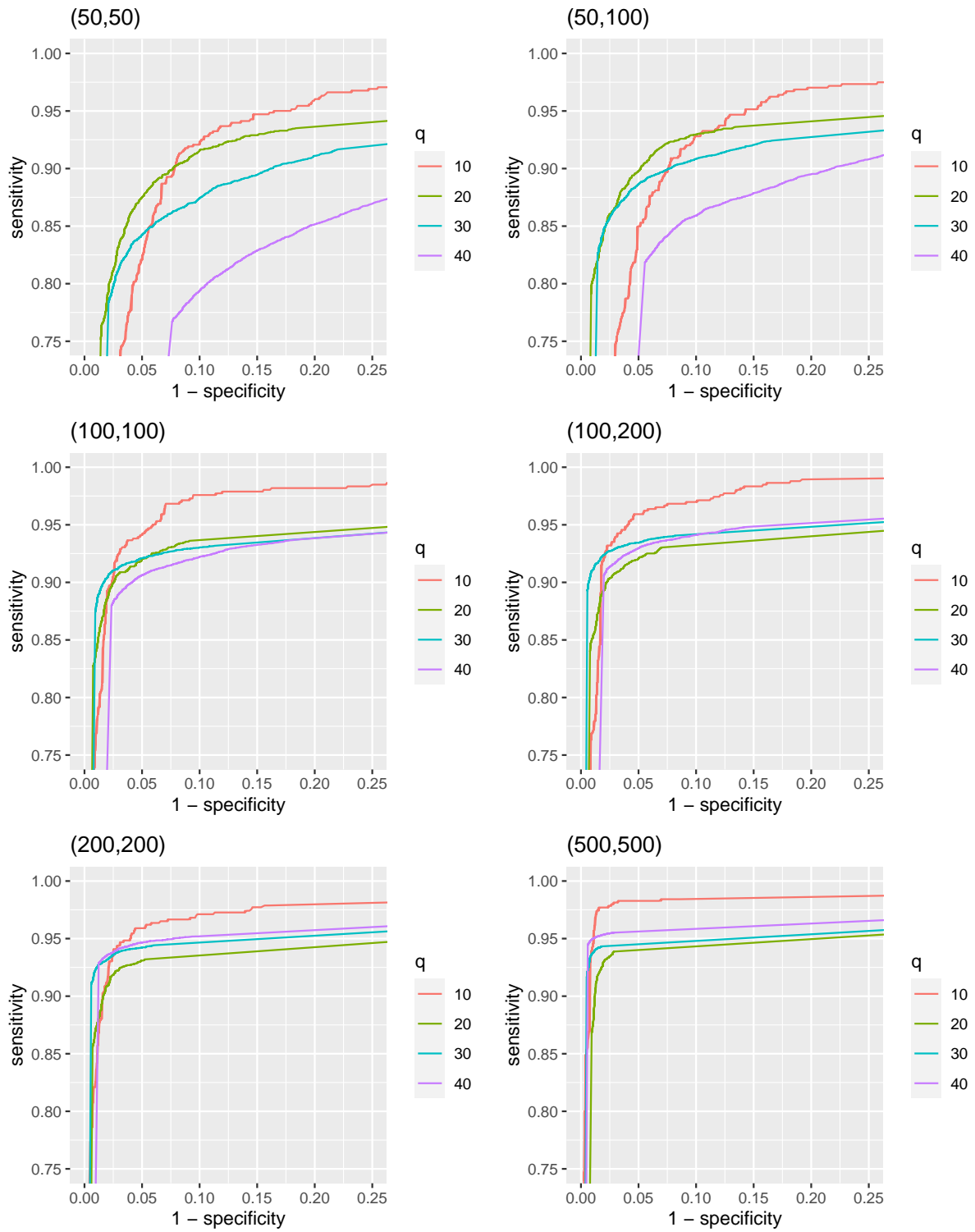


Figure 17: ROC for $\xi = 0.3$. Each plot is for different sample sizes (n_1, n_2) . Different colors represent different DAG sizes, q .

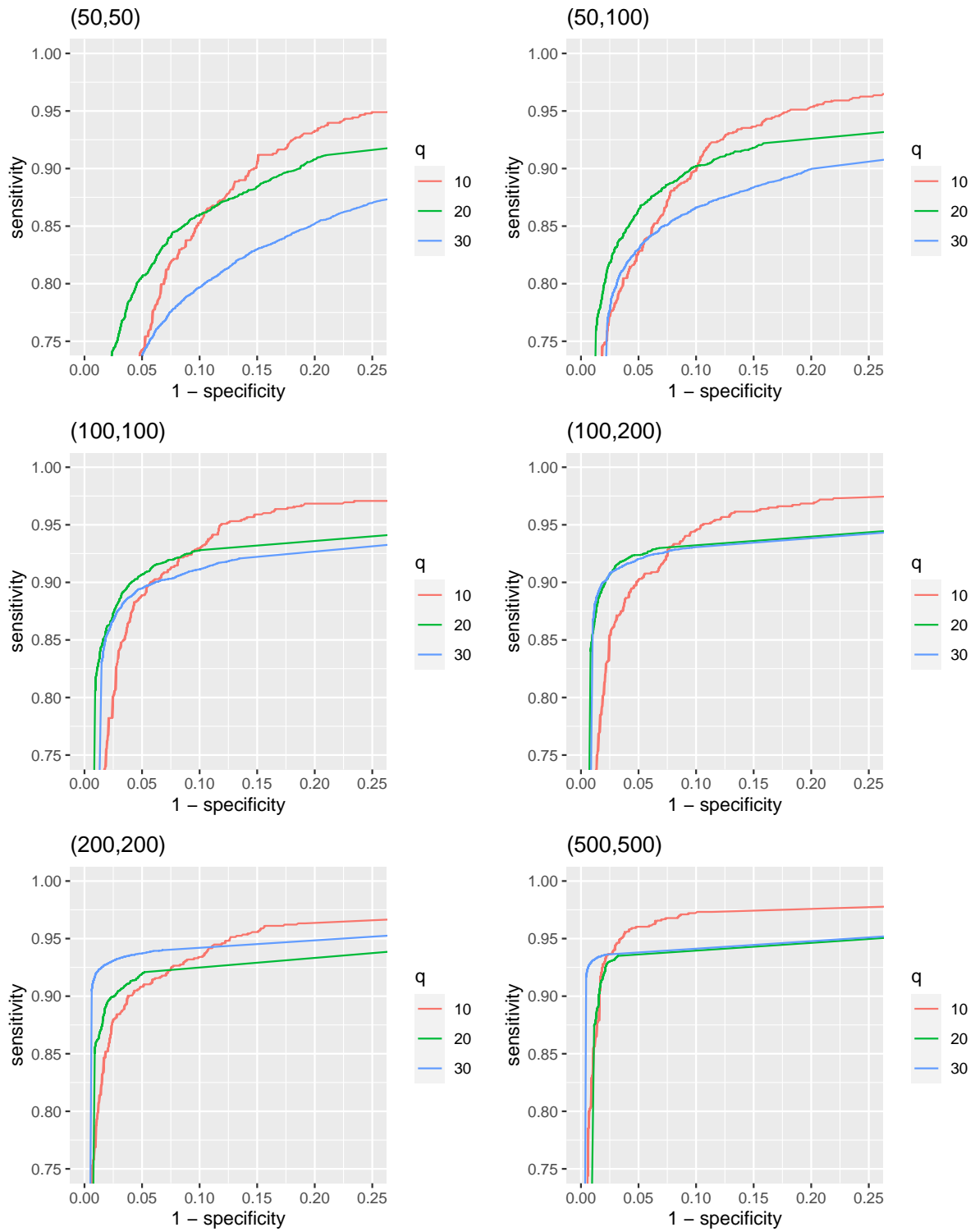


Figure 18: ROC for $\xi = 0.4$. Each plot is for different sample sizes (n_1, n_2) . Different colors represent different DAG sizes, q .

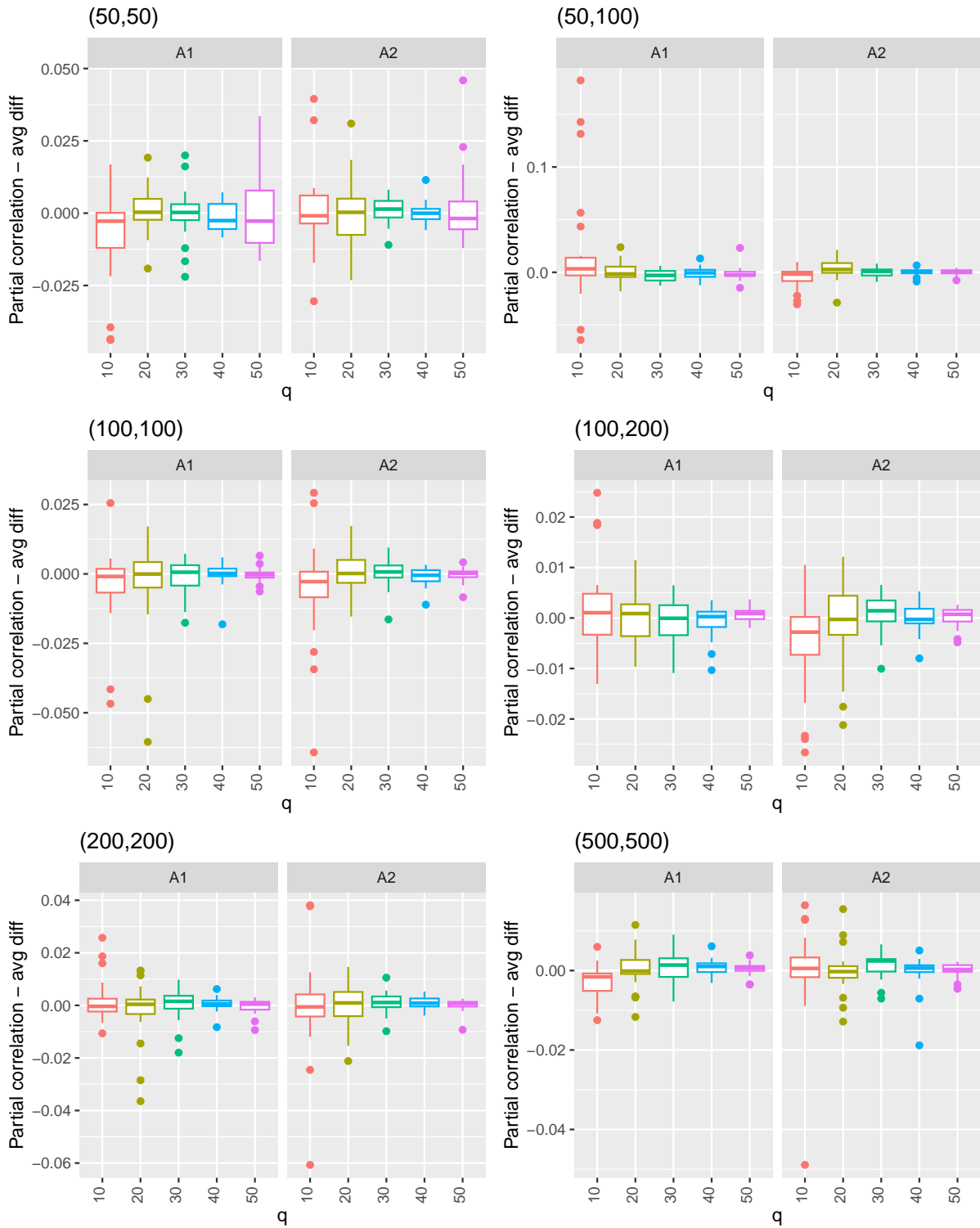


Figure 19: Box plot for the difference between the estimated and true partial correlations defined in (41) for $T = 5,000$ iterations and $\xi = 0.2$.

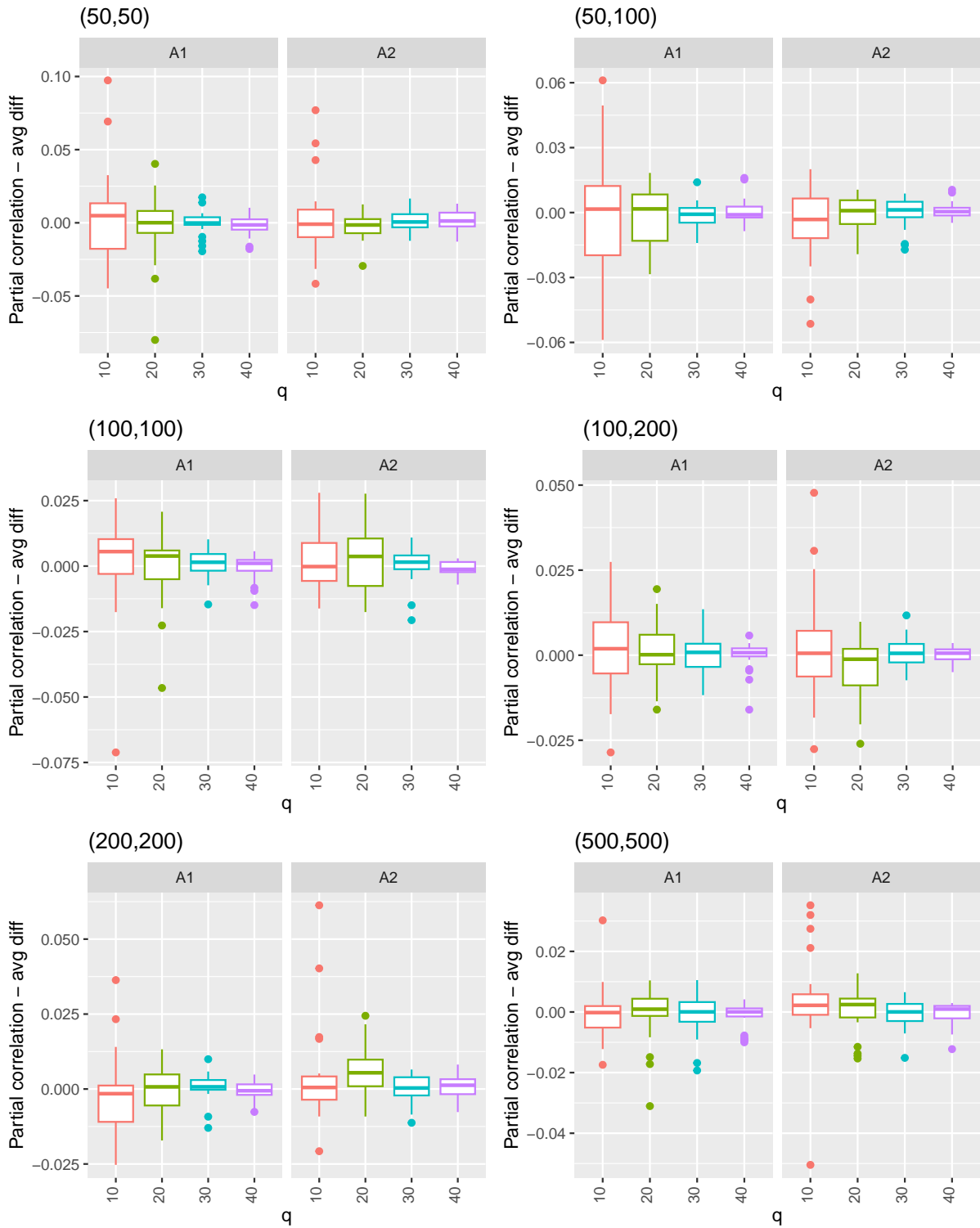


Figure 20: Box plot for the difference between the estimated and true partial correlations defined in (41) for $T = 5,000$ iterations and $\xi = 0.3$.

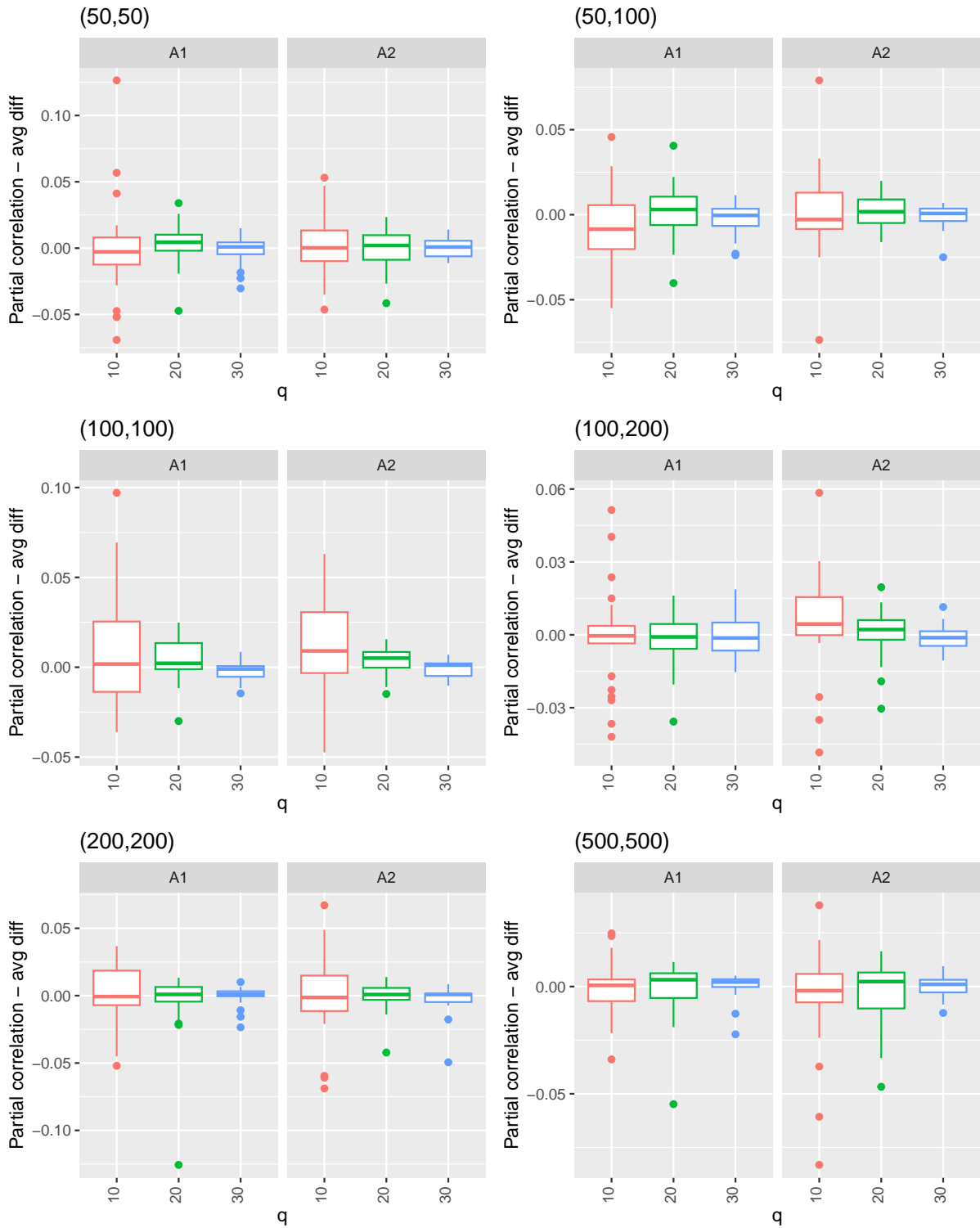


Figure 21: Box plot for the difference between the estimated and true partial correlations defined in (41) for $T = 5,000$ iterations and $\xi = 0.4$.

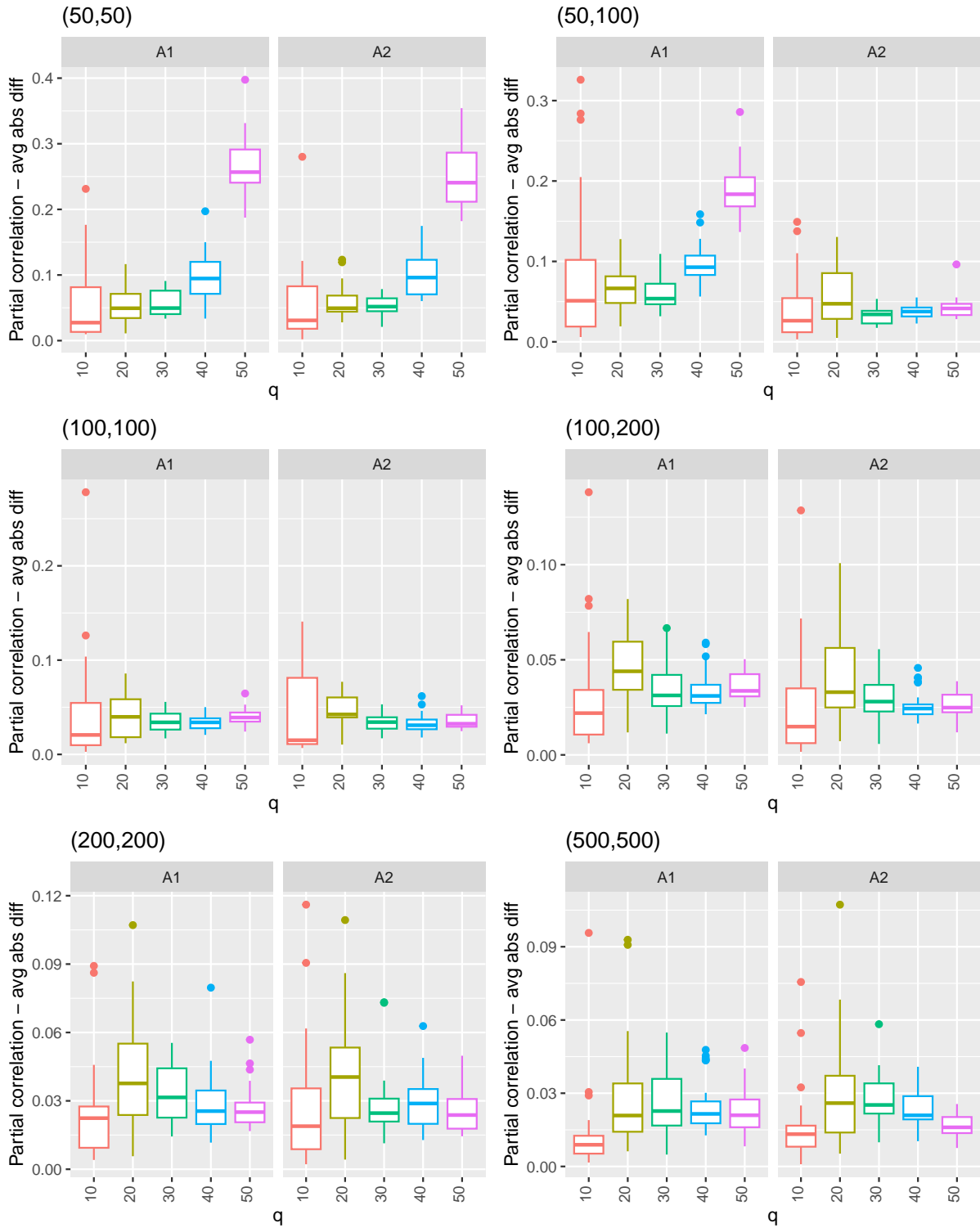


Figure 22: Box plot for the absolute difference between the estimated and true partial correlations defined in (41) for $T = 5,000$ iterations and $\xi = 0.2$.

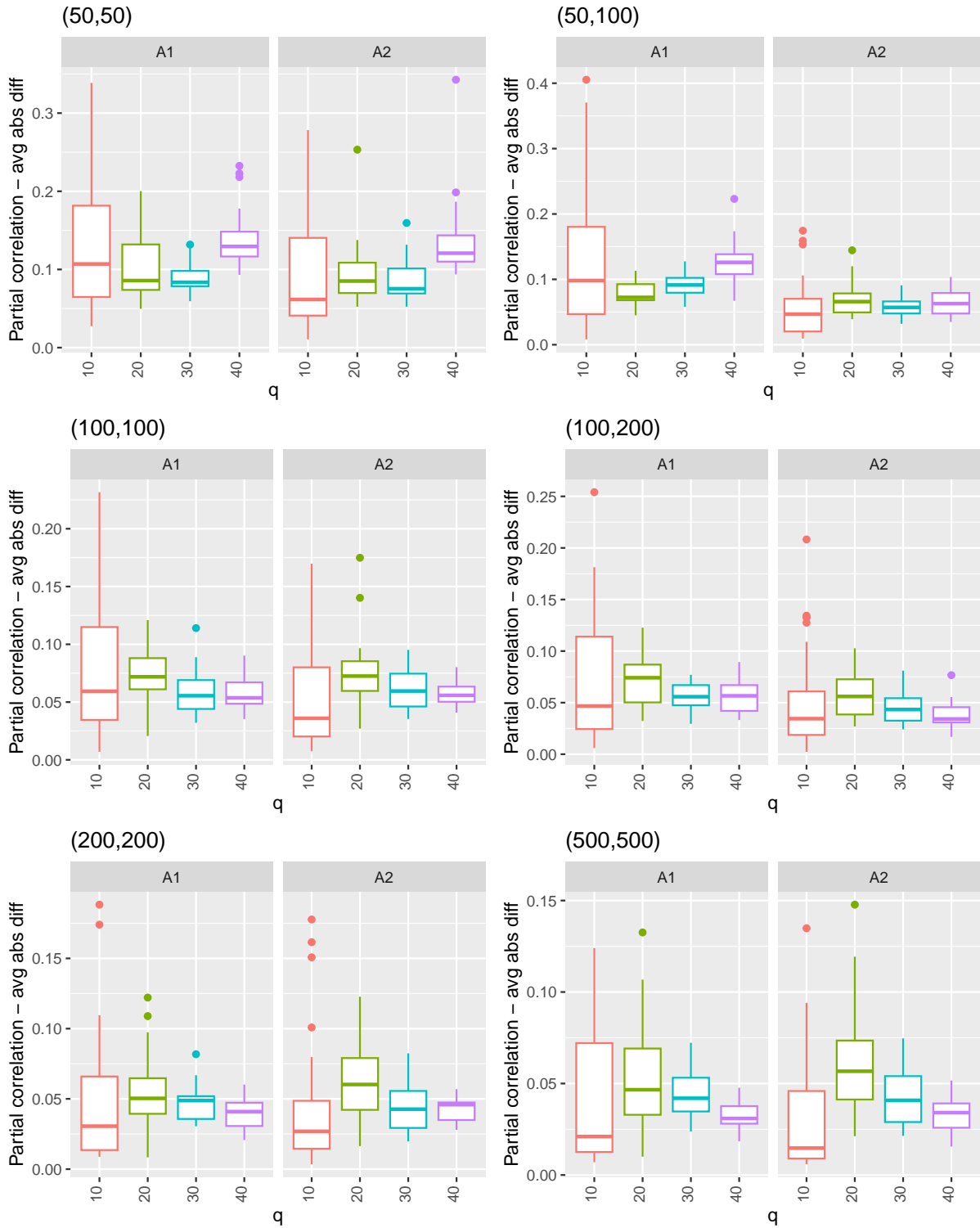


Figure 23: Box plot for the absolute difference between the estimated and true partial correlations defined in (41) for $T = 5,000$ iterations and $\xi = 0.3$.

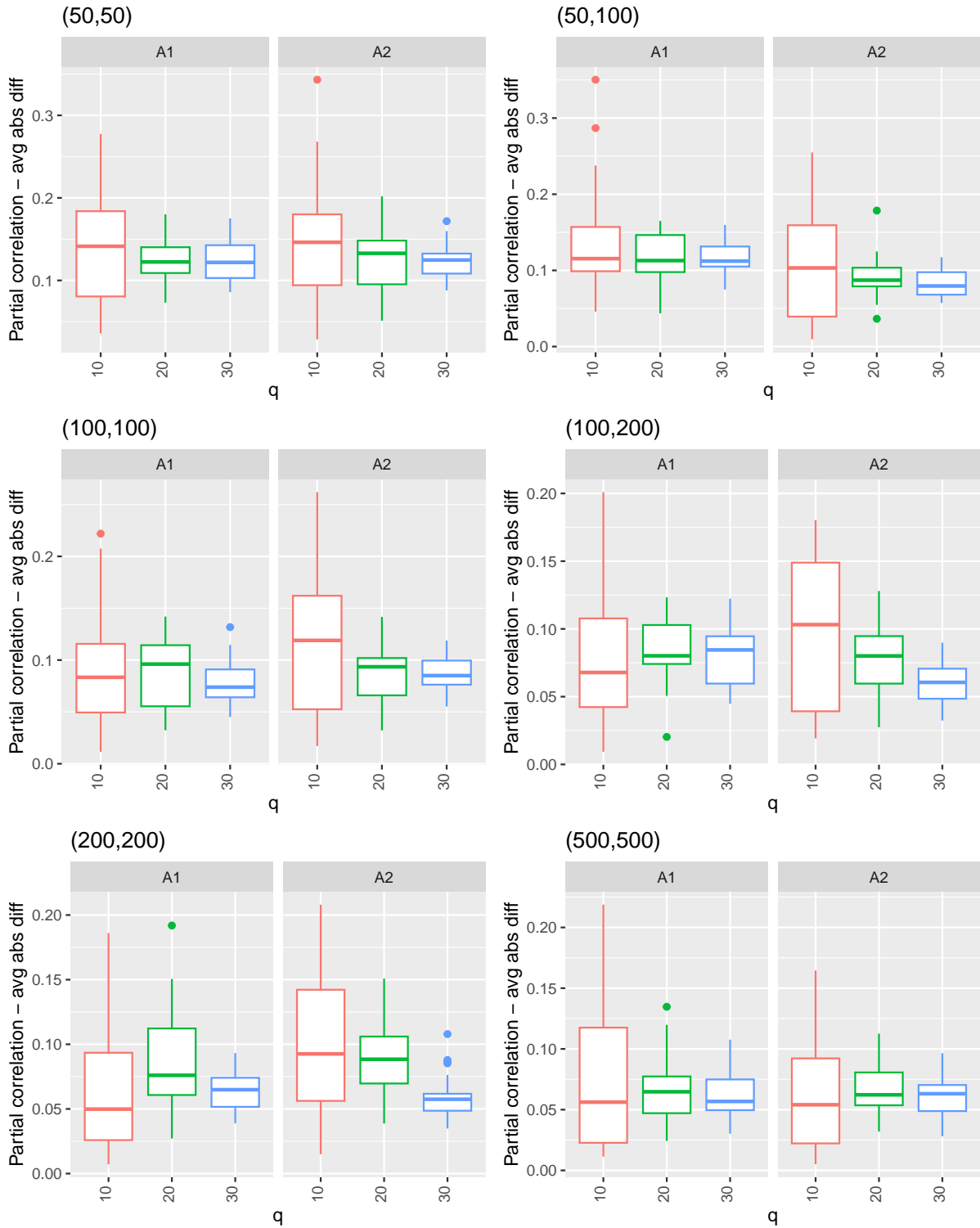


Figure 24: Box plot for the absolute difference between the estimated and true partial correlations defined in (41) for $T = 5,000$ iterations and $\xi = 0.4$.